E.O. Paton Electric Welding Institute of the National Academy of Sciences of Ukraine

International Scientific-Technical and Production Journal

The Paton WELDING JOURNAL

Issue 02 2020

Published Monthly Since 2000

English Translation of the Monthly «Avtomatychne Zvaryuvannya»
(Avtomaticheskaya Svarka/Automatic Welding) Journal Published in Ukrainian and Russian Since 1948

Founders
E.O. Paton Electric Welding Institute
International Association «Welding»

Publisher
International Association «Welding»

Translators
A.O. Fomin, I.M. Kutianova
Editor
N.G. Khomenko
Electron galley
D.I. Sereda, T.Yu. Snegiryova

Address
E.O. Paton Electric Welding Institute,
International Association «Welding»
11 Kazymyr Malevych Str. (former Bozhenko),
03150, Kyiv, Ukraine
Tel.:/Fax: (38044) 200 82 77
E-mail: journal@paton.kiev.ua
www://patonpublishinghouse.com/eng/journals/tpwj

State Registration Certificate
KV 4790 of 09.01.2001
ISSN 0957-798X
DOI: http://dx.doi.org/10.37434/tpwj

Subscriptions
12 issues per year, back issues available.
$384, subscriptions for the printed (hard copy) version, air postage and packaging included.
$312, subscriptions for the electronic version (sending issues of Journal in pdf format or providing access to IP addresses).
Institutions with current subscriptions on printed version can purchase online access to the electronic versions of any back issues that they have not subscribed to.
Issues of the Journal (more than two years old) are available at a substantially reduced price.

CONTENTS

SCIENTIFIC AND TECHNICAL

Piskun N.V., Falchenko Yu.V., Petrushinets L.V., Ustinov A.I., Melnichenko T.V. and *Statkevich I.I.* Formation of the structure and mechanical properties of joints of TiAlNb intermetallic alloy in diffusion welding 2

Akhonin S.V., Bilous V.Yu., Selin R.V. and *Petrychenko I.K.* Impact of TIG welding on the structure and mechanical properties of joints of pseudo-β-titanium alloy 9

Korzhik V.M., Shcheretskii V.O., Chaika A.A. and *Jianglong Yi.* Calculated evauation of application of nanosized particles in modifying the cast structure of weld metal 16

Dmytryk V.V., Glushko A.V. and *Iglin S.P.* Structural changes in the metal of welded joints of long-term operating steam pipelines 22

Stefaniv B.V., Nyrkova L.I., Larionov A.V. and *Osadchuk S.O.* Corrosion resistance of composite material deposited by TIG method using flexible cord TeroCote 7888T 26

INDUSTRIAL

Nesterenkov V.M., Zagornikov V.I., Orsa Yu.V. and *Ignatenko O.M.* Features of applying electron beam welding in manufacture of the cathode assembly of the electron gun 30

Koval V.A., Labur T.M. and *Yavorska T.R.* Properties of joints of V1341T grade alloy under the conditions of TIG welding 35

Matviichuk V.A. and *Nesterenkov V.M.* Additive electron beam equipment for layer-by-layer manufacture of metal products from powder materials 41

Poklyatsky A.G., Fedorchuk V.E., Motrunich S.I., Falchenko Yu.V. and *Kisla G.P.* Influence of scandium on mechanical properties of welded joints of D16 alloy produced using filler wires of different alloying systems 47

https://doi.org/10.37434/tpwj2020.02.01

FORMATION OF THE STRUCTURE AND MECHANICAL PROPERTIES OF JOINTS OF TiAlNb INTERMETALLIC ALLOY IN DIFFUSION WELDING

N.V. Piskun, Yu.V. Falchenko, L.V. Petrushinets, A.I. Ustinov, T.V. Melnichenko and **I.I. Statkevich**
E.O. Paton Electric Welding Institute of the NAS of Ukraine
11 Kazymyr Malevych Str., 03150, Kyiv, Ukraine. E-mail: office@paton.kiev.ua

The impact of technological measures in vacuum diffusion welding on formation of the structure and mechanical properties of joints of TiAlNb intermetallic alloy was studied in the work. It is shown that welding of intermetallic alloy by the method of vacuum diffusion welding at temperature T_w = 1050 °C, pressure P_w = 10 MPa, for 20 min does not ensure producing sound joints. After welding, the joint line is visible in the butt, along which there is a considerable number of defects in the form of pore lines. Increase of welding parameters up to temperature T_w = 1200 °C, pressure P_w = 30 MPa, welding time of 30 min, as well as application of a ductile interlayer from NbTi alloy 1 mm thick allows improving the conditions of welded joint formation and greatly reducing the number of defects in the butt joint. During welding, common grains and diffusion zone 25–35 μm thick form between the interlayer material and the intermetallic alloy. Application of nanolayered interlayer of Al−Ti system of the total thickness of 25 μm in welding of TiAlNb intermetallic alloy, combined with cyclic loading in the form of 3 cycles of loading-unloading leads to a change of the nature of the structure in the joint zone. In the microstructures of welded joints obtained by optical metallography, the joint line is not visible. Application of electron microscopy allows detecting in the butt joint a diffusion zone 15 to 20 μm thick, close by its chemical composition to that of the intermetallic alloy. Investigation of the compressive strength of welded joints demonstrated that the average strength of joints of TiAlNb intermetallic alloy, produced using an interlayer from NbTi alloy, is equal to 988.2 MPa, and application of a nanolayered interlayer of Al–Ti system in welding allows increasing the average strength of the samples up to 1279.8 MPa. 16 Ref., 2 Tables, 8 Figures.

Keywords: TiAlNb intermetallic alloy, diffusion welding, interlayers, joint microstructure

Titanium aluminides represent an important class of alloys which have a unique set of physico-mechanical properties that makes them highly promising for manufacture of aviation engine elements. The main disadvantage of the above alloys is low ductility at room temperature that makes their technological processing and industrial application more complex.

One of the directions of possible solution of the problem of increasing the ductility and adaptability to fabrication, respectively, is creation of alloys with ortho- or B_2-structure. It is known that niobium addition to γ-TiAl promotes increase of its ductility [1]. With this purpose, titanium aluminides are alloyed by a rather large quantity of niobium (up to 25 at.%) and other β-stabilizers. However, alongside many positive characteristics orthorhombic alloys with up to 25 at.% niobium content, have higher density (6.9 g/cm^3). In addition, high niobium content leads to considerable increase of the alloy price.

A modern tendency in development of the technology of heat-resistant TiAl-based intermetallics is creation of a class of alloys, having third β-phase in their composition. Presence of this phase facilitates the technological processing of materials, including also rolling and hot pressing [2−4]. γ-TiAl alloys contain 42–46 at.% aluminium and also transient metals in the sum of up to 10 at.% total, as master alloy, which stabilize the primary β-Ti phase (known in the low-temperature ordered state as B_2-phase with BCC lattice) In addition to obligatory alloying by Nb, such β-stabilizers as Mo, Ta, Zr, Cr, W, and V can be used. Their application leads to preservation in the alloy of a small volume fraction of residual B_2-phase at solidification, which is ductile both at room, and at high temperatures. Molybdenum having high β-stabilizing activity, can be used for creation of B_2-phase (thus, TNM abbreviation TiAl–Nb–Mo appeared) [5−7]. Development of TNM type alloys allows solving the problem of low room temperature ductility of intermetallics, as well as increasing the high temperature resistance of the products.

At this moment, researchers are paying attention to creation of intermetallic alloys of Ti−Al−Nb ternary system. The complexity of producing joints by

N.V. Piskun — orcid.org/0000-0003-1459-2310, Yu.V. Falchenko — orcid.org/0000-0002-3028-2964,
L.V. Petrushinets — orcid.org/0000-0001-7946-3056, A.I. Ustinov — orcid.org/0000-0002-8855-3499,
T.V. Melnichenko — orcid.org/0000-0002-1460-5532, I.I. Statkevich — orcid.org/0000-0001-9403-2123

diffusion welding method consists primarily, in the presence of an oxide layer on their surface, which prevents formation of a welded joint. Alloys of this group also have insufficient ductility that, in its turn, prevents bonding of the contact surfaces at the stage of physical contact. The works on diffusion welding of titanium aluminides are known.

The authors of [8] studied the possibility of diffusion welding of γ-TiAl alloy. It was found that the highest values of shear strength were obtained in the following mode: T_w = 1000 °C, P_w = 10 MPa, t = 300 min (388.4 MPa). Despite the absence of defects in the joints, all the samples failed at shear strength values on the level of 25 % from that of the base metal, which is caused by the presence of brittle α_2-Ti_3Al phase along the butt joint.

In [9] it was shown that at the same mode of welding TiAl alloy with a high Nb content (T_w = 1100 °C, P_w = = 30 MPa, t = 45 min), roughness lowering from 0.261 to 0.062 μm allows increasing the shear strength by 100 MPa (to 383 MPa). Control of sample surface roughness also has a positive effect on joint structure formation — with its refinement α_2-Ti_3Al phase disappears in the butt joint. Heat treatment promotes removal of the joint line, this way somewhat increasing the shear strength, but greatly changing the base material microstructure. It becomes coarse-grained, completely platelike.

With the purpose of intensification of the process of formation of joints of TiAl alloy with a high Nb content in diffusion welding, the authors of [10] use pulsed current as the heat source. It is assumed that plasma, which forms in the gaps between the surfaces, activates and cleans them, removing the oxides and contamination. Optimum welding parameters were as follows: T_w = 1200 °C, P_w = 15 MPa, t = 60 min. In this mode, the initial lamellar microstructure in the joint zone is transformed into the duplex one, having higher mechanical properties. Pressure increase up to 30 MPa at welding temperature of 1200 °C, promotes intensive grain growth, leading to decrease of the joint rupture strength from 657 to 574 MPa.

The authors of [11] point to the need for running of recrystallization processes in the butt joint, in order to produce a sound joint of TiAl alloy with a high Nb content. Diffusion welding at the temperature higher than 1100 °C and 30 MPa pressure leads to recrystallization on the contact boundary, promoting migration of the interface. Shear strength of the joints rises with temperature and pressure of welding, and reaches the highest value (approximately 400 MPa) at the following mode parameters: T_w = 1150 °C, P_w = 30 MPa, t = = 45 min, T_w = 1100 °C, P_w = 40 MPa, t = 45 min.

One of the methods for welding surface activation is using interlayers, application of which allows localizing plastic deformation directly in the butt joint, and minimizing the requirements to roughness and quality of surface preparation.

Work [12] is a study of the possibility of diffusion welding of γ-TiAl, using a mixture of powders of titanium, aluminium and high-purity carbon as an interlayer. Powders were cold-pressed into cylindrical samples 0.5 mm thick. The thus obtained interlayer was placed between the samples, which were welded and heated up to the aluminium melting temperature (660 °C) under the pressure of 15–55 MPa. The powder mixture entered into a reaction, and formed a $TiAl_3$ layer on the boundary with titanium aluminide, and a porous mixture of γ-TiAl and TiC phases in the central section of the joint zone. The highest values of rupture strength (approximately 70 MPa) were obtained at welding pressure of 30 MPa. Its smaller or larger values lead to porosity increase and, as a consequence, to lowering of mechanical property values.

In order to reduce the chemical inhomogeneity in the joint zone, there is a need for application of thinner foil, capable, however, of plastic deformation during welding. Foils produced by the method of electron beam evaporation and condensation in vacuum can be regarded as such materials. As shown by previous studies, during welding they can be transformed into a structure, close in its chemical composition to the material being welded [13].

The objective of this work is investigation of the impact of vacuum diffusion welding of TiAlNb alloy with application of interlayers of Nb–Ti or Al–Ti systems, on formation of the structure and mechanical properties of the joints.

Investigation procedures, materials and sample preparation for welding. TiAlNb intermetallic alloy (Ti–28.80Al–11.27Nb–Cr3.51–3.1Zr, wt.%) was used for investigations. The alloy was developed at PWI and produced by the method of electron beam melting with application of lighter β-stabilizers, namely Cr and Zr at reduction of Nb concentration and Al content reduced to 28.80 wt.%.

The developed alloy has the following advantages.

First, Nb increases the creep resistance as a result of lowering of diffusion mobility of the elements, strengthens γ and α_2- phases, as well as improves TiAl oxidation resistance.

Secondly, Zr and Cr, similar to molybdenum, stabilize β-phase. Zr and Cr are lighter than molybdenum, so that the developed alloy has lower density that is a weighty argument for the aerospace industry. Density of the produced alloy is 4.11 g/cm^3, that is almost 1.7 times smaller than for TNM alloys (6.9 g/cm^3). In addition, Cr, particularly in microquantities, improves the corrosion resistance.

The initial ingot produced by the method of electron beam melting, had a nonuniform coarse microstruc-

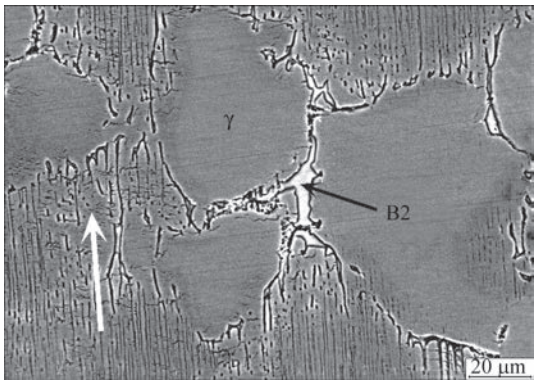

Figure 1. Microstructure of intermetallic alloy after ICZM in the initial condition (white arrow shows the direction of the alloy crystallization in melting)

ture, inhomogeneous distribution of elements through the ingot field, as well as many of pores and cracks. All these disadvantages exactly determined its low mechanical properties at room temperature. It is known that before application of the cast intermetallic material, it should be subjected to gas-static isothermal pressing, many hour heat treatment or rolling [14].

Ingot treatment was performed by the method of induction crucibleless zone melting (ICZM) [15]. Sample microstructure (Figure 1) after zone remelting consists of grains of 31.5 μm average size, elongated in one direction, which also have internal lamellar structure that consists of $\gamma+\alpha_2$ lamellar colonies, along which precipitates of light-coloured layers of β-phase and acicular precipitates of α-hase appear. In the sample center the intergranular boundaries are thin and have the thickness of 2 μm [16].

Metal cutting up into samples for welding was conducted in an EDM machine. Samples of 10×10×5 mm size were cut out for welding. Surfaces to be joined were ground on a diamond ring and degreased in alcohol.

Welding of intermetallic alloy was performed in U-394M unit. The uniformity of sample heating was ensured due to application of electron beam heater of a circular shape, which was mounted on the butt level. The welding process parameters were as follows: welding temperature T_w = 1050–1200 °C, welding pressure P_w = 10–30 MPa, welding time t = 20−30 min, vacuum in the working chamber was maintained on the level of $1.33\cdot10^{-3}$ Pa. Sample welding was performed with application of static and cyclic loading. Figure 2 gives the cyclograms of welding process.

After the rarefaction on the level of $1.33\cdot10^{-3}$ Pa has been achieved in the vacuum chamber, sample heating was performed. After reaching the required temperature and soaking at the mode for several minutes, welding pressure is applied, to equalize the temperature field (duration is determined by sample size).

The total welding time at application of static loading was equal to 20 min, and at application of cyclic loading it was 30 min. At cyclic loading three cycles of sample loading-unloading were applied.

Sample welding was conducted both without application of interlayers, and with interlayers in the form of foil. Niobium-titanium alloy or nanolayered foil of Al−Ti system were used as interlayers.

The interlayer from NbTi alloy was produced by the technology of cold-hearth electron beam melting of intermetallic alloy of TiAl system and niobium alloy 5VMTs. Niobium in the alloy promotes an increase of heat resistance, ductility and oxidation resistance. The composition of the produced NbTi alloy was as follows: Nb–43.49Ti−3.06W−2.35Al, wt.%.

As shown by investigations, metal hardness is uniform and equal to *HV*–1810–1930 MPa over the ingot cross-section. The interlayer from NbTi alloy was cut out in the EDM machine, which was followed by grinding its surfaces. The interlayer thickness was 1 mm.

Nanolayered foil based on Al–Ti system was produced by electron beam evaporation and condensation in vacuum. The deposition process consists in layer-by-layer condensation of elements on a horizon-

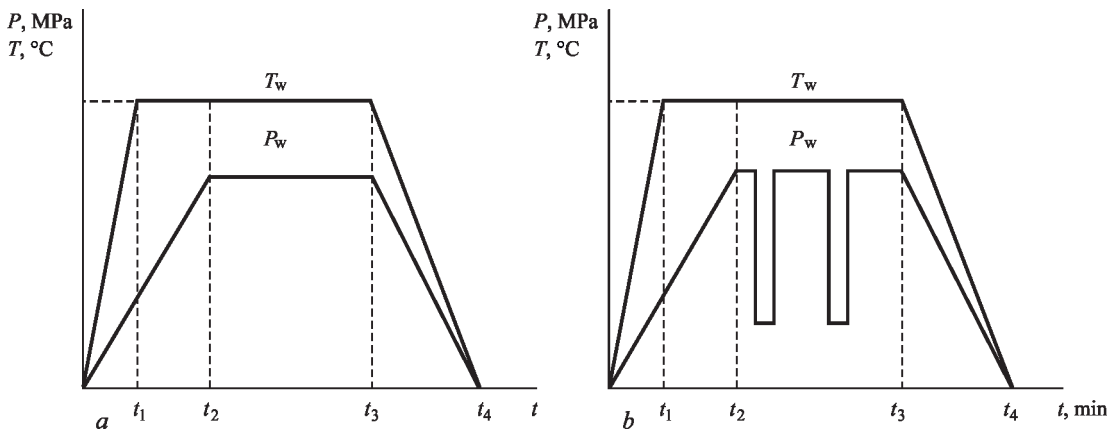

Figure 2. Cyclogram of VDW process: *a* — VDW with static loading; *b* — VDW with cyclic application of pressure; T_w — welding temperature; P_w — force of pressing the samples together; t_1 — duration of heating to T_w; t_2 — duration of soaking at T_w; t_3 — welding time; t_4 — cooling time

tal substrate, which rotates and which is fixed on the shaft of UE204 unit.

Nanolayered foil (Table 1) for application as an interlayer was selected proceeding from the composition of materials, which were welded, so that the interlayer components acted as base material alloying elements. The foil is characterized by uniform distribution of elements across the thickness.

Investigations of the structure and phase composition of the produced joints were conducted using the methods of optical microscopy in Neophot-32 microscope and scanning electron microscopy (SEM) in CAMSCAN 4 microscope, fitted with energy-dispersive analysis system Oxford Inca Energy 200. In order to determine the chemical composition of elements in the joint zone, investigations were conducted on flat samples, which were prepared by the standard procedure, using grinding-polishing equipment of Struers Company. This procedure was used to prepare transverse macrosections of both the foil and the welded joints.

In order to reveal the sample microstructure by optical metallography method, etching was performed in a reactive consisting of a mixture of hydrofluoric and nitric acid, in the following proportion: 1 part of hydrofluoric acid (HF) and 3 parts of nitric acid (HNO_3). The photos of the joint microstructure were taken by a digital camera C-3000 of OLYMPUS Company.

Sample microhardness was measured in hardness meter M-400 of LECO Company with a diamond pyramid. The load was 25 g.

Samples for mechanical testing were cut out of welded joints by EDM machine. The sample size was 4×4×8 mm. Metallographic studies of the structure and chemical composition were conducted on one of the samples obtained after welding, and the others were used for evaluation of mechanical properties of the welded joints.

Welding of intermetallic alloy TiAlNb without application of interlayers. Welding of intermetallic TiAlNb alloy was conducted at temperature T_w = = 1050 °C, pressure P_w = 10 MPa, for 20 min. As shown by metallographic investigations of the samples, the joint line is visible in the butt. A considerable number of defects are located in the form of a pore sequence along this line, that is readily revealed at chemical etching of the joint (Figure 3, *a*).

Table 1. General characteristics of Al/Ti foil

Foil	Total foil thickness, μm	Layer thickness, nm		Foil composition, at.%		Foil composition, wt.%	
		Al	Ti	Al	Ti	Al	Ti
Al/Ti	25	30	25	47.14	52.86	33.45	66.55

Increase of welding mode parameters to T_w = = 1200 °C, P_w = 30 MPa at soaking for 30 min, allows greatly reducing the number of defects in the butt joint (Figure 3, *b*). Material microhardness directly in the joint zone is equal to *HV* 4800 MPa, at 20 μm distance from the butt it is *HV* 4730, and at 50 μm distance it is *HV* 4180 MPa, respectively.

Welding of intermetallic alloy TiAlNb using an interlayer based on NbTi alloy. Application of an interlayer of a softer material than the intermetallic alloy in welding allows improving the conditions of welded joint formation (Figure 4). In welding in the following mode: T_w = 1050 °C; P_w = 15 MPa and t = = 30 min, a diffusion zone is observed in the butt joint, where the metal structure differs from that of the intermetallic TiAlNb alloy (Figure 4, *a*). This zone is separated from two sides (relative to the interlayer) from the intermetallic alloy by clearcut lines, along which clustering of defects is observed.

At increase of welding parameters up to temperature T_w = 1200 °C and pressure value P_w = 30 MPa and preservation of soaking time t = 30 min, the number of defects in the butt joint becomes much smaller (Figure 4, *b*).

Application of electron microscopy allows revealing significant diffusion of chemical elements in the butt joint (Figure 5). Figure 5, *a*, shows half of the welded joint.

As one can see from Figure 4, *b* and Figure 5, *a*, common grains form in the butt joint between the interlayer material and the intermetallic alloy during welding.

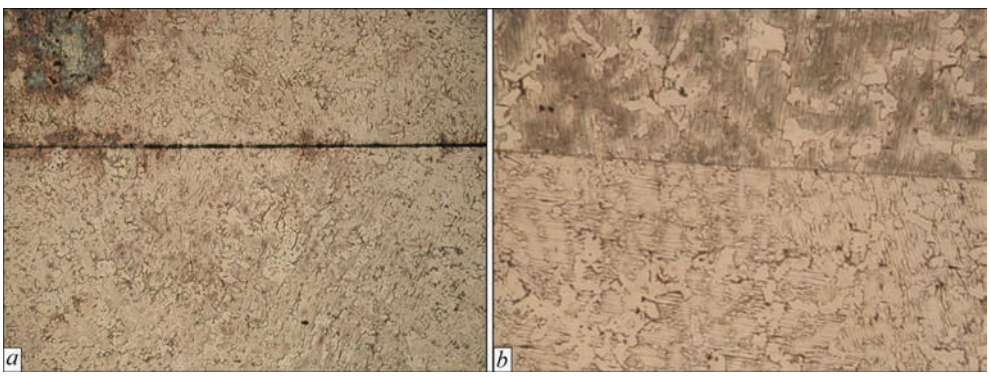

Figure 3. Microstructure (×25) of TiAlNb alloy joint zone in welding in the following mode: *a* — T_w = 1050 °C, P_w = 10 MPa, t = = 20 min; *b* — T_w = 1200 °C, P_w = 30 MPa, t = 30 min

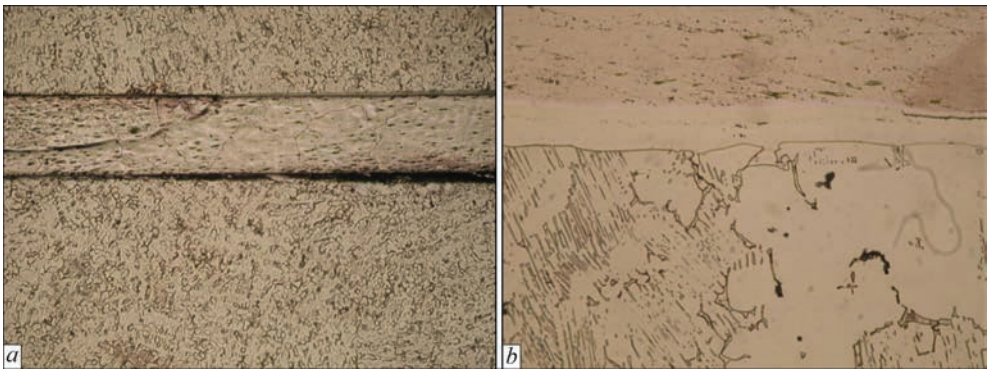

Figure 4. Microstructure of TiAlNb alloy joint zone in welding with application of an interlayer from NbTi alloy in the following mode: *a* — T_w = 1050 °C, P_w = 15 MPa, t = 30 min (×25); *b* — T_w = 1200 °C, P_w = 30 MPa, t = 30 min (×200)

A diffusion zone 25–35 μm thick is observed along the interlayer — TiAlNb alloy interface. Chemical composition of this zone corresponds to the following element content: 47.04Ti–29.31Nb–20.28Al–1.97Cr–1.4W, wt.%. In the middle part the chemical composition of the interlayer (66.34Nb–28.83Ti–3.48W–1.35Al, wt.%) is preserved due to its considerable thickness.

As shown by investigation results, an increased level of microhardness values up to *HV* 5090 MPa is observed in the near-contact zone of the interlayer — intermetallic alloy. Microhardness in the intermetallic alloy proper at 0.1 mm distance from the butt joint, is equal to *HV* 3670 MPa, at 2 mm it is *HV* 4120 MPa, and in the interlayer central part it is *HV* 2440 MPa, respectively.

Welding of intermetallic alloy TiAlNb using nanolayered interlayer of Al-Ti system. Welding of intermetallic alloy TiAlNb, using nanolayered interlayer of Al–Ti system of total thickness of 25 μm was conducted at the following parameters: temperature T_w = 1200 °C, pressure P_w = 30 MPa, soaking time t = 30 min. Analysis of joint microstructure shows that during welding a diffusion zone approximately 20–25 μm thick forms in the place of location of the nanolayered interlayer (Figure 6, *a*). Finely-dispersed precipitates are observed in the middle of the diffusion zone. The lines of interface with the intermetallic alloy pass on both sides from this zone. No cracks or pores were found in the butt joint.

Application of cyclic loading in welding (3 loading and unloading cycles) leads to a change of the nature of the structure in the joint zone. No contact line is found in welded joint microstructure, obtained by optical metallography. The line of contact of the nanolayered interlayer with the intermetallic alloy as an element of the microstructure is absent (Figure 6, *b*).

Electron microscopy allows revealing in the butt joint a diffusion zone approximately 15–20 μm thick (Figure 7, *a*), close in its composition to the intermetallic alloy.

Chemical composition of elements in the joint zone is equal to: 67.12Ti–31.31Al–1.57Cr, wt.%. That is after welding of the intermetallic alloy, using a nanolayered

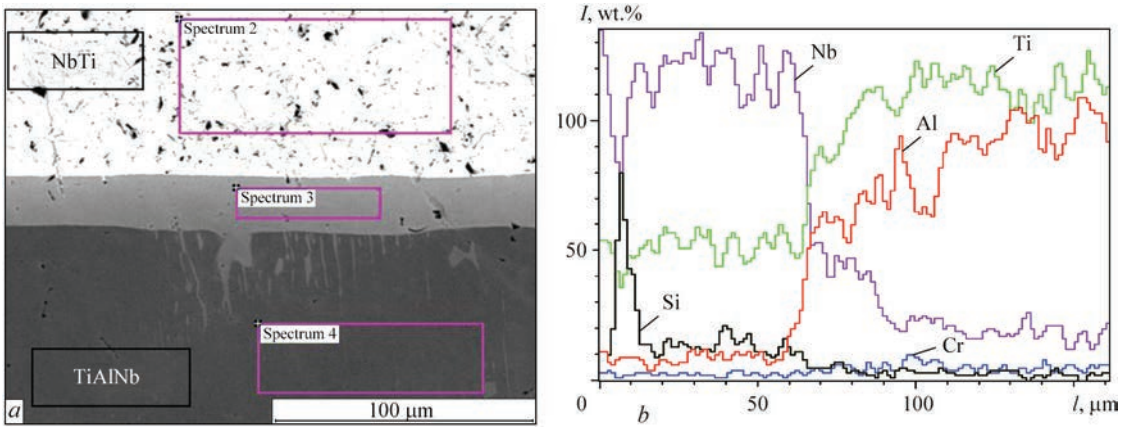

Spectrum	Chemical composition, wt.%				
	Al	Ti	Cr	Nb	W
2	1.35	38.83	–	66.34	3.48
3	20.28	47.04	1.97	29.31	1.4
4	31.38	56.56	2.56	9.49	–

Figure 5. Microstructure of the zone of TiAlNb alloy joint, produced with application of an interlayer from NbTi alloy in the following mode: T_w = 1200 °C, P_w = 30 MPa, t = 30 min (*a*); distribution of chemical elements in the butt joint (*b*); content of chemical elements in individual regions in the joint zone (*c*)

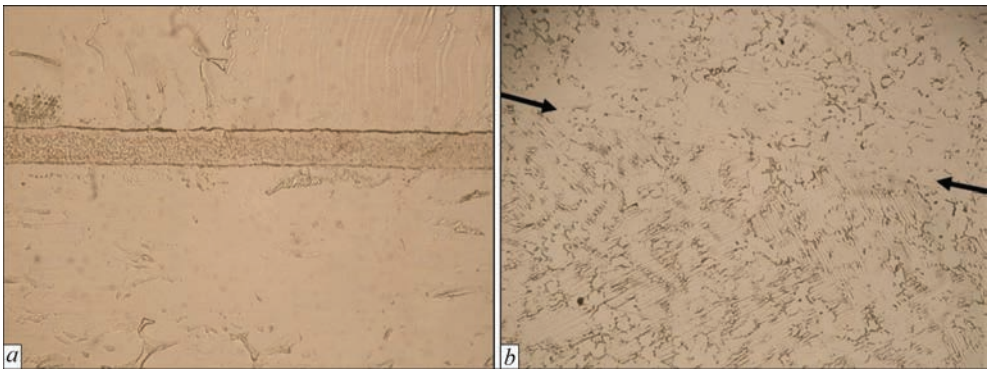

Figure 6. Microstructure of TiAlNb alloy joint zone in welding using a nanolayered interlayer of Al–Ti system in the following mode: *a* — T_w = 1200 °C, P_w = 30 MPa, (×500); *b* — T_w = 1200 °C; 3 cycles of pressure P_w = 30 MPa; t = 30 min (×50)

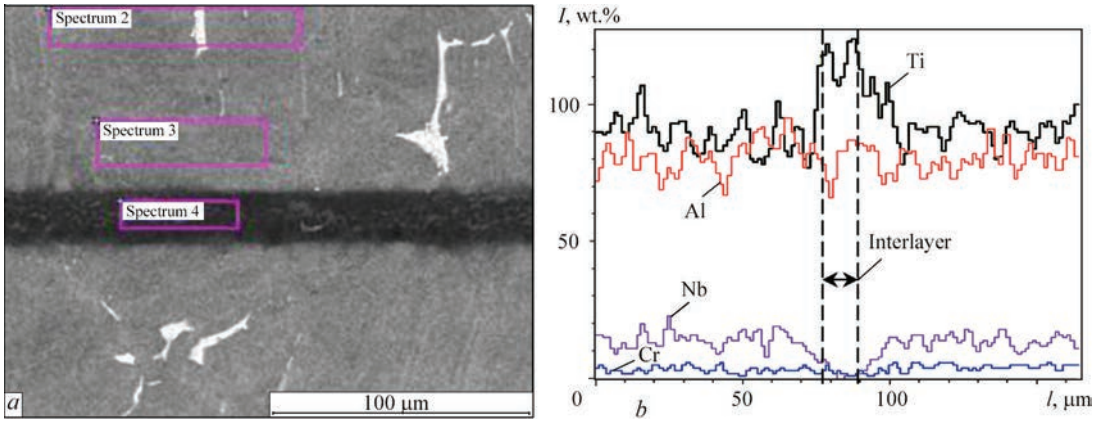

Spectrum	Chemical composition, wt.%			
	Al	Ti	Cr	Nb
2	32.83	55.84	3.28	8.05
3	35.14	55.93	2.88	6.05
4	31.31	67.12	1.57	–

Figure 7. Microstructure of zone of TiAlNi alloy joint, produced using a nanolayered interlayer of Al–Ti system in the following mode: T_w = 1200 °C, 3 cycles of pressure P_w = 30 MPa, t = 30 min (*a*); distribution of chemical elements in the butt joint (*b*) and chemical element content in individual regions of the joint zone

interlayer, a diffusion zone forms in the butt joint, in which an increased content of titanium (67.12 %), aluminium (31.31 %), and a small content of chromium on the level of 1.57 wt.% (Figure 7, *b*) are found.

As shown by investigation results, an increase of microhardness values up to *HV*–5160–5400 MPa is observed in the diffusion zone. Microhardness values in the intermetallic alloy are equal to *HV* 4370 MPa.

Investigations of mechanical properties of welded joints. Investigations of compressive strength of welded joints were conducted according to ASTM D695 standard. Mechanical properties of the alloys at room temperature were studied by uniaxial compression, using INSTRON 8802 testing machine and extensometer 2620-601. Strain rate was $2 \cdot 10^{-4} \cdot s^{-1}$. Application of the compression method is the most effective, when samples dimensions are small. A diagram in σ-ε coordinates is realized. Table 2 gives the parameters of samples and results of compressive testing of the samples.

Table 2. Parameters of samples and results of compressive testing of samples

Sample number	Joint type	Sample area F, mm	Tensile strength, σ_t	Yield limit $\sigma_{0.2}$	Relative reduction in area at maximum force $\delta^{(\sigma)}$, %	Modulus of elasticity E_t, MPa
1-1	Welding with interlayer of NbTi alloy	15.52	1021.2	637.0	10.5	71893.0
1-2		16.10	1044.4	608.0	11.8	87872.0
1-3		15.54	898.8	600.0	9.7	84306.0
2-1	Welding with nanolayered interlayer	16.28	1153.1	605.0	12.3	90327.0
2-2		16.34	1435.3	628.0	19.1	84784.0
2-3		16.92	1250.9	615.0	13.6	95480.0

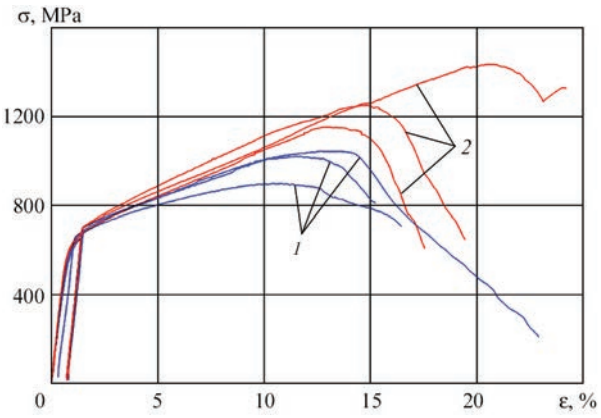

Figure 8. Diagram of testing samples from TiAlNb alloy, produced in welding with an interlayer of NbTi alloy (*1*) and in welding with nanolayered interlayer (*2*)

Proceeding from test results, a series of diagrams was derived in σ-ε coordinates, which are given in Figure 8.

Mechanical testing of the joints for compression revealed that the average strength of the joints from TiAlNb intermetallic alloy, produced using an interlayer from NbTi alloy, is equal to 988.2 MPa, and average strength of samples, produced with a nanolayered interlayer of Al−Ti system is 1279.8 MPa.

Conclusions

1. Welding of intermetallic alloy TiAlNb by vacuum diffusion process at temperature T_w = 1050 °C, pressure P_w = 10 MPa, for 20 min, does not ensure producing sound joints. After welding, a contact line is observed in the butt joint, along which a large number of defects are located in the form of linear porosity.

2. Increase of welding mode parameters up to temperature T_w = 1200 °C, pressure P_w = 30 MPa, soaking time t = 30 min, and use of a ductile interlayer from NbTi alloy 1 mm thick allows improving the conditions of welded joint formation and greatly reducing the number of defects in the butt joint. Common grains and a diffusion zone 25–35 μm thick form along the interlayer-intermetallic alloy boundary between the interlayer material and the intermetallic alloy during welding.

3. Application of nanolayered interlayers of Al–Ti system of the total thickness of 25 μm and cyclic loading in the form of 3 cycles of loading-unloading in welding the intermetallic alloy TiAlNb leads to a change of the nature of the structure in the joint zone. No joint line is visible in the microstructure of welded joints, produced by optical metallography. Application of electron microscopy allows revealing in the butt joint a diffusion zone 15 to 20 μm thick, close in its composition to that of the intermetallic alloy.

4. Investigations of compressive strength of welded joints showed that the average strength of joints from intermetallic alloy TiAlNb, produced using an interlayer from NbTi alloy, is equal to 988.2 MPa, and application of nanolayered interlayer of Al−Ti system in welding allows increasing the average strength of the samples up to 1279.8 MPa.

1. Bochvar, G.A., Salenkov, V.A. (2004) Investigation of alloys based on titanium aluminide with orthorhombic structure. *Tekhnologiya Lyogkikh Splavov*, **4**, 44–46 [in Russian].
2. Clemens, H., Mayer, S. (2013) Design, processing, microstructure, properties, and applications of advanced intermetallic TiAl alloys. *Advanced Engineering Materials*, **4**. 191–215.
3. Huber, D., Werner, R., Clemens, H., Stockinger, M. (2015) Influence of process parameter variation during thermo-mechanical processing of an intermetallic β-stabilized γ-TiAl based alloy. *Materials Characterization*, **109**, 116–121.
4. Godor, F., Werner, R., Lindemann, J., Clemens, H. (2015) Characterization of the high temperature deformation behavior of two intermetallic TiAl–Mo. *Materials Sci. and Eng., A*, **648**, 208–216.
5. Appel, F. Paul, J.D.H., Oering, M. (2011) *Gamma titanium aluminide alloys: Science and technology*. Weinheim, WILEY-VCH.
6. Huang, Z.W., Cong, T. (2010) Microstructural instability and embrittlement behaviour of an Al-lean, high-Nb γ-TiAl-based alloy subjected to a long-term thermal exposure in air. *Intermetallics*, **18**, 161–172.
7. Schwaighofer, E., Clemens, H., Mayer, S. et al. (2014) Microstructural design and mechanical properties of a cast and heattreated intermetallic multi-phase γ-TiAl based alloy. *Ibid*., **44**, 128–140.
8. Cam, G., Ipekoglu, G., Bohm, K.-H., Kocak, M. (2006) Investigation into the microstructure and mechanical properties of diffusion bonded TiAl alloys. *J. of Materials Sci*., **16**, 5273–5282.
9. *Lei* Zhu, Xiang-Yi Xue, Bin Tang et al. (2016) The influence of surface roughness on diffusion bonding of high Nb containing TiAl alloy. In: *Proc. of the 2nd Annual Int. Conf. on Advanced Material Engineering (AME 2016)*, 635–643.
10. *Kun* Zhao, Yong Liu, Lan Huang et al. (2016) Diffusion bonding of Ti–45Al–7Nb–0.3W alloy by spark plasma sintering. *J. of Materials Processing Technology*, **230**, 272–279.
11. *Bin* Tang, Xian Sheng Qi, Hong Chao Kou et al. (2016) Recrystallization behavior at diffusion bonding interface of high Nb containing TiAl alloy. *Advanced Engineering Materials*, **4**, 657–664.
12. Cao, J., Feng, J.C., Li, Z.R. (2007) Effect of reaction heat on reactive joining of TiAl intermetallics using Ti–Al–C interlayers. *Scripta Materialia*, **5**, 421–424.
13. Ustinov, A.I., Falchenko, Yu.V., Ishchenko A.Ya. et al. (2008) Diffusion welding of γ-TiAl based alloys through nano-layered foil of Ti/Al system. *Intermetallics*, **8**, 1043–1045.
14. Pflumma, R., Donchev, A., Mayer, S. et al. (2014) High-temperature oxidation behavior of multi-phase Mo-containing γ-TiAl-based alloys. *Ibid*., **53**, 45–55.
15. Kartavykh, A.V., Asnis, E.A., Piskun, N.V. et al. (2015) Microstructure and mechanical properties control of c-TiAl(Nb, Cr, Zr) intermetallic alloy by induction float zone processing. *J. of Alloy and Compounds*, **643**, 182–166.
16. Kartavykh, A.V., Asnis, E.A., Piskun, N.V. et al. (2017) Room-temperature tensile properties of float-zone processed β-stabilized γ-TiAl(Nb,Cr,Zr) intermetallic. *J. Materials Letters*, **188**, 88–91.

Received 20.12.2019

https://doi.org/10.37434/tpwj2020.02.02

IMPACT OF TIG WELDING ON THE STRUCTURE AND MECHANICAL PROPERTIES OF JOINTS OF PSEUDO-β-TITANIUM ALLOY

S.V. Akhonin, V.Yu. Bilous, R.V. Selin and **I.K. Petrychenko**
E.O. Paton Electric Welding Institute of the NAS of Ukraine
11 Kazymyr Malevych Str., 03150, Kyiv, Ukraine. E-mail: office@paton.kiev.ua

Structural pseudo-β-titanium alloys attract a lot of interest in fabrication of complex constructions for critical purposes. This alloy class includes alloys with the structure represented by one β-phase after hardening or normalizing from the β-region. The alloy weldability is an important factor at application of pseudo-β-titanium alloys in aircraft and rocket engineering. By their mechanical characteristics, the welded joints of modern pseudo-β titanium alloys should match the level of base metal mechanical properties. In this work, the impact of argon arc welding, as well as further heat treatment on the phase composition, structure and mechanical properties of welded joints of pseudo-β-titanium alloy was studied. It was established that as a result of the impact of thermal cycle of welding predominantly β-phase in the quantity of 77 % is recorded in the weld metal of joints of pseudo-β alloy VT19. Application of VT1-00sv filler wire enhances the quantity of dispersed α-phase particles and reduces the quantity of β-phase in the weld metal to 60 %, respectively. Annealing results in formation of a uniform, homogeneous finely-dispersed two-phase (α+β)-structure with tensile strength values of welded joints on the level of σ_t = 1010 MPa, that exceed the respective base metal values by 12 %. 16 Ref., 5 Tables, 8 Figures.

Keywords: pseudo-β titanium alloys, TIG welding, mechanical properties

Structural pseudo-β titanium alloys attract a lot of interest in manufacture of complex constructions for critical purposes. This class covers alloys with the structure, presented by one β-phase after hardening or normalizing from β-area. As-annealed structure of these alloys is presented by α-phase and a large amount of β-phase. The coefficient of β-stabilization of such alloys K_β = 1.4–2.4. They undergo β-phase transformation by β→(β+α) scheme. In the stable state they have (β+α)-structure [1−4].

An important factor at application of pseudo-β titanium alloys in aviation and rocket engineering is their weldability. By their mechanical characteristics, welded joints of modern pseudo-β titanium alloys should correspond to the level of those of base metal [5, 6].

Tungsten electrode argon-arc welding (TIG welding) became the most widely accepted for titanium alloy welding. Welding can be performed with and without filler metal application. Welding wires or rods from titanium alloys are used as filler metal [7, 8]. In order to increase the efficiency of arc heat utilization and arc penetrability in TIG welding of titanium, a number of variants of this process have been developed, such as submerged-arc welding, through-penetration welding, and semisubmerged-arc welding. The latter allows producing tight welds without pores [9]. Application of fluxes leads to reduction of weld pool dimensions, shortening of the time of metal being in the molten state and provides cracking resistance of welded joints, close to base metal values [10, 11].

The objective of this work is investigation of the impact of TIG welding with and without filler wire application, TIG welding over a layer of flux, as well as further heat treatment on phase composition, structure and mechanical properties of welded joints of pseudo-β titanium alloy.

Material and equipment. Pseudo-β titanium alloy, studied in the work, was developed by complex alloying theory, and contains, wt.%: Ti as base; 2.5–3.5 Al; 5–6 Mo; 3−4 Y; 4−5 Cr; 0.5–1.5 Zr; not more than 0.15 Si, 0.10 C, 0.15 O_2, 0.05 N_2, 0.015 H_2 [12]. The alloy contains β-stabilizers with coefficient of distribution greater and smaller than a unity, as well as with coefficient of distribution that is equal to a unity. Content of β-stabilizing elements is equivalent to 13.7–17.0 % Mo at average content equivalent to 15.3 % Mo. The ratio of isomorphous (equivalent to 7.8 % Mo) and eutectic-forming β-stabilizers (equivalent to 7.5 % Mo), expressed in molybdenum equivalent values, is equal to 1:1. The alloy is produced by cold-hearth electron beam remelting.

The impact of argon-arc welding on the properties and structure of joints of pseudo-β titanium alloy was

S.V. Akhonin — https: //orcid.org/0000-0002-7746-2946, V.Yu. Bilous — https: //orcid.org/0000-0002-0082-8030,
R.V. Selin — https: //orcid.org/0000-0002-2990-1131, I.K. Petrychenko — https: //orcid.org/0000-0002-0476-3983

Table 1. Modes of TIG welding of pseudo-β titanium alloy VT19

Mode number	Welding current I_w, A	Arc voltage U_a, V	Welding speed v_w, m/h	Arc length L_a, mm	Wire feed rate $v_{w.f}$, m/h	Quantity of filler wire in weld metal, %
1	310	12	10	1	–	0
2	380	12	8	1	30	10–12
3	420	12	8	1	60	22–24
4	240	11	10	2	–	0

studied. In particular, through-penetration TIG welding without filler wire, with filler wire and over a layer of flux was performed. Also studied was further heat treatment of the produced welded joints: annealing at the temperature of 760 °C for 1 hour and cooling in the furnace.

Unalloyed titanium welding wire VT1-00sv of 2 mm diameter was used as filler metal. This allowed variation of weld metal alloying in a narrow range. The quantity of filler metal was determined by examination of the macrostructure of transverse macrosections of the welds.

ANT-25 flux developed at PWI was used. It is designed for single-pass welding of 3–6 mm thick metal [13].

Samples of 200×100×6 mm size were welded. The mode of TIG welding of pseudo-β titanium alloy VT19 is given in Table 1. An example of transverse macrosection of the welded joint is shown in Figure 1.

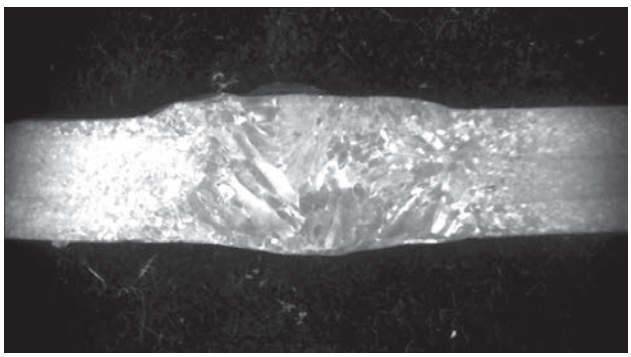

Figure 1. Transverse macrosection of the welded joint of pseudo-β titanium alloy VT19 produced by TIG welding with filler wire application

Calculation of the quantity of filler metal in the weld metal was performed by the results of studying the obtained transverse macrosections. It is found that in welding in mode 2 the quantity of wire in the weld metal is 10–12 %. In welding in mode 3 the quantity of filler metal VT1-00 in the weld metal is equal to 22–24 %, respectively [14]. The structures in the middle of a 6 mm thick sample are given. The quantity of β-phase in the weld metal, HAZ and base metal was determined on microsections and is based on the fact that different phases are etched and coloured differently. So, β-phase is of a light colour on microsections, α- and α′-phases are dark-coloured. Etching results allow revealing the shape and dimensions of individual grains, and quantity of β-phase, depending on the location of the region and thermal conditions of their formation.

Results. *Through-penetration argon-arc welding without filler wire.* Weld metal of the joints produced by TIG welding without filler wire in mode 1 (see Table 1), consists of β-phase grains, equiaxed and elongated in the direction of heat removal. Their hairlike borders are manifested against the background of the dendritic structure (Figure 2, *a*). Quantity of β-phase in this area is equal to 77 %. Fusion zone (Figure 2, *b*) is located at 5.4 mm distance from weld axis, on the right are weld grains against the background of the dendritic structure, on the left are equiaxed β-grains of HAZ area in the fusion zone. The quantity of β-phase in this area is equal to 81 %. Directly in the fusion zone one can see partially melted grains that belong simultaneously both to HAZ and to weld metal.

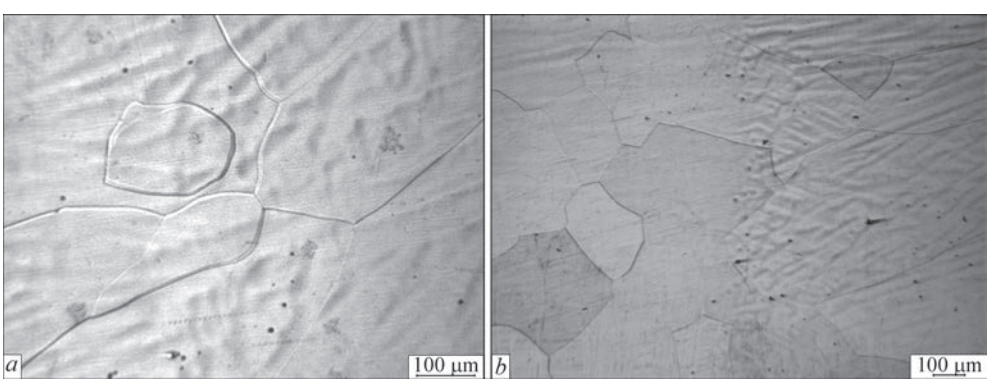

Figure 2. Microstructure of weld metal of the joint of pseudo-β titanium alloy VT19 produced by TIG welding without filler wire application in mode 1: *a* — weld center; *b* — fusion zone

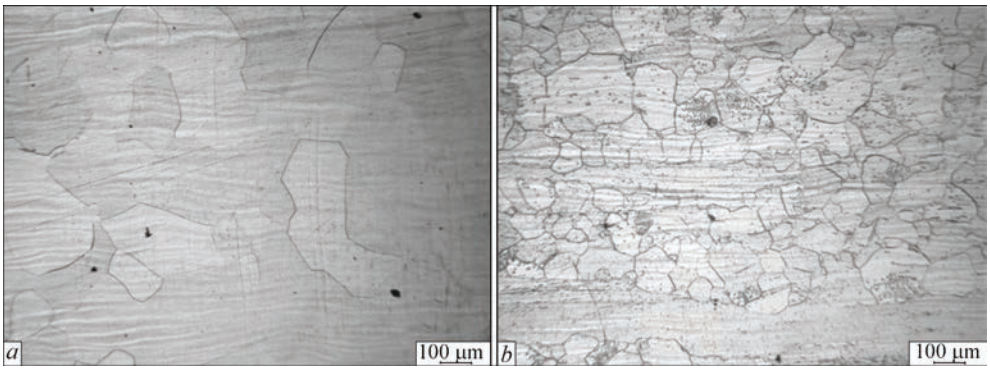

Figure 3. Microstructure of metal of the HAZ of welded joint of pseudo-β titanium alloy VT19, produced by TIG welding without filler wire application in mode 1: *a* — area of complete polymorphous transformation; *b* — zone of incomplete polymorphous transformation

HAZ area, where complete polymorphous transformation has occurred, consists of equiaxed β-grains (Figure 3, *a*), and its width is 4.75 mm. Quantity of β-phase is on the level of 80 %. HAZ area, where incomplete polymorphous transformation is observed, has a width of 2.5 mm (Figure 3, *b*), β-grains contain just the particles of other phases, which occur in the base metal, in particular β-phase. Quantity of β-phase is 75 %.

On the boundary of transition from the area of incomplete polymorphous transformation to base metal the quantity of β-phase is equal to 57 %. In the base metal the quantity of β-phase is 31 %.

Thus, microstructural investigations showed that predominantly β-phase in the quantity of 77 % is found in the metal of welded joint, produced without the filler wire, and in different HAZ areas it varies from 75 % to 80 %. In order to ensure decomposition of the formed metastable phases and provide equal strength, the welded joints produced without filler wire, should be further subjected to heat treatment — annealing.

Through penetration argon-arc welding with application of filler wire VT1-00sv. Microstructure of weld metal in welded joint of pseudo-β titanium alloy VT19, produced by TIG welding in mode 2 (see Table 1), is presented in Figure 4, *a*. Weld metal has a dendritic structure, against the background of which β-phase grains formed, which are elongated in the direction of heat removal. Dispersed particles of α-phase of approximately 1 μm size and smaller, are observed in β-grains. These particles are nonuniformly distributed in the grain volume. Quantity of β-phase in the weld metal is equal to 69.1 %.

Microstructure of weld metal in welded joint of pseudo-β titanium alloy VT19, made in mode 3 (see Table 1), is shown in as-welded condition in Figure 4, *b*. Weld metal consists predominantly of β-phase, the boundaries of which are manifested against the background of the dendritic structure. In weld metal structure dispersed precipitates of α-phase of approximately 1 μm size are also observed. The highest density of such precipitates is found in the weld upper part near the alloy zone. Here, the size of some particles is equal to 2–3 μm. The quantity of β-phase in the weld metal is equal to 60.3 %.

Microstructure of HAZ metal of welded joints of VT19 alloy, produced using filler wire VT1-00 in modes 2 and 3 is similar to that of this zone in joints made without application of filler wire VT1-00 in mode 1.

Thus, in welded joints produced with filler wire application, the quantity of dispersed particles of α-phase becomes greater and their size increases up to 2–3 μm in welds with 20 % of VT1-00sv wire. Temperature mode during welding and cooling promoted increase of the density and size of dispersed phase particles. Quantity of β-phase in the weld metal decreased to 60 % due to disalloying of weld metal and HAZ [15].

Argon-arc welding over a layer of flux. Microstructure of metal of the weld and near-weld zone of

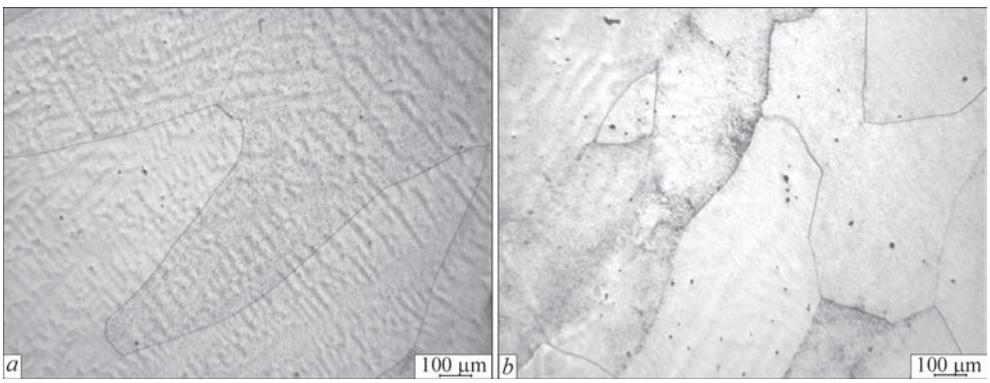

Figure 4. Microstructure of weld metal in welded joint of pseudo-β titanium alloy VT19, produced by TIG welding with filler wire VT1-00: *a* — in mode 2; *b* — in mode 3

Table 2. Quantity of β-phase in base metal and weld metal of TIG-welded joints of titanium alloy VT19

Sample number	Sample type, welding speed, filler material	Quantity of β-phase, %
Base metal		55.7
1	Welded joint, 10 m/h, without filler	77.1
2	Welded joint, 8 m/h, quantity of filler is 10 %	69.1
3	Welded joints, 8 m/h, quantity of filler is 22 %	60.3
4	Welded joint over a layer of flux, 10 m/h, without filler	97.2

welded joint produced at welding speed of 10 m/h (mode 4, Table 1) is given in Figure 5. Weld metal consists of equiaxed and nonequiaxed grains of β-phase with thin boundaries against the background of the dendritic structure; metal of the near-weld zone consists of equiaxed grains of β-phase.

Metal of the weld and near-weld zone of the HAZ of samples 1, 2, 3 and 4, while differing by the parameters and configuration of the zones, and direction of crystallite growth, has an identical microstructure, which consists of β-phase grains. Quantity of β-phase in the weld metal is equal to 60–70 % for samples 2 and 3, 77 % for sample 1, and 97 % for sample 4 (Table 2).

Analysis of mechanical properties of welded joints (Table 3) shows that the lowest strength and impact toughness is demonstrated by welded joints, made by TIG welding without filler wire over a layer of flux, in modes 1 and 4, where σ_t = 860 MPa, and σ_t = = 857 MPa, respectively. Thus, application of fluxes in TIG welding does not have any particular impact on the strength and impact toughness of welded joints, and promotes an increase of β-phase content in the weld metal due to reduction of energy input and increase of weld metal cooling rate.

Joints produced with application of filler wire VT1-00sv in modes ensuring VT1-00 metal quantity on the level of 22–24 % in the weld metal (mode 3, Table 1), have the highest strength.

Joints produced with application of filler wire VT1-00sv, in which the content of VT1-00 metal in the weld is on the level of 10–12 %, have intermediate strength values. This is attributable to a large content of β-phase in the weld metal of joints made without filler wire application. Metastable β-phase has a low strength that is why welded joints have low strength values.

Impact toughness *KCV* of samples with a sharp notch of weld metal in welded joints produced with application of filler wire VT1-00sv with feed rate in the mode, ensuring the content of VT1-00 metal in the weld on the level of 22–24 %, is also maximum and is equal to 32 J/cm^2.

Thus, the properties of welded joints of pseudo-β alloy VT19, produced by tungsten electrode argon-arc welding, both without filler wire and with application of filler wire VT1-00sv were studied, and it was established that the joints made with application of filler wire VT1-00sv in the quantity of 22 % have the strength equal to that of base metal, and the quantity of β-phase in the weld metal decreases from 77 % to 60 %. To ensure the uniform structure, decomposition of metastable phases and produce equal strength

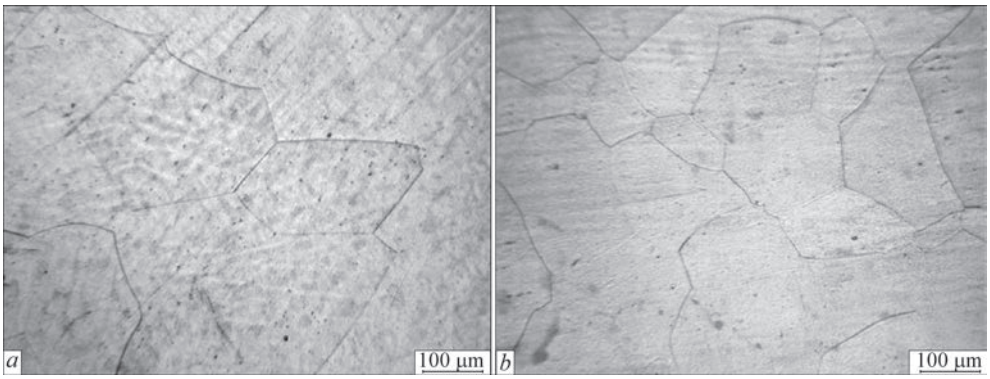

Figure 5. Microstructure of the metal of weld (*a*) and near-weld zone (*b*) of welded joint of pseudo-β titanium alloy VT19, produced by TIG welding (mode 4) with tungsten electrode over a layer of flux

Table 3. Mechanical properties of welded joints of pseudo-β titanium alloy VT19

Mode number	Sample type	Tensile strength σ_t, MPa	Yield limit σ_y, MPa	Relative elongation δ, %	Reduction in area ψ, %	Impact toughness *KCV*, J/cm^2	
						weld	HAZ
BM		887	958	12	42	22	
1	As-welded	860	839	13.3	60	19	22
2		895	868	7.3	23.4	28	26
3		963	942	6	24.5	32	24
4		857	815	13.3	55	14	26

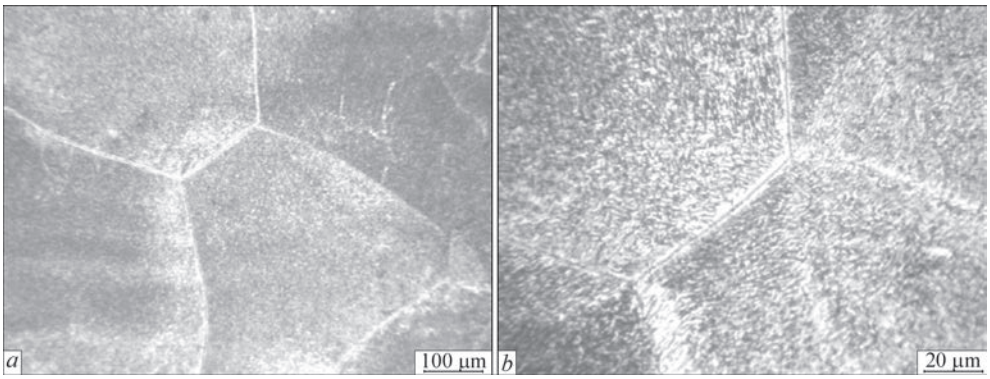

Figure 6. Microstructure of HAZ metal (*a*) of welded joint of pseudo-β titanium alloy VT19, produced by tungsten electrode argon-arc welding with through penetration after annealing at 760 °C; *b* — intragranular structure

joints, made without application of commercial titanium VT1-00 as filler material, and because of weld metal disalloying, the joints should be subjected to further heat treatment [16].

Selected as heat treatment was annealing which envisages heating up to the temperature of 750–760 °C, soaking and further cooling in the furnace.

Microstructure of HAZ metal of welded joint, made in mode 1 (without application of flux or filler wire) is shown in Figure 6.

HAZ metal consists of equiaxed polyhedral grains with homogeneous two-phase (α+β)-structure inside the grain. The intragranular structure of the HAZ metal consists of lamellar α-phase 2–5 μm long and up to 1 μm thick. Located between the plates are dispersed particles of α- and β-phase, the size of which is below 1 μm. In some grains, dispersed globular particles of up to 1μm size precipitate in β-matrix. Microstructure of weld metal of this welded joint is shown in Figure 7. Weld metal of the joint consists predominantly of nonequiaxed, elongated in the direction of heat removal primary β-grains (Figure 7, *a*) with highly refined intragranular structure that formed after decomposition of metastable phases (mainly β-phase), as a result of annealing of this welded joint at the temperature of 760 °C for 1 h (Figure 7, *b*).

After stabilization of weld metal structure finely-dispersed two-phase (α+β)-structure formed, which was uniform and homogeneous for the entire weld. The α-phase plates have the length of 2–4 μm, and thickness close to 0.5 μm, dispersed globular particles are of 0.5–1.0 μm size and smaller. A continuous or intermittent α-fringe 1.0–1.5 μm wide was observed along the grain boundaries. Finely-dispersed structure of the weld metal can provide its high strength.

For comparison, Figure 8 shows the microstructure of weld metal in welded joint of pseudo-β titanium alloy VT19, produced by through penetration argon-arc welding with filler wire VT1-00sv in modes that ensure VT1-00 metal content on the level of 22–24 % in the weld. The weld metal consists of elongated in the direction of heat removal primary β-grains (Figure 8, *a*) with two-phase intragranular structure, which consists of dispersed α- and β-phases (Figure 8, *b*). Thickness of α-phase particles is less than 1 μm at the length of 0.7–5.0 μm. An α-fringe up to 2 μm width is present on the boundaries of β-grains.

Application of filler wire at argon-arc welding of VT19 alloy allows reducing the content of β-phase in the weld metal and in as-annealed condition. So, after annealing the metal of welds, made with application of VT1-00 in the quantity of 22 %, contains β-phase on the level of 30 % (Table 4). In welds without filler wire application, the quantity of β-phase after annealing is fixed on the level of 43 %.

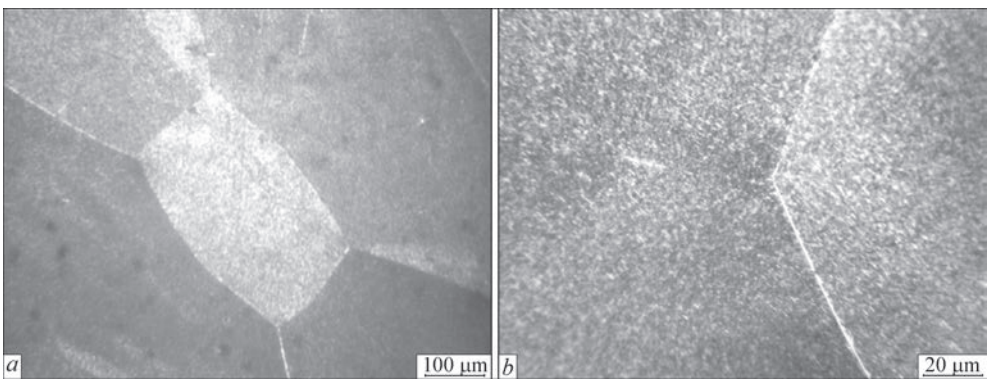

Figure 7. Microstructure of the metal of weld (*a*) of the joint of pseudo-β titanium alloy VT19, produced by tungsten electrode argon-arc welding with through penetration after annealing at 760 °C; *b* — intragranular structure

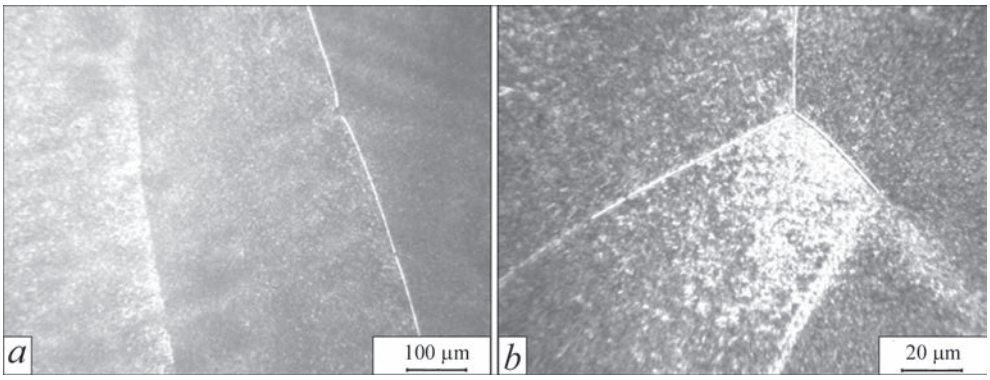

Figure 8. Microstructure of the metal of weld (*a*) of welded joint of pseudo-β titanium alloy VT19, produced by tungsten electrode argon-arc welding with through penetration with application of filler wire VT1-00 (22–24 % content in the weld) after annealing at 760 °C; *b* — intragranular structure

Table 4. Quantity of β-phase in the base metal and metal of welded joints of VT19 alloy

Sample type	Sample condition	Quantity of β-phase, %
Base metal	After annealing at 760 °C, 1 h, cooling with the furnace	22.98
Weld metal without filler, after annealing	After annealing at 760 °C, 1 h, cooling with furnace	43.72
Weld metal with VT1-00sv filler, 22–24 % content in the weld		29.87

Table 5. Mechanical properties of welded joints of pseudo-β titanium alloy VT19, produced by argon-arc welding (AAW) after annealing at 760 °C, 1 h, cooling with furnace

Sample type	Tensile strength σ_t, MPa	Yield limit σ_y, MPa	Relative elongation δ, %	Reduction in area ψ, %	Impact toughness *KCV*, J/cm^2
AAW without filler	981	946	9.7	15.3	29.4
AAW with filler wire VT1-00sv, in the quantity of 22–24 %	1011	989	9.1	15.1	25.9

Thus after annealing, the weld metal demonstrated a uniform, homogeneous for the entire weld finely-dispersed two-phase (α+β)-structure with plates of β-phase 2–4 μm long and 0.5 μm thick, and a 1.0–1.5 μm wide α-fringe formed along the grain boundaries. Finely-dispersed structure of the weld metal ensures its high strength. In the metal of the weld produced with application of filler wire VT1-00sv in the quantity of 20 %, the size of α-phase particles is larger: thickness of α-phase particles is close to 1 μm at the length of 0.7–5.0 μm. In the HAZ metal the thickness of α-phase increased to 1.5–2.0 μm as a result of annealing.

Studying the mechanical properties of welded joints of pseudo-β titanium alloy VT19, produced by tungsten electrode argon-arc welding, both without filler wire, and with application of filler VT1-00sv showed that both in as-welded condition and in the condition after annealing at 760 °C the joints produced without filler wire (Table 5) have the lowest strength values (Table 5).

However, the degree of strengthening as a result of annealing is different in different joints. So, joints produced by argon-arc welding with through penetration became stronger by 120 MPa after annealing, and joints made with filler wire application, became stronger by 48 MPa. During further investigations, it will be rational to study the impact of strengthening heat treatment on the structure and properties of welded joints of pseudo-β titanium alloy VT19.

Conclusions

1. As a result of the impact of welding thermal cycle, predominantly β-phase is found in the weld metal of joints of pseudo-β alloy VT19 produced by TIG welding without filler wire application; dispersed particles of α-phase of approximately 1 μm size, are observed in β-grains, and the quantity of β-phase in welded joint metal is maximum and equal to 77 %.

2. In welds of pseudo-β alloy VT19, made by TIG welding with application of filler wire VT1-00sv in the quantity of 10 and 20 %, the number of dispersed particles of α-phase becomes greater and their size increases up to 2–3 μm in welds with 20 % of VT1-00sv wire, and the quantity of β-phase in the weld metal decreases to 60 %.

3. Joints of VT19 alloy, made by TIG welding with application of filler wire VT1-00sv in the quantity

of 22 %, have tensile strength values on the level of σ_t = 965 MPa and equal strength to that of the base metal. Joints of VT19 alloy, produced by argon-arc welding without filler material application, have tensile strength values on the level of σ_t = 860 MPa. In order to ensure decomposition of metastable phases and equal strength of these joints, they should be subjected to further heat treatment by annealing.

4. As a result of the impact of annealing at the temperature of 760 °C, the metal of TIG-welded joints of VT19 alloy forms a uniform, homogeneous, finely-dispersed two-phase (α+β)-structure with α-phase plates, 2–4 μm long and 0.5 μm thick, and with tensile strength values on the level of σ_t = 980 MPa. Joints of VT19 alloy made by argon-arc welding with application of filler wire VT1-00sv in the modes, which provide filler metal content of 22–24 % in the weld after annealing at 760 °C have tensile strength values on the level of σ_t = 1010 MPa.

1. Iliin, A.A., Kolachev, B.A., Polkin, I.S. (2009) *Titanium alloys. Composition, structure, properties*: Refer. Book. Moscow, VILS-MATI [in Russian].
2. Khorev, A.I. (2012) Development of titanium β-alloy VT19 on the base of complex alloying. *Vestnik Mashinostroeniya*, **7**, 69–71 [in Russian].
3. Khorev, A.I. (2012) Titanium superalloy VT 19. *Tekhnologiya Mashinostroeniya*, **6**, 2–5 [in Russian].
4. Moiseev, V.N. (1998) β-titanium alloys and prospects of their development. *Metal Science and Heat Treatment*, **12**, 11–14 [in Russian].
5. Khorev, A.I. (2002) Titanium is a high-speed aviation and cosmonautics. *Tekhnologiya Lyogkikh Splavov*, **4**, 92–97 [in Russian].
6. Cui, C., Hu, B., Zhao, L., Liu, S. (2011) Titanium alloy production technology, market prospects and industry development. *Materials & Design*, 32(**3**), 1684–1691.
7. Blashchuk, V.E., Shelenkov, G.M. (2005) Fusion welding of titanium and its alloys (Review). *The Paton Welding J.*, **2**, 35–42.
8. Patel, N.S., Patel R.B. (2014) A review on parametric optimization of TIG welding. *Int. J. of Computational Engineering Research*, 4(**1**), 27–31.
9. Huang, J.L., Warnken, N., Gebelin, J.C. (2012) On the mechanism of porosity formation during welding of titanium alloys. *Acta Materialia*, 60(**6–7**), 3215–3225.
10. Zamkov, V.N., Prilutsky, V.P. (2004) Theory and practice of TIG-F (A-TIG) welding (Review). *The Paton Welding J.*, **9**, 11–14.
11. Dey, H.C., Albert, S.K., Bhaduri, A.K., Mudali, U.K. (2013) Activated flux TIG welding of titanium. *Welding in the World*, 57(**6**), 903–912.
12. Kostin, K.V. et al. (2016) Influence of complex alloying on improvement of mechanical properties and strength of titanium alloys. *Omsky Nauchny Vestnik*, 148(**4**), 45–47.
13. Gurevich, S.M., Zamkov, V.N., Prilutsky, V.P. et al. *Welding flux*. USSR author's cert. 439363 [in Russian].
14. Akhonin, S.V., Belous, V.Yu., Petrichenko, I.K., Selin, R.V. (2016) Influence of filler metal on structure and properties of welded joints of high-strength two-phase titanium alloys produced using argon arc welding. *The Paton Welding J.*, **1**, 39–43.
15. Akhonin, S.V., Belous, V.Y., Berezos, V.A., Selin, R. V. (2018) Effect of TIG welding on the structure and mechanical properties of the pseudo-β-titanium alloy VT19 welded joints. *Mat. Sci. Forum*, **927**, 112–118.
16. Hryhorenko, S.G., Achonin, S.W., Belous, W.J., Selin, R.W. (2016) Heat treatment effect on the structure and properties of electron beam welded joints made of high-alloy titanium. *Biuletyn Instytutu Spawalnictwa*, 60(**5**), 90–95.

Received 07.11.2020

https://doi.org/10.37434/tpwj2020.02.03

CALCULATED EVAUATION OF APPLICATION OF NANOSIZED PARTICLES IN MODIFYING THE CAST STRUCTURE OF WELD METAL

V.M. Korzhik[1], **V.O. Shcheretskii**[1], **A.A. Chaika**[1] and **Yi Jianglong**[2]
[1]E.O. Paton Electric Welding Institute of the NAS of Ukraine
11 Kazymyr Malevych Str., 03150, Kyiv, Ukraine. E-mail: office@paton.kiev.ua
[2]Guangdong Institute of Welding (China-Ukraine E.O. Paton Institute of Welding)
363 Chiansin Str., 510650, Guangzhou, Tianhe. E-mail: wuby@gwi.gd.cn

The work deals with the features of application of promising nanosized particles of TiC, WC, TiB_2 for modifying the weld microstructure in aluminium alloy welding. Evaluation of their applicability was performed from the viewpoint of thermodynamic stability in the melts of commercial weldable alloys, which contain: Cu, Fe, Zn, Mn, and Ti. It is shown that despite their relative instability, nanosized TiC particles can be used with success as modifiers of aluminium alloys of Al−Mg system. Here, presence of silicon lowers titanium carbide resistance in aluminium melt and, therefore, is undesirable, whereas titanium, contrarily, improves the stability of TiC particles. WC particles can be used with success for modifying the structure of alloys of Al–Si system, presence of silicon increasing their stability in the melt. Particles of titanium diboride TiB_2 are the most stable compound of the studied ones. Its small modifying effect on aluminium alloys is compensated by its stability in aluminium melts at overheating. 16 Ref., 1 Table, 5 Figures.

Keywords: automatic welding of aluminium, nanosized particles, modifying, thermodynamics, filler materials

Tendencies in development of modern mechanical, automotive engineering and shipbuilding point to a steady growth of the demand for light-alloy structural elements, in order to reduce the weight of components and mechanisms, as well as fuel consumption, that is particularly important in the period of transport transition from hydrocarbon to electric engines. In a modern car with internal combustion engine the weight of aluminium alloy elements relative to overall car weight increases every year. In batch-produced cars with an electric motor this value already is on the level of 50–85 %. Here, welding remains to be the main method of joining aluminium alloy parts in automotive and aviation engineering. A high demand for aluminium structures motivated materials scientists to create new light-alloy materials based on aluminium, as well as composite materials. Appearance of new aluminium alloys and materials on their base, sharply raises the question of ensuring their reliable joining in the structure. Here, the classical weldable filler alloys based on Al−Mg and Al−Si alloying systems, do not provide the required level of mechanical properties of the weld metal relative to modern alloy characteristics, to say nothing of the composite materials. Alongside application of advanced high-strength aluminium alloys, the number of composite materials consisting of aluminium alloy matrix and filler, namely particles, fibres, whiskers, etc, is growing. Such an approach allows an essential increase of service properties of the welded joint, compared to monometallic weld. Welding of the new high-strength aluminium alloys, as well as aluminium matrix composites on their base, today has some difficulties, which require a solution. The main problem of welding new multicomponent aluminium alloys is an insufficient level of the properties of the weld, formed using commercial welding wires, as well as alloying element loss during welding, both from the part body and from the filler material. On the other hand, the welded joint of composite materials, using standard aluminium welding wires a priori has the mechanical property level, lower than that of the composite materials, manufactured on the base of aluminium alloys, strengthened by a composite component.

The structure of metal of the weld of aluminium and its alloys depends on many parameters, and if we ignore the structural features of welding equipment, the other can be conditionally divided into two groups: first group of parameters is determined by physico-chemical properties and phenomena, associated with base and filler materials; the other group includes the temperature-time mode of the welding process, impact of fluxing and modifying additives, rate of pool cooling and other parameters, which di-

V.M. Korzhik — https://orcid.org/0000-0001-9106-8593, V.O. Shcheretskii — https://orcid.org/0000-0002-8561-4444,
Yi Jianglong — https://orcid.org/0000-0002-2018-7138

rectly affect the solidification parameters. Modifiers of the second kind have a significant impact on the solidification parameters, and on the weld macro- and microstructure, accordingly. Their impact is related to contact effect on the process of crystallization center nucleation. At addition to the melt of a modifier which has or forms bonds with a structure isomorphous to the alloy crystallites, an essential reduction of the range of melt metastability occurs, and, hence, microstructure refinement. The content of this type of modifier usually does not exceed 0.1 wt.% [1].

The work is devoted to the problem of modifying the weld microstructure by nonmetallic nanosized particles, namely to investigation of resistance of carbides and borides in aluminium melts, which act as microstructure modifiers, when added to the composition of weldable filler material for aluminium alloy welding.

At modification of aluminium and its alloys, titanium, zirconium, scandium, etc. can be regarded as classical metal modifiers of aluminium alloys. In welding, burning out or leveling of their action always occurs, due to interaction with interstitial elements and flux components. An optimum modifier is a chemically resistant, superfine (nanosized) particle, that maximally meets the requirements of crystalline compliance, that is it effectively refines the grain at minimum concentration, stays in an inert (stable) dispersed condition in the melt; has minimum structural difference from the filler alloy crystalline lattice; does not lose its modifying properties at remelting. One of the obvious solutions is adding to the weld metal of the welded joint the submicro- and nanosized nonmetallic hardeners (modifiers in the form of refractory particles, for instance carbides, oxides, borides, etc.), which, on the one hand, can modify the weld structure and are «insensitive» to local overheating during welding, and on the other hand, increase the overall strength level of the material by Orowan mechanism, creating obstacles to the movement of dislocations and cracks, which initiate.

The following can be regarded as typical nonmetallic modifiers of aluminium microstructure: TiC (at lattice parameter a = 0.4328 nm), as well as TiB_2, AlB_2, in which compliance with aluminium lattice occurs only between the close packing directions, between the second close packed plane of the aluminium matrix and second close packed plane of modifier particles. There is also data on the effectiveness of application of WC particles as modifiers for aluminium alloys of Al–Si alloying system. These particles can refine the primary and eutectic silicon in the cast structure [2, 3].

At this moment, there exists a group of modifying additives, the action of which is based on interaction in Al–Ti–C system [4, 5]. In these modifiers TiC particles are used as nucleating agents. The main advantage of such modifying additives is the possibility of their application in aluminium alloys, where the alloying components (Zr, Cr, Li, etc.) block the effect of B- and Ti-based modifiers [6, 7].

Despite the fact that the modifying effect of TiC particles has been proved in practice [8], there is also data on instability and degradation of titanium carbide particles with formation of thermally unstable and hygroscopic aluminium carbide Al_4C_3 and silicon carbide SiC [9].

Thus, at application of titanium carbide, it is necessary to study the conditions of its stability as to thermal modes of its application and alloying components of aluminium alloys. A number of studies are devoted to problems of phase interaction at interaction of carbides with aluminium alloys [10–12]. Interphase interaction in these systems can occur rather actively, and it depends on many factors, namely presence of oxide film, diffusion rate, temperature modes, interface cleanliness, etc. Direct thermodynamic calculation of phase transformations yields results, which are not always confirmed experimentally, but it is rather difficult to purely experimentally study such processes, as result repeatability is relatively low. This is the cause for availability of contradictory data in publications on carbide and boride interaction in the form of superfine particles with aluminium-based melts in solid-liquid contact. As the effectiveness of modifying impact of nonmetallic compounds on the aluminium matrix will be directly proportional to the effective contact area of the surface of these particles with aluminium melts, refinement of their dimensions to nanosized values should increase their reactivity and crystal forming ability to the same extent. Thus, such nanosized particles can vigorously react in the presence of thermodynamic conditions of reaction running and its rate that in the case of «slow» solid-phase reactions can be compensated by a large area of their running owing to the developed surface. Thus, modifying effect of nanosized particles can be leveled out, because of interaction aluminium melt components, even during the short time of existence of liquid metal weld pool.

Thermodynamic evaluation of interphase interaction of the mentioned nanosized particles was performed by a procedure, described in work [13], which is based on CALPHAD thermodynamic calculation of heterogeneous systems and takes into account the equilibrium processes in systems, proceeding from thermodynamic data for binary and ternary element

systems that participate in the calculation. This method allows optimizing the data from different sources, calculating the dependencies, which quite well agree with experimental data.

In order to calculate the Gibbs energy functions of pure elements, their stable and unstable phases were taken from SGTE data bases [14], the majority of thermodynamic functions for binary and ternary compounds were taken from CIST2 base, data for ternary compounds and optimization of Al–C–Ti system were taken from work [15].

The model of substitution solution was used to describe the liquid phases:

$$G_{\rm m}^{\rm liq} = \sum_i x_i \, {}^0G_i^{\rm liq} + RT \sum_i x_i \ln(x_i)_{\rm m}^{\rm liq} + {}^EG_i^{\rm liq},$$

where x_i is the molar fraction of the i-th component; ${}^0G_i^{\rm liq}$ *is* the Gibbs molar energy of the pure component and in the liquid state; R, T are the universal gas constant and absolute temperature, respectively; ${}^EG_{\rm m}^{\rm liq}$ is the excess molar Gibbs energy, defined as:

$${}^EG_{\rm m}^{\rm liq} = \sum_i \sum_{j>1} x_i x_j L_{i,j}^{\rm liq} + \sum_i \sum_{j>i} \sum_{k>j} x_i x_j L_{i,j,k}^{\rm liq},$$

where $L_{i,j}^{\rm liq}$ and $L_{i,j,k}^{\rm liq}$ are the parameters of double and triple interaction, respectively, which are described by Redlich–Kister polynomial

$$L_{i,j}^{\rm liq} = \sum_i (x_i - x_j)^n \, {}^nL_{i,j}^{\rm liq},$$

Thermodynamic parameters (Gibbs energy and enthalpy) of solid phases were determined using the regular solution model [16], in which the Gibbs energy of the i-th phase $\Delta G_i = \Delta G_i(T)$, which consists of three components A, B, and C, where A is the solid solution base, the Gibbs energy of which is described as

$$G_i = \chi A G_i A = \chi B G_i B + \chi C G_i C = \chi A \chi B L_i A, B = \\ = \chi A \chi C L_i A, C + \chi B \chi C L_i B, C + \chi A \chi B \chi C L_i A, B, C + \\ + RT(\chi A \ln \chi A + \chi B \ln x B + \chi C \ln \chi C),$$

where χn, n = A, B, C is the molar concentration of component n in the solid solution in units of one ($\chi A + \chi B + \chi C = 1$), $G_{in} = G_{in}(T)$ is the Gibbs energy of n-th component of the solution (i-th phase); L_i is the parameter of pair (A–B, A–C, and B–C) and triple (ABC) interaction of atoms in phase i, which characterize the excess entropy of component mixing relative to an «ideal solution», in which $L_i = 0$.

Calculation of the initial equilibrium state in the system was performed using as initial values the thermodynamic data for the chemical elements and TiC, which were considered as the system initial elements. Thus, in order to study the multicomponent systems of aluminium alloy–superfine particle, the following boundary conditions were established:

- a closed heterogeneous system of particle-melt is considered;
- a particle is an independent component of calculation, the quantity of which is defined as a function of the solubility limit of the metal component in the aluminium melt at the set temperature (quantity of secondary phases that form as a result of interaction is determined by the equilibrium of chemical potentials and limited maximum content of reacting particles of up to 5 wt.%);
- final result of calculations is the thermodynamic phase equilibrium.

Phase calculation was performed from 500 °C (temperature below solidus temperature of commercial aluminium alloys) up to the temperature of 900 °C.

Used as filler materials in aluminium welding are aluminium alloys, which have such alloying, modifying and impurity elements as Cu, Mg, Si, Mn, Ti, and Fe in their composition.

In accordance with the performed calculation, the interaction of tungsten carbide with aluminium-based melts occurs in keeping with the Table and phase diagrams of secondary compounds (shown are the areas and quantity of secondary phases, which formed as a result of interaction of aluminium melt with tungsten carbide), Figures 1–3.

WC particles rather actively interact with aluminium, leading to formation of Al_4W intermetallics and aluminium carbide, the area of existence of which goes beyond the temperature limits of calculation towards higher temperatures. Al_4C_3 compound is a high-temperature brittle one; it readily interacts with moisture with formation of aluminium hydroxide $Al(OH)_3$ in the form of looseness. It is obvious that presence of aluminium carbide in the weld on the interphases is highly undesirable.

Results of calculation of the probable interaction of tungsten carbide particles with aluminium melts in the temperature range of 500–900 °C showed, that tungsten carbide particles can interact with aluminium melt with formation of Al_4W intermetallics and aluminium carbide in the quantity of up to 0.96 %. It is obvious that such a calculation does not take into account the kinetic component of such a reaction. However, as we noted above, at contact of nanosized particles with a developed surface, the relatively slow processes can be greatly accelerated due to a large contact area of such a material. Manganese and iron practically do not affect the interphase interaction of tungsten carbide with aluminium melts, even though they form intermetallic compounds with aluminium. Formation of an intermetallic with copper, Al_2Cu,

Calculated parameters of interphase interaction in Al-modifying particle system

System	(Al)+WC		(Al)+TiC		(Al)+TiB_2	
Alloying element	T_{sol}, °C	Secondary phases	T_{sol}, °C	Secondary phases	T_{sol}, °C	Secondary phases
	659	Al_4C_3, Al_4W	659	Al_4C_3, Al_3Ti, $N(Ti_3AlC_2)$	660	–
1 % Si	647	Al_4C_3, WSi_2, Al_4W	651	TiSi, Al_3Ti, $N(Ti_3AlC_2)$	602	–
5 % Si	573	SiC, WSi_2	640	Al_4C_3, TiSi, $TiSi_2$, $N(Ti_3AlC_2)$, Al_8SiC_7	577	–
1 % Mn	657	Al_4C_3, Al_4W, Al_6Mn	653	Al_4C_3, Al_6Mn, Al_3Ti, $N(Ti_3AlC_2)$	659	Al_6Mn
5 % Cu	551	Al_4C_3, Al_4W, Al_2Cu	553	Al_4C_3 Al_3Ti, $N(Ti_3AlC_2)$	554	–
1 % Fe	655	Al_4C_3, Al_4W, Al_3Fe	653	Al_4C_3, Al_3Fe, Al_3Ti, $N(Ti_3AlC_2)$	654	$Al_{13}Fe_4$
1 % Ti	659	Al_4C_3, TiC,Al_4W	659	Al_4C_3, Al_3Ti, $N(Ti_3AlC_2)$	664	Al_3Ti
1 % Mg	643	Al_4C_3, Al_4W	645	Al_4C_3, Al_3Ti, $N(Ti_3AlC_2)$	644	–
5 % Mg	583	Al_4C_3, Al_4W	567	Al_4C_3, Al_3Ti, $N(Ti_3AlC_2)$	659	–
5 % Zn	639	Al_4C_3, Al_4W	640	Al_4C_3, Al_3Ti, $N(Ti_3AlC_2)$	640	–

only slightly activates aluminium carbide formation; copper content of 5 % in the aluminium melt increases the probability of aluminium carbide content rising by 0.03 % from 0.96 up to 0.99 %.

Titanium presence in the base melt leads to appearance of titanium carbide TiC, formation of which is energetically more beneficial than that of aluminium carbide, i.e. this is a competitive process for Al_4C_3 formation, which lowers the probability of its appearance, and its quantity in this system, respectively (Figure 2). On the other hand, in such a system the rate of WC interaction should increase, as the process of TiC formation, as was shown above, is energetically more favourable.

Similar to copper, silicon in small quantities (up to 1 wt.%) only slightly affects WC interaction with aluminium; tungsten silicide WSi_2 forms, reducing the quantity of Al_4W intermetallic. At increase of its quantity to 5 wt.%, the mechanism of interaction in Al–WC–Si system changes completely (Figure 3). The place of Al_4W intermetallic is completely taken up by tungsten silicide WSi_2, and silicon carbide SiC forms instead of aluminium carbide Al_4C_3. Thus, silicon in the quantity greater than 5 % completely blocks the probability of aluminium carbide formation, phase equilibrium shifts towards formation of tungsten silicide and silicon carbide. Both these compounds are highly resistant in aluminium melts. If we assume that the interaction of tungsten carbide particles with the aluminium melt is initiated by dissolution of the contact layer surface, then WSi_2 formation in the interphase zone should block further contact interaction, as the silicide on the surface of dispersed particles isolates the interphase zone from further interaction. Presence of alloying titanium has a positive impact on the stability and formation of secondary modifying phases. Among the secondary compounds, formation of tungsten carbide is possible, which can act as modifier of aluminium solid solution.

Calculation of probable interaction in the system of aluminium–particles of titanium carbide TiC, the results of which are presented in the Table, showed

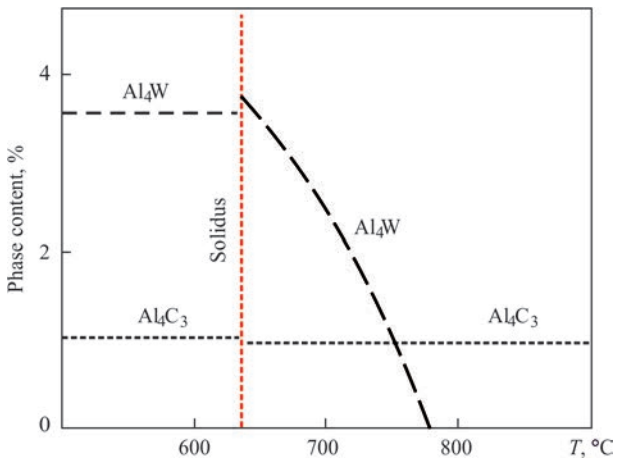

Figure 1. Calculated phase ratio (wt.%) in Al–5 % WC system

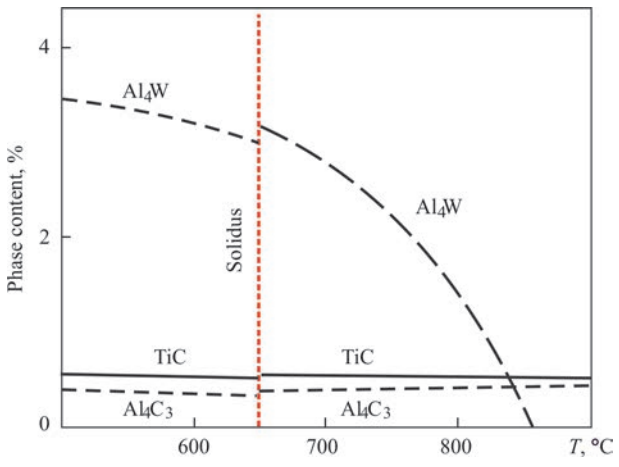

Figure 2. Calculated phase ratio (wt.%) in 99Al1Ti–5 % WC system

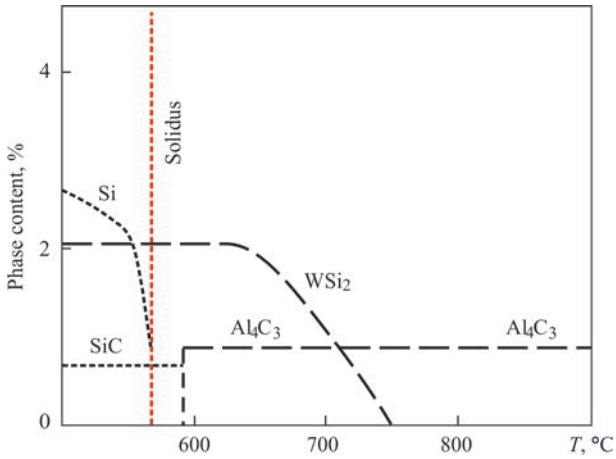

Figure 3. Calculated phase ratio (wt.%) in 95Al5Si–5 % WC system

limited thermodynamic instability of Al–TiC system in the studied temperature range with formation of aluminium carbide, as a result of titanium carbide dissolution. It is obvious that the maximum quantity of formed aluminium carbide is proportional to maximum solubility of titanium in aluminium for the specified temperature. That is, increase of weld pool temperature can nominally lead to increase of the quantity of formed aluminium carbide, as temperature increase raises the limit of titanium solubility in aluminium. As interaction of TiC and aluminium melt proceeds through dissolution in liquid aluminium, it is obvious that if the alloy being welded is first alloyed by titanium or boron-titanium modifier, such an interaction will be blocked, and titanium carbide particles will be thermodynamically stable.

As one can see from the Table, in the main study the chemical elements only slightly alter the interaction in this system, except for silicon, the action of which highly increases the probability of matrix alloy

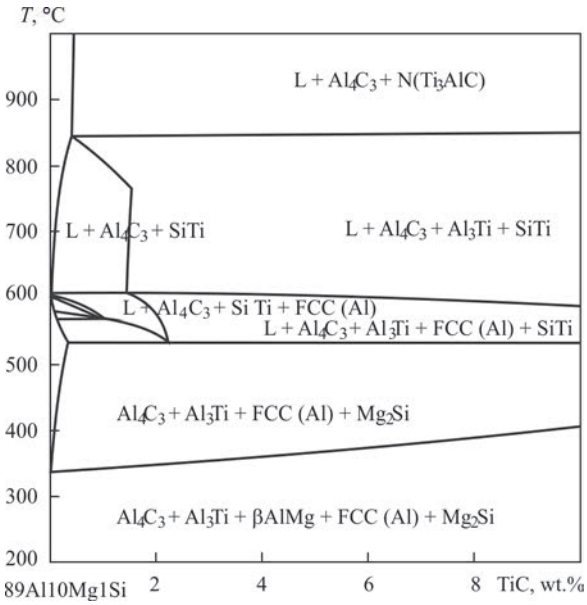

Figure 4. Calculated phase diagram of Al10Mg1Si–TiC

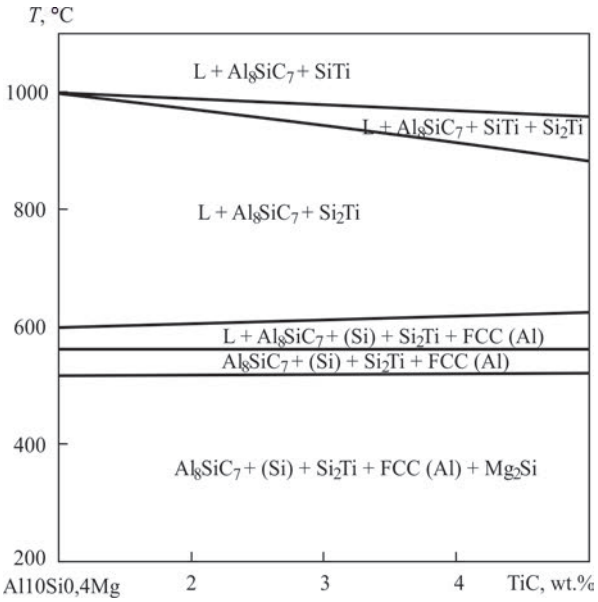

Figure 5. Calculated phase diagram of Al10Si0.4Mg–TIC

interaction with the filler that is, primarily related to silicon reactivity and its ability to form titanium silicides. Silicon presence in the quantity of up to 1 % practically does not affect the interaction of titanium carbide particles with the aluminium melt. At silicon concentration below 1 % in the system, N-phase with the decrease undergoes U-type transformation with aluminium melt (L + N↔ε(Al_3Ti) + TiSi), forming phases, which can act as effective modifiers of aluminium solid solution (Figure 4). Silicon interaction with titanium carbides is thermodynamically favourable already at temperatures of solid-phase interaction, where titanium silicide TiSi can actively form due to interaction with silicon. Considering that the solid-phase diffusion processes run several orders of magnitude slower than the liquid phase processes and the negligibly small solubility of silicon in aluminium solid solution, the probability of such interaction is extremely small.

At higher concentrations of silicon in the system above 5 wt.% (Figure 5), N-phase below 1200 °C goes into chemically more stable titanium silicides, which have no modifying effect. Chemical interaction of aluminium with carbon and reduction of aluminium oxide proceed through oxicarbides and carbides. Reduction results in formation of simple (SiC, Al_4C_3) and complex refractory carbides (Al_4SiC_4 = Al_4C_3·SiC; Al_8SiC_7 = 2Al_4C_3·SiC), which together with oxicarbides can slow down the process of further interaction of TiC particles. Depending on silicon concentration, equilibrium carbide can appear in different compositions: Al_4C_3 or in the form of Al_2OC — at a low content of silicon and presence of aluminium oxide (from the aluminium surface). At higher silicon content Al_8SiC_4 already forms. If silicon content in

the system is above 30 %, SiC formation will be thermodynamically favourable. At 1740 °C, high-temperature ternary N-phase (Ti_3AlC_2) starts forming by quasibinary peritectic transformation, as a result of interaction of initial TiC particles with the melt [15].

Particles of titanium diboride turned out to be the most stable compound in this system among the studied ones (Table). It remains thermodynamically stable in the entire studied range of temperatures, and presence of alloying elements typical for weldable aluminium alloys practically does not affect the system, and it remains inert to aluminium melts at the specified temperatures.

Conclusions

Thus, thermodynamic calculations were used to analyze the probability and establish the parameters of contact interaction of nanosized particles (WC, TiC, TIB_2) with filler material melts for weldable aluminium alloys. Established regularities of interphase interaction in the considered systems of aluminium alloy–dispersed particles, allow formulating the recommendations on selection of combinations of aluminium matrix alloy and strengthening modifying additive in the form of refractory particles, taking into account their probable interaction and modifying effect on weld metal microstructure.

It was established that finely-dispersed particles of tungsten carbide WC are a promising material for strengthening weldable aluminium systems Al−Si (AK type), containing 5 wt.% Si and more, which modify the silicon phase in the alloy microstructure.

Silicon presence in the quantity of up to 1 wt.% in Al–TiC system practically does not affect the interaction of titanium carbide particles with aluminium melt. Increase of silicon concentration leads to formation of titanium silicides (TiSi, $TiSi_2$) from the liquid phase. Further increase of silicon content just enhances the interaction in this system, which can create a threat for interaction, and lead to degradation of nanosized particles of titanium carbide, when they are used as a modifying additive for welding filler materials, which contain more than 5 % Si. Therefore, superfine particles of titanium carbide will predictably be more efficient as modifiers for alloys of Al−Mg system (AMg type), where their interaction with the melt is less probable, and the reaction products do not lower the modifying effect.

The modifying additive of titanium diboride to filler materials based on aluminium alloys can be regarded as thermodynamically stable, but also such, the modifying effect of which is small, compared to other additives, studied in this work.

This work was performed under a project fulfilled within the framework of Bilateral Agreement on Science and Technology Cooperation between the Government of Ukraine and Government of the People's Republic of China and Technical Project of Guangdong Province # 20180508).

1. Zadiranov, A.N., Kats, A.M. (2008) *Theoretical principles of solidification of metals and alloys*. Moscow, RUDN [in Russian].
2. Lekatou, A., Karantzalis, A.E., Evangelou, A. et al. (2015) Aluminium reinforced by WC and TiC nanoparticles (exsitu) and aluminide particles (in-situ). *J. Materials & Design*, **65**, 1121–1135.
3. Borodianskiy, K., Zinigrad, M. (2016) Modification performance of WC nanoparticles in aluminum and an Al–Si casting alloy. *Metallurgical and Materials Transact. B*, **47**, 1302–1308.
4. Banerji, A., Reif, W. (1986) Development of Al–Ti–C grain refiners containing TiC. *Metallurgical and Materials Transact. A*, **17A**, 2127–2137.
5. Cibula, A. (1949/1950) The mechanism of grain refinement of sand casting in aluminum alloys. J. *of the Institute of Metals*, **76**, 321–360.
6. McCartney, D.G. (1989) Grain Refining of aluminum and its alloys using inoculants. *Int. Materials Reviews*, 34(**5**), 247–260.
7. Jones, G.P., Pearson, J. (1976) Factors affecting the grain refinement of aluminum using titanium and boron additives. *Metallurgical Transact. B*, 7(**2**), 223–234.
8. *Peng* Yu, Zhi Mei S.C. (2005) *Materials chemistry and physics*, **93**, 109–116.
9. Greer, A.L., Cooper, P.S., Meredith, M.W. et al.(2003) Tronche grain refinement of aluminium alloys by inoculation. *Advanced Engineering Materials*, **5**, 81–91.
10. In-Hyuck Song, Do Kyung Kim, Yoo-Dong Hahn, HaiDoo Kim. (2004) *Materials Letters*, **58**, 593–597.
11. Viala, J.C., Peillon, N., Bosselet, F., Bouix, J. (1997) *Materials Sci. and Engineering A*, **229**, 95–113.
12. Bouix, J., Berthet, M.P., Bosselet, F. (2001) *Composites Sci. and Technology*, **61**, 355–362.
13. Shcheretsky, A.A., Shcheretsky, V.A. (2006) *Protsessy Litia*, 3, 18–214 [in Russian].
14. Dinsdale, A.T. (1991) SGTE data for pure elements. *Calphad*, **15**, 317–425.
15. Witusiewicz, V.T., Hallstedt, B., Bondar, A.A. et al. (2015) Thermodynamic description of the Al–C–Ti system. *J. of Alloys and Compounds*, **623**, 480–496.
16. Kaufman, L., Bernstein Kh. (1972) *Computer calculation of phase diagrams*. Moscow, Mir [in Russian].

Received 06.11.2019

https://doi.org/10.37434/tpwj2020.02.04

STRUCTURAL CHANGES IN THE METAL OF WELDED JOINTS OF LONG-TERM OPERATING STEAM PIPELINES

V.V. Dmytryk, A.V. Glushko and **S.P. Iglin**
National Technical University «Kharkiv Polytechnic Institute»
2 Kyrpychova Str., 61002, Kharkiv, Ukraine. E-mail: alyonaglushko@gmail.com

Increasing the service life of steam pipelines is a very urgent task for heat power engineering. The investigation of peculiarities of changing the metal structure in the areas of heat-affected-zone of welded joints of steam pipelines, which are operated for a long time in the conditions of creep, makes it possible to reduce the level of their damage and, consequently, increase the operating time. In the work the features of dislocations movement, dependence of creep rate on the structural state of welded joints are considered, and features of forming vacancies and creep pores are given. It was established that the formation of nuclei pore in the conditions of creep depends on the degree of deformation of metal in welded joints, as well as on its structural state. 10 Ref., 7 Figures.

Keywords: structural changes, welded joints, operation, steam pipelines, dislocation, pores, damage, operating time

In the process of long-term operation of steam pipelines made of chromomolybdenum vanadium heat-resistant pearlite steels, at the service parameters T_e = = 545−585 °C and P_e = 25 MPa, their metal is deformed, i.e. a manifestation of creep occurs [1, 2].

The yield strength of welded joints of steels 12Kh1MF and 15Kh1M1F is 320−370 MPa, which is much higher than the value of a mentioned operating stress. When the service period of steam pipelines is increased to more than 270,000 h, the deformation of their metal, corresponding to the second stage of creep, grows with a certain acceleration [3]. The deformation of the steam pipeline metal in accordance with the requirements of the standard documentation [1, 2], should not exceed 1 %. However, the metal of the heat-affected-zone (HAZ) areas of welded joints is deformed to a greater extent [3, 4]. For example, the deformation of the area of partial recrystallization amounts to 3−7 % and that of the overheating area is 2−3 %. The deformation of welded joint metal during their long-term service period is associated with degradation of their structure, which contributes to the formation of creep pores and cracks and leads to decrease in the service characteristics of welded joints (Figure 1) [3−5].

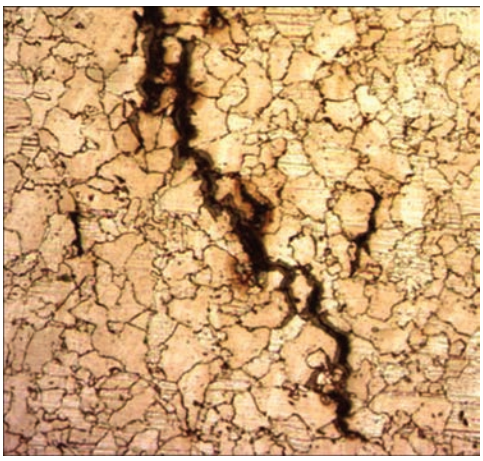

Figure 1. Microstructure (×200) of HAZ metal area of welded joint of steel 12Kh1MF (280,000 h)

The aim of the work is to study the peculiarities of structural changes in the metal of welded joints of steam pipelines, which have been long time operated under the conditions of creep. The study of structural changes will allow specifying the mechanism of damage of the metal of welded joints by pores and cracks of creep.

The metal of the areas of partial recrystallization and overheating of the HAZ at a long-term service under creep conditions (more than 270,000 h) deforms with a certain acceleration, depending on the structural state [3]. The deformation of the areas under consideration corresponds to the second stage of a stable creep. It is advisable to reveal the features of the structural state and the damage during the transition from the second to the third stage of creep, which is important in order to specify the mechanism of formation of pores and cracks, which develop mainly according to a brittle mechanism.

Creep is facilitated by the movement of dislocations, which is associated with the physicochemical processes taking place in the metal of welded joints during their long-term service [3, 5−8]. The main factors that provide the running of diffusion and dislocation processes are thermal activation and stress. It is important to establish both the features of the running of such processes as well as their relationship, which will reduce the level of their occurrence. Reducing the level of occurrence physicochemical occurrence is possible by increasing the stability of the structure of welded joints.

At a long-term service of welded joints, the creep of their metal in the process of returning is negligible

V.V. Dmytryk — https://orcid.org/0000-0002-1085-3811

and noticeable at the initial stage of the recrystallization process. We should note that their mechanisms are different from the mechanisms of returning and recrystallization occurring at annealing the cold-deformed metal. The level of deformation ε is represented as a static dependence of creep rate on time *t* (Figure 2), in which the value of the degree m depends on the structural state of the metal of welded joints. It was found that the dependence of creep on time at the presence of increase in the structural heterogeneity of the HAZ areas will accordingly accelerate. For example, for the partial recrystallization area, the acceleration will be higher than for the normalization area, as well as for the weld metal and the base metal. Let us write:

$$E = kt^m,$$

where *k* is the coefficient of proportionality, which is a function of both temperature and stress, corresponding to the conditions of creep.

It is important to establish the relationship between the deformation of the metal of welded joints, their softening and damage, which is provided by the conditions of the return process at a stable stage of creep. The strength of metal of welded joints at a service period of more than 270,000 h is decreased by about 15–20 % [1–4]. It was found that when establishing the dependence, the movement of dislocations through the barriers (precipitation of carbides of the 1st group) should be considered. It is partially confirmed by the assumption of Wirtman that in the conditions of creep, the main process is climb of dislocations initiated by thermal activation and stress [6, 7]. However, in his theory it was not considered what barriers overcome dislocations when moving under creep conditions. It was taken into account that in the metal of welded joints of steam pipelines a movement of dislocations occurs simultaneously according to two mechanisms: gliding and climb. It is advisable to study the peculiarities of revealing the abovementioned mechanisms, which will allow slowing down their proceeding.

The hindering of dislocations moving under the conditions of creep according to the gliding mechanism contributes to the stability of their structure. It was found that the hindering of dislocations is accordingly provided by the following main factors: Peierls–Nabarro forces (8–11 %); availability of dislocation clusters (9–10 %); atmospheres of impurity atoms (3–5 %); dispersed precipitations of the other phases (74–80 %). We should note that the effect of hindering dislocations can vary qualitatively, which depends on the self-diffusion of chromium, molybdenum, vanadium, and to a lesser extent on silicon, as well as the formation of segregations and new carbides of VC, Mo_2C, $M_{23}C_6$ and M_7C_3.

It was found that the stability of the structural state of the metal of welded joints depends significantly on

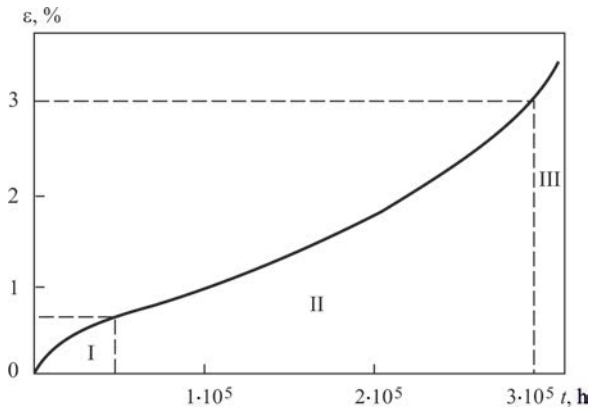

Figure 2. Curve of creep of HAZ metal overheating area of welded joint of steel 15Kh1M1F (I–II are the areas corresponding to the creep stages)

the shape, sizes and distribution density and peculiarities of the other phase precipitations [7]. Such precipitations that intersect the planes of gliding dislocations hinder their movement. Dislocations, when overcoming obstacles, which are the precipitations of especially fine-dispersed carbides of VC and Mo_2C, pass them over. When overcoming obstacles, the dislocations in a form of elongated carbides $M_{23}C_6$ and M_7C_3, located along the grain boundaries, which are perpendicular to the operating stress, can destroy carbides, which requires specification (Figure 3). It was found that the greatest contribution to the system of hindering dislocations (about 80 %) is made by the carbides of VC and Mo_2C, which are not prone to coagulation. In the conditions of creep it is advisable to reduce the rate of coagulation of carbides $M_{23}C_6$ and M_7C_3 (when creating new steels), or replace them with more stable carbides.

It was found that according to the considerations of R. Honeycomb [9], the activation energy of dislocations climb in the metal of welded joints does not fully correspond to the energy of self-diffusion of chromium and molybdenum. It was assumed that the activation energy provides climbing and gliding of dislocations as well as overcoming obstacles during their movement. It was accepted that the crystals of α-phase are characterized by a high energy of packing defects, as well as by the presence of a large number of equilibrium dislocation steps, which contribute to the formation of point defects (vacancies). When the service of welded joints is more than 270,000 h, the diffusive displacement of chromium decreases and that of molybdenum increases [8]. Accordingly, the ability of transformation of the initial structure (recommended by the standard documentation [1, 2]) into a ferrite-carbide mixture changes. Let us complete the expression of Wirtman [9], which

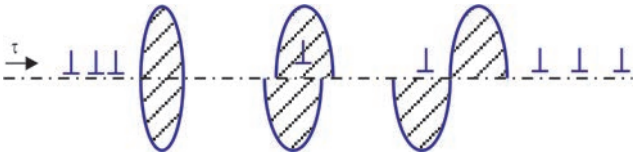

Figure 3. Scheme of damage of elongated carbides $M_{21}C_6$ and M_7C_3

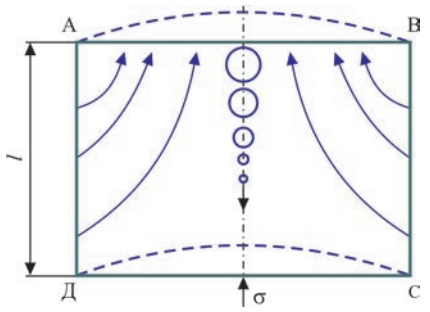

Figure 4. Scheme of vacancy creep (ABCD is the contour of a deformed fragment of the HAZ metal area: O are the pores; --- is the change of contour shape on stress σ

determines the dependence of creep rate on stress and temperature and by the dependence on the structural state. The account of the mentioned dependence allows specifying the level of deformation of metal of welded joints at the presence of changes of external stress (starts-stops of power units). Let us write:

$$\varepsilon = \text{const}\frac{\sigma^P}{kT}\exp\left(-\frac{U_S{}^n}{kT}\right),$$

where σ is the working stress; k is the Boltzmann constant; P is the exponent of power that characterizes the change in stress and temperature; n is the exponent of power depending on the structural state; U_S is the activation energy; T is the temperature.

It was found that at the end of the second stage of creep (see Figure 2), the strain rate begins to increase with the approach to the exponent. In the process of long-term service, the structure of welded joints (ferrite-bainite, ferrite-sorbite or ferrite-troostite) is transformed into a mechanical mixture (ferrite + carbides) at a different rate. At the same time, in the near-boundary zones of α-phase crystals segregations, new carbides of VC and Mo_2C are formed and also $M_{23}C_6$ and M_7C_3 coagulate, the creation and coalescence of vacancies occurs. In the metal of the areas of overheating and partial recrystallization of the HAZ of welded joints when their service life is more than 270,000 h, an increasing gliding along grain boundaries (up to 3−7 %) over time is observed. Let us introduce a specification into the mechanism of the viscous Nabarro−Herring flow [6], which allows using it for the metal of welded joints, deformed in a different extent. It was found that directional diffusion of point defects facilitates displacement of dislocations during creep. The pores are formed in the most deformed fragments of the area and then move in the direction where the deformation is smaller (Figure 4). Accordingly, the diffusive displacement of atoms proceeds in the opposite direction. It was assumed that the origin of vacancies occurs along the grain boundaries, and the rate of creep is provided by their diffusion movement.

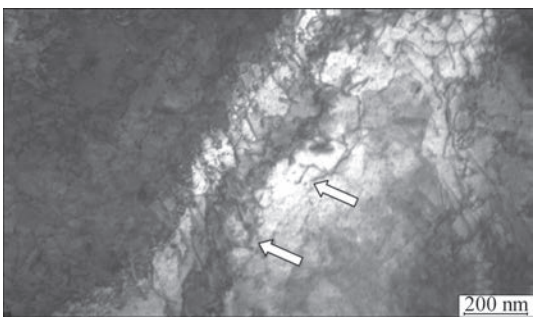

Figure 5. Dislocation structure of HAZ metal fusion area of welded joint of steel 12Kh1MF. Service period is 280,000 h (examples of steps on dislocations are indicated by arrows)

In the centre of the AB boundary (see Figure 4), the concentration of vacancies is the highest. Following [9] let us write:

$$C - C_0 = C_0\frac{\sigma b^3}{kT},$$

where C is the formed concentration of vacancies; C_0 is the equilibrium concentration; b^3 is the volume of vacancy.

The number of vacancies along the boundary between the AD and BC will be the lowest. Then the diffusion rate of displacement of chromium and molybdenum will be:

$$\frac{dV}{dt} = \frac{U_s b^3 l Д_n}{kT},$$

where U_S is the activation energy; l is average grain size; D_n is the coefficients of self-diffusion of chromium and molybdenum.

In determining the creep rate of the HAZ metal, the activation energy and diffusion coefficients of chromium and molybdenum were taken into account [10]. Let us write:

$$\varepsilon = \frac{1}{l^3}\frac{dV}{dt} = \frac{2U_s b^3 Д_n}{l^3 kT}.$$

The creep rate is in the linear dependence on the activation energy and on the diffusion coefficients of chromium and molybdenum, it depends on the level of vacancies nucleation intensity, their displacement and coalescence and the subsequent transformation of vacancies into pores. On the dislocation lines (areas of fusion and HAZ overheating), the steps are formed (Figure 5), which occurs at the mutual intersection of moving dislocations with «sedentary» dislocations as well as during passing of dislocations through the clusters of dislocations. The shape of the steps depends on the angle of intersection of dislocations. The intersection of dislocations leads to vacancies formation. Therefore, the creep occurs at a simultaneous formation of vacancies and the activation energy of creep is in compliance with the activation energy of self-diffusion.

In the conditions of creep, the steps on dislocations are climbing, which is facilitated by the moving (along the line of dislocations) vacancies that feed the steps. A number of steps on the lines of dislocations,

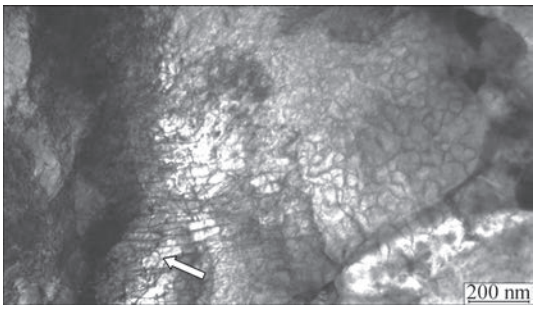

Figure 6. Dislocation structure of area of partial recrystallization of HAZ metal of welded joint of steel 12Kh1MF. Service period is 280,000 h (examples of steps on dislocations are indicated by arrows)

which depends on the number of intersections of moving dislocations with «sedentary» dislocations, is controlled by the level of the metal deformation. For example, a number of steps on the dislocations at the area of partial recrystallization will be higher than at other areas of HAZ metal (Figure 6).

The permissible overheating in the temperature range T_0 = 630–650 °C (emergency steam discharge) contributes to the formation and development of creep pores, which are mostly formed along the grain boundaries, where coagulating carbides of the first group are located [5]. A number of nuclei pores n (size of 0.1–0.3 μm) is increased in a linear dependence on the overheating temperature and also its duration. Let us write:

$$n = \alpha(T)t + n_0,$$

where $\frac{dn}{dt} = \alpha(T)$ is the rate of nuclei pores formation; n_0 is the initial number of pores.

The formation of pores in the metal of welded joints is noticeably influenced by the increase in the number of starts-stops of power units, which is characterized by the presence of variable stresses and requires a further study.

It was found that the creep pores are mainly formed at grain boundaries, located at the angles of 70–90° to the tension axis. However, at the presence of coagulating carbides at their boundaries, the pores are formed also at the angles of 20–60° which should be studied further. It was found that the formation of pore nuclei in the conditions of creep depends on the degree of deformation of the welded joints metal, as well as on its structural state (Figure 7). The assumption of R. Honicomb finds confirmation of the fact that the pores arise as a result of simultaneous manifestation of such processes as coalescence and gliding of vacancies along the grain boundaries, which also requires further specification in the metal of welded joints with respect to their service period of more than 270,000 h.

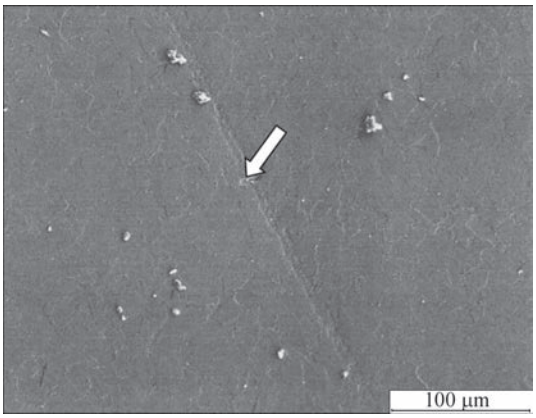

Figure 7. Formation of creep nuclei pores (arrow) during overheating of HAZ metal of welded joint of steel 12Kh1MF (280,000 h)

Conclusions

1. It was grounded that structural changes in the metal of welded joints, which have been long-time operated under creep conditions, facilitate increasing its deformation capacity and the formation of creep pores.

2. It was found that structural changes in the metal of welded joints of steam pipelines are interconnected with the processes of creep and diffusion of alloying elements of chromium and molybdenum.

3. The peculiarities of vacancies formation in the structure of welded joints were revealed, which is provided by the conditions of creep and depend on the structural state of welded joints.

1. (2005) *Procedural guidelines on evaluation of viability of equipment of thermal power plants* (SO153-34.17.456). Moscow, TsPTI ORGRES [in Russian].
2. (2001) *Express-method for evaluation of residual service life of welded joints of boiler and steam pipeline collectors on structural factor* (RD 153-34.1-17.467). Moscow, TsPTI ORGRES [in Russian].
3. Glushko, A.V., Dmitrik, V.V., Syrenko, T.A. (2018) Creep of welded joints of steam pipelines. *Metallofizika i Novejshie Tekhnologii*, 40(**5**), 683–700 [in Russian].
4. Khromchenko, F.A. (2002) Service life of welded joints of steam pipelines. Moscow, Mashinostroenie [in Russian].
5. Dmitrik, V.V., Sobol, O.V., Pogrebnoj, M.A. et al. (2015) Structural changes in metal of welded joints of steam pipelines in operation. *The Paton Welding J.*, **12**, 24–28.
6. Suzuki, T., Yoshinaga, H., Takeuchi, S. (1989) *Dislocation dynamics and plasticity*. Moscow, Mir [in Russian].
7. Glushko, A. (2016) Researching of welded steam pipe joints operated for a long time. *Eastern-European J. of Enterprise Technologies*, 6, 1(**84**), 14–20.
8. Dmitrik, V.V., Sobol, O.V., Pogrebnoj, M.A., Syrenko, T.A. (2015) Peculiarities of degradation of metal in welded joints of steam pipelines. *The Paton Welding J.*, **7**, 10–15.
9. Honeycomb, R. (1972) *Plastic deformation of metals*. Moscow, Mir [in Russian].
10. Dmitrik, V.V., Syrenko, T.A. (2012) To the mechanism of diffusion of chromium and molybdenum in the metal of welded joints of steam pipelines. *The Paton Welding J.*, **10**, 20–24.

Received 06.05.2019

https://doi.org/10.37434/tpwj2020.02.05

CORROSION RESISTANCE OF COMPOSITE MATERIAL DEPOSITED BY TIG METHOD USING FLEXIBLE CORD TeroCote 7888T

B.V. Stefaniv, L.I. Nyrkova, A.V. Larionov and **S.O. Osadchuk**
E.O. Paton Electric Welding Institute of the NAS of Ukraine
11 Kazymyr Malevych Str., 03150, Kyiv, Ukraine. E-mail: office@paton.kiev.ua

Increasing the corrosion resistance of drill bits with protective coatings is an urgent problem in Ukraine. For drilling tool, the main indices of physical and mechanical properties of wear-resistant coatings are abrasive wear, corrosion resistance and hardness (microhardness). It allows effectively resisting wear of working bodies of blades and a body of drill bits under the conditions of alternating and shock loads, hydroabrasive wear, corrosion, erosion, etc. It was investigated that a uniform distribution of tungsten carbide particles throughout the whole volume of deposited layer causes the same hardness over the coating depth and significantly increases the resistance of coating to corrosion wear. It is shown that microhardness of the matrix of a composite material TeroCote 7888T based on NiCrBSi exceeds the microhardness of steel 30Kh by 2.2 times. According to the results of corrosion tests, it was established that the protection of steel 30Kh by a deposited layer on the basis of a composite material TeroCote 7888T under the conditions simulating operating ones allows reducing the corrosion rate of working bodies of steel drill bit by almost 53 times. 10 Ref., 1 Table, 4 Figures.

Keywords: surfacing, tungsten carbides, microstructure, microhardness, wear resistance, corrosion rate, corrosion spot

Drill bits are operated in different climatic zones, under aggressive conditions and are subjected to different loads. The classic types of wear of a drilling tool in industry are: abrasion, erosion, shock, friction, heating, corrosion and cavitation one. The losses as a result of wear are manifested not only in the loss of funds for the purchase of new equipment, but also in the idle period during repair. For more than a century history, it was shown that the application of protective coatings to the working parts of drill bits can significantly increase the life of a drilling tool.

To protect the drilling tool from different types of wear, composite materials based on Ni, Fe, NiCr, NiCrBSi, brass, etc., strengthened with tungsten carbides [1] are widely used. First of all, this is associated with the unique properties of the reinforcing phase of such alloys as tungsten carbides. The most widespread use in the industry belongs to tungsten monocarbide WC with a stoichiometry of 6.13 % C. It is characterized by a high hardness *HV* 2200, compressive strength of 5–7 GPa and elasticity modulus of 700 GPa, preserves mechanical properties over a wide range of temperatures, resistant to friction corrosion and capable of forming a strong bond with metals [2, 3].

The problem of corrosion, along with an intensive wear, is very important for working bodies of a drill bit during drilling of oil and gas wells. The stability and performance of drilling using steel bits with a protective coating, including bits with rock destruction elements in the form of polycrystalline diamond cutters, directly depends on the ability of the elements of «cutting structure» of bits to resist abrasive wear of the brazing alloy and the areas of blades around these elements that seek to destroy the system of fastening these rock destruction elements. Therefore, the protective coating of steel areas of the working bodies of the blades located around the cutting and calibrating elements keeps them from tearing, causes baring, increasing the size of the projection and a gradual fallout of separate elements.

The carried out investigations of wear resistance of composite materials under the conditions of hydro-abrasive wear [4] showed that the wear resistance of a protective coating applied with TeroCote 7888T with chipped tungsten carbide particles exceeds the wear resistance of coatings applied with the use of relite «LZ-11-7» (spherical granules of tungsten carbide) and Diamax M (grinded tungsten carbide particles) by 1.7 and 2.9 times, respectively. Based on the results of investigations of hydroabrasive wear of composite materials, the main attention was paid to the composite alloy TeroCote 7888T, which belongs

B.V. Stefaniv — http://orcid.org/0000-0002-7159-8762, L.I. Nyrkova — http://orcid.org/0000-0003-3917-9063,
S.O. Osadchuk — http://orcid.org/0000-0001-9559-0151

to the category of corrosion-resistant protective materials.

Taking into account the abovementioned, the aim of the work was to investigate the corrosion resistance of the metal deposited using TeroCote 7888T composite material under the laboratory conditions simulating the operation of a drill bit during drilling wells (temperature, chemical composition, wear, etc.).

Materials and methods. As the object of the investigations a composite material flexible cord TeroCote 7888T was selected. The examination of microstructure was performed using the standard procedure in the optical metallographic microscope MMT-1600B. The digital image of the microstructure was obtained with the use of the Carl Zeiss ICc5 camera. The microhardness was measured in keeping with the standard procedure according to GOST 2999 [5] in the PMT-3 microhardness meter. The corrosion tests were performed using the method of massometry according to GOST 9.908 [6].

Results of investigations. To deposit protective coating on the specimens, the composite material (self-fluxing brazing alloy TeroCote 7888T in the form of a flexible cord with a diameter of 5 mm according to DIN 8555: G21−350−GR) was used. The cord had a core of nickel wire of 1.2 mm diameter and a sheath of a matrix alloy of the NiCrBSi system with a high content of tungsten carbide. The working temperature of surfacing was 1170 °C (±50 °C). The size of particles of a chipped tungsten carbide was 0.10−0.70 mm. The content of tungsten carbide in the matrix alloy does not exceed 65 wt.%.

The arc surfacing of test specimens was performed with the help of the PRS-3M welding machine. The application of deposited layer was performed in an arc method by a non-consumable tungsten electrode in a shielding gas — technical argon. The optimal conditions with the lowest heat input were as follows: U = 10−12 V; I = 50−60 A, deposition rate was 2−4 m/h. The surfacing was carried out in a horizontal position on all the sides of the rectangular specimen. The average thickness of the deposited layer was 8−10 mm. After surfacing, the specimens were grinded, the thickness of the deposited layer on each side was approximately 1.5−1.8 mm.

To determine the microstructure, a microsection was made from the specimen with the deposited layer. Metallographic examinations showed that the deposited layer and the base metal are combined by a thin transition layer of a diffusion origin (Figure 1), which indicates that the base metal did not melt and the filler metal did not dissolve in it. The microstructure of the deposited alloy contains a solid solution based on nickel-chromium strengthened with tungsten carbides

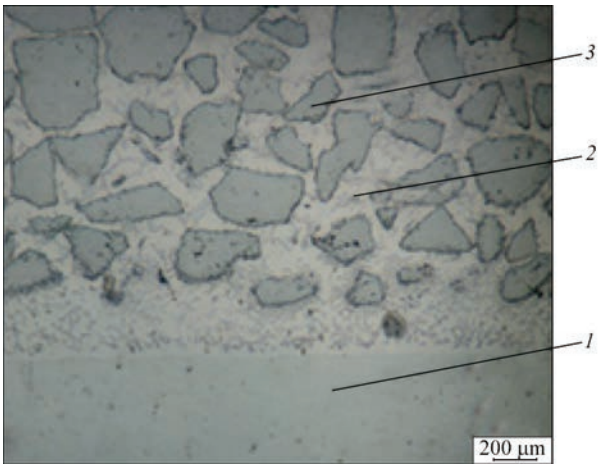

Figure 1. Microstructure of deposited layer (30Kh steel): *1* — base metal; *2* — matrix based on alloy NiCrBSi; *3* — tungsten carbides

and the content of silicon and boron depressants. The presence of boron and silicon in the composition of filler wires provides self-fluxing properties to them during surfacing on steel. The tungsten carbides of irregular shape (of different sizes) are distributed throughout the whole microsection field.

It is known from the literature that a high-quality wear-resistant coating should have a uniform distribution of solid phases with a distance between these phases being smaller than the size of abrasive particles [7]. Such a uniform distribution of tungsten carbide particles throughout the volume of the deposited layer provides the same hardness throughout the depth and considerably improves the resistance of coating to corrosion wear.

The measurements of microhardness on the surface of the deposited layer and the base metal were performed in the PMT-3 microhardness meter at a magnification of ×130 at a ratio of the load to the indentation area. The loads of 50 g weight (for the base metal) and 200 g (for the deposited layer) were used. The specimen was divided into three areas for measurements: the base metal, the matrix in the middle of the deposited layer, the tungsten carbide particles (Figure 1). At each area

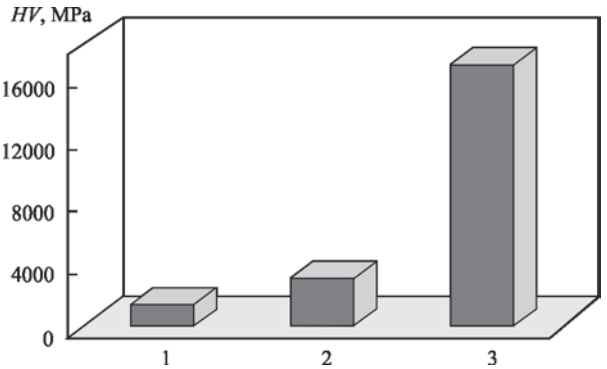

Figure 2. Average value of microhardness of specimen areas: 1 — steel 30Kh; 2 — matrix based on alloy NiCrBSi; 3 — tungsten carbides

Rate and penetration depth of corrosion of steel 30Kh and deposited layer

Characteristics of specimen	Corrosion rate, g/(m²·h)	Corrosion penetration depth, mm/year
Specimen with deposited layer	0.257–0.261	0.18
Steel 30Kh	8.42	9.5

ten measurements were performed at a holding time of 15 s. According to the obtained data, the average values for each area were determined (Figure 2): 1 — base metal (steel 30Kh) — 1400.8 MPa; 2 — matrix based on NiCrBSi alloy — 3123.5 MPa; 3 — tungsten carbides — 16850 MPa (16.8 GPa).

The corrosion resistance of the deposited metal based on the alloy TeroCote 7888T was evaluated on two specimens (Figures 3, 4). For comparison, the corrosion resistance of steel 30Kh was evaluated.

The resistance of the deposited metal layer to the action of the moving medium was evaluated by the appearance of the specimens and the corrosion rate. To simulate the effect of the corrosive medium and solid particles present in the drilling cuttings during drilling wells, the study was performed in a moving medium based on 3 % NaCl solution of the following composition: 400 ml of H_2O + 12 g of NaCl + 200 g of quartz sand in the mlw MR25 installation at a room temperature. The time of holding specimens in the moving medium was 95 h, the fluid flow rate was 60–90 rpm and the total duration of tests (with and without stirring) was 172 h. After the tests were finished, the corrosion products were removed from the specimen surface according to GOST 9.907 [8]. Inspection of the surface of the specimens before and after the examinations was performed visually. The area of corrosion damages of the base metal was evaluated according to GOST 9.311 [9], item 5. The rate of corrosion of the specimens was determined by the method of massometry in compliance with the indices according to GOST 9.908 [6] in g/(m²·h):

$$V_p = \frac{\Delta m}{Sl}, \quad (1)$$

where Δm is the weight loss of the specimen, g; S is the surface area of the specimen, m²; t is the duration of investigations, h.

The depth of corrosion penetration in mm/year was calculated by the formula:

$$V_h = 8.76\frac{V_p}{\rho}, \quad (2)$$

where V_p is the corrosion rate, g/(m²·h); ρ is the density of the metal, g/cm³.

For steel 30Kh — ρ = 7.8 g/cm³, for composite alloy TeroCote 7888T — ρ = 12.4 g/cm³.

The results of the investigation are shown in Table and in Figures 3, 4.

Specimens with deposited layer. The surface of the specimen before testing is uniform and has a metallic color (Figure 3, *a*). After testing on the entire surface, on both sides, darkening spots of the deposited layer and pits with a diameter not more than 1 mm are visible. Corrosion damages have the appearance of corrosion spots of different sizes: from (10×1) mm to (5×3) mm and tiny pits (Figure 3, *b*). The total area of corrosion damages is close to 0.00004 m² (at the total surface area of the specimen being 0.0045 m²).

The area of corrosion damages of the base metal is about 2 % (Figure 3, *c*) and is estimated by the point

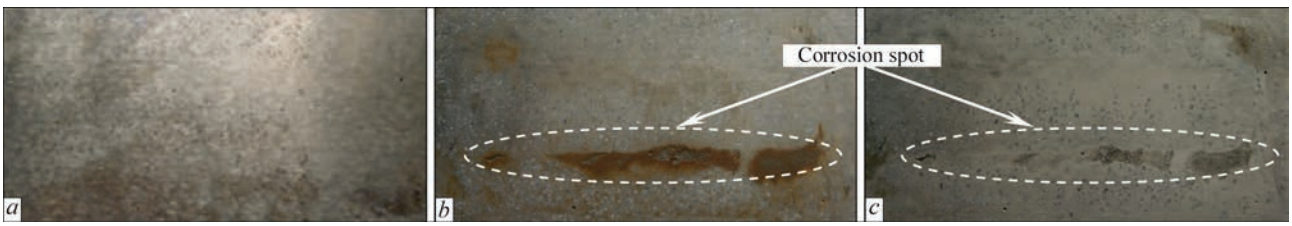

Figure 3. Outer appearance of specimen surface of deposited layer on the basis of NiCrBSi: *a* — in the initial state; *b* — with corrosion products; *c* — after removal of corrosion products

Figure 4. Outer appearance of specimen surface of deposited layer on the basis of steel 30Kh: *a* — in the initial state; *b* — with corrosion products; *c* — after removal of corrosion products

6 (the area of damages of the base metal is from 1 to 2.5 %) according to Table 2 GOST 9.311 [9] by a ten-point scale. The corrosion rate of the specimen was 0.257 g/(m^2·h), the corrosion penetration depth was 0.18 mm/year (Table).

Specimen of steel 30Kh. Before the tests the surface of the 30Kh steel specimen (Figure 4, *a*) has a metallic color. After tests, the entire surface is covered with brown corrosion products (Figure 4, *b*), after removal of which corrosion spots are present occupying more than 70 % of the total area (at a total surface area of the specimen being 0.0035 m^2), Figure 4, *c*. According to GOST 9.908 [6], the type of corrosion is identified as a continuous uniform. The corrosion rate was 8.42 g/(m^2·h), the depth of corrosion penetration was 9.5 mm/year (see Table).

According to GOST 9.502 [10], if the corrosion rate of iron and ferrous metals is from 0.1 to 0.5 mm/year, which is estimated by a point 6, the resistance of the metal to uniform corrosion is considered to be lowered. If the corrosion rate is from 5.0 to 10.0 mm/year (point 9), the metal is considered to be weak resistant.

Conclusions

1. According to the results of investigations, it was found that during TIG surfacing using a flexible cord TeroCote 7888T, during the formation of the deposited layer the tungsten carbide particles are uniformly distributed over the entire deposited layer volume, which determines the uniform distribution of hardness over the depth of the coating.

2. The results of carried out investigations showed that the use of protective coating deposited with flexible cord TeroCote 7888T allows reducing the corrosion rate of working bodies of drilling tool of 30Kh steel by approximately 53 times, which will promote extending its service life.

1. *Wear-resistant materials*. https://docplayer.ru/32381351Iznosostoykie-materialy-i-tvyordye-splavy-na-osnovekobalta.html [in Russian].
2. Samsonov, G.V., Vitryanyuk, V.N., Chaplygin, F.I. (1974) *Carbides of tungsten*. Kiev, Naukova Dumka [in Russian].
3. Pierson, H.O. (1996) *Handbook of refractory carbides and nitrides*. New Jersey, Noyes Publ.
4. Stefaniv, B.V. (2016) Investigation of wear resistance of protective coatings under conditions of hydroabrasive wear. *The Paton Welding J.*, **9**, 26–29.
5. *GOST 2999–75:* Vickers hardness test [in Ukrainian].
6. *GOST 9.908–85* (USCAP): Metals and alloys. Methods for determination of corrosion and corrosion resistance indices [in Russian].
7. *Wear-resistant materials*. http:// www.svarka 52.ru/upload/osnovnoj_katalog_po_paike_i_Terocote_BRAZING_1.pdf [in Russian].
8. *GOST 9.907–83* (USCAP): Metals, alloys, metallic coatings. Methods for removal of corrosion products after corrosion tests [in Russian].
9. *GOST 9.311–87* (USCAP): Metal and non-metal inorganic coatings. Method of corrosion damage evaluation [in Russian].
10. *GOST 9.502–82* (USCAP): Inhibitors of metals corrosion for aqueous systems. Methods of corrosion tests [in Russian].

Received 05.11.2019

https://doi.org/10.37434/tpwj2020.02.06

FEATURES OF APPLYING ELECTRON BEAM WELDING IN MANUFACTURE OF THE CATHODE ASSEMBLY OF THE ELECTRON GUN

V.M. Nesterenkov, V.I. Zagornikov, Yu.V. Orsa and **O.M. Ignatenko**
E.O. Paton Electric Welding Institute of the NAS of Ukraine
11 Kazymyr Malevych Str., 03150, Kyiv, Ukraine. E-mail: office@paton.kiev.ua

The efficiency of using electron beam welding in producing permanent joints of structural materials of all thicknesses and shapes is well-known. The work for the first time considers the possibility of using electron beam welding for the production of high-precision parts of optical system in cathode unit, providing the necessary parameters and their joining with electron beam gun insulator in future. The use of electron beam welding at the final stage of manufacturing cathode unit opens the opportunity of minimizing the number of further technological operations. It is noted that to create the welding technology, in which the operation of welding would become a final assembly operation, the development of new designs of welded joints and schemes for assembly of cathode unit are required. Due to a correct design of welding units and compliance with the accuracy of assembling for welding, it became possible to preserve geometric dimensions after electron beam welding and to provide the operational reliability of the design as a whole. 5 Ref., 6 Figures.

Keywords: electron beam welding, pulsed mode, nickel alloy, cathode unit, welding equipment

In the industry new tasks are emerging that are successfully solved by using electron beam welding (EBW). In this process welding guns of different power are used to provide the formation of welded joints with a thickness from 0.5 to 150 mm or more.

Cathode units (CU) of optical systems are the base of electron beam guns and are subjected to increased requirements during manufacturing. Taking into account the capabilities of EBW, it is very promising to use it in the manufacture of CU, which represent a complex metal-ceramic product. Considering a high cost of equipment for electron beam welding, the task of manufacturing and at the same time extending the service life of CU is very important. In order to increase the long-term and stable formation of electron beam welds, high-precision parts of a cathode part of the electron beam gun (EBG) were designed and manufactured using EBW.

In the manufacture of such units it is necessary to solve a number of problems related to the presence of residual inherent stresses caused by the difference of thermal coefficients of linear expansion of metal and ceramics [1].

As is known, cathodes for electron welding guns are made of tungsten and lanthanum hexaboride LaB_6. Tungsten is much more resistant to vapors of welding metals and residual gases, while the cathodes of lanthanum hexaboride are rapidly contaminated by vapors of welded metals and lose their emission capacity [2]. However, the power of heating required for the normal operation of the tungsten cathode is 3–4 times higher than the heating power of the cathode of LaB_6. Due to the influence of high operating temperatures, the cathode can be shifted relative to the optical axis and the focusing of the electron beam can be violated.

As a consequence, the operating temperature of the tungsten cathode holder and the elements connected with it prevent the use of brazed joints in the cathode assembly design. The paper for the first time considers the possibility of using EBW to join high-precision parts of the optical system (CU) with the necessary parameters.

The problem solved in this work consisted in developing a technology that allows the EBW operation to be a finishing operation of the CU electrode connection while maintaining its full operational properties.

The experimental works were carried out in the SV112 installation of the design of the E.O. Paton Electric Welding Institute (PWI) with the computer control of EBW parameters. Carrying out EBW in a small-sized SV112 installation in difficult-to-weld places (interelectrode spaces), where the use of a standard monitoring system in the secondary electrons was problematic, became possible due to the presence of a coaxial monitoring system on the base of digital videocamera.

V.M. Nesterenkov — http://orcid.org/0000-0002-7973-1986

To produce welded joints from the parts of kovar used during the manufacture of CU it is necessary to minimize residual stresses by minimizing penetration depth and overheating of the base metal [3]. This is achieved by optimizing the welding parameters: welding speed V_w, beam current I_w, focusing lens current I_f and working distance, which provide the formation of welds with penetration to a partial thickness with a minimum recrystallization zone. The weld formation is significantly influenced by the position of the electron beam focus relative to the surface of the product. The best results are achieved by placing the focus below its surface. The welding modes are selected such that to provide that the value of the weld shape factor was close to H_p/B = 1.8−2.0 mm. Such shape is predetermined by the need in a minimal heat input to reduce the probability of arising burns out, cuts, increased spattering and periodic hump shape of the weld.

For the same purpose EBW pulsed mode is successfully used. Pulsed EBW due to a low heat input has become irreplaceable during welding in the direct vicinity from the place of soldered joints of metal with ceramics. The heat input during welding is minimized and the welding speed is maximized to reduce the size of the weld pool and crystallization period.

The EBW pulsed mode parameters are the following:

- rigidity of the *G* mode (ratio of pulse duration to pause duration between them);
- frequency of transmission of current pulses of electron beam *F*.

A significant influence on the value of input energy and quality of welded joint during welding in a pulsed mode is also provided by the welding speed V_w, the choice of which in each specific case depends on duration of an individual pulse and length of the path traveled by the beam during a pause between the pulses, which determines the factor of the overlap.

To keep with the conditions of formation of a sealed (vacuum-tight) welded joint, the overlap factor of welding points is set not less than 0.6−0.7. Based on the carried out calculations and experiments, the pulsed mode parameters of EBW were determined.

EBW pulsed mode parameters

U_p, kV	60
Beam current, mA	10−12
Working distance, mm	150−300
Pulse frequency *F*, Hz	30
Pulse duration τ_{pulse}, ms	16.5
Pause duration τ_{pause}, ms	16.5

The welding speed on different types of welded joints of CU varied from 3 to 10 mm/s. The further increase in speed resulted in the Humping effect.

The reduced welding speed threatens with overheating of the product right up to distortion of its shape.

In addition, the EBW pulsed mode allows reducing the requirements to the accuracy of aligning thin-walled structural elements and, first of all, the value of gap between these elements. Our previous investigations have shown that the gap in the joints of CU should not exceed 0.06−0.08 mm. In this case the error of 0.09 mm is admitted. The excess of edges should be not more than 0.5 mm or 20−25 % of the thickness. Welding on the edge flange while maintaining the assembly gap within 0.06−0.08 mm also did not cause any difficulties.

All the welds in the considered welded design of CU were circumferential. It is known that the products, the parts of which substantially differ in thickness, are welded with a preliminary treatment of the edge to equalize the temperature field, which provides a symmetrical shape of penetration. In order to minimize the heat removal into the product during welding of circumferential welds of CU, the designing samplings were used (Figure 1).

The welding process is also critical as to the accuracy of the heating spot location with respect to the butt. In case of its deviation from the trajectory of the butt, lacks of penetration, burns out and undercuts are possible. Lacks of penetration and burns out do not provide the vacuum density of welds and are the main rejection criteria as the most dangerous defects. Such defects are difficult to eliminate during remelting. Repeated passes lead to the formation in weld of a coarse-grained columnar structure and hot cracks to which nickel alloys are prone. Therefore, the number of passes should not be more than two.

Based on the results of previous investigations of EBW, a small chart of technological production of CU was created, consisting of six parts: Wehnelt electrode bushing, cathode bushing, heater bushing, lid and pin of cathode heater (Figure 2).

In Figure 3 the chart is supplemented with a photo of macrosection of typical types of welded joints.

The parts of CU (cathode bushing with a high-voltage input and bushing of the heating device with a high-voltage input) were manufactured and joined (weld No.2 and weld No.3) in two design variants: *a* — butt joint of CU electrodes; *b* — butt joint of CU electrodes with the use on flanging.

The use of the design as to the variant (*b*) made it possible to reduce the criticality of a butt gap value. The welded joint with edge flanging was also produced when the pin of the heating device was installed to the CU lid (weld No.5).

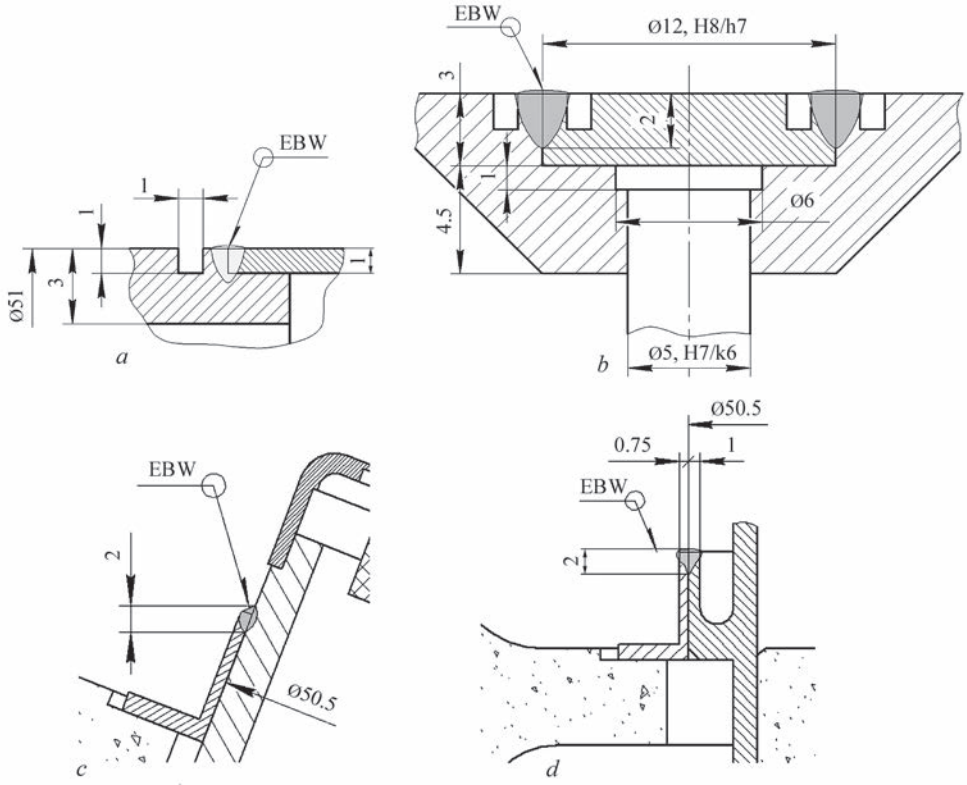

Figure 1. Examples of design of welded joints of CU (*c*, *b*): *a* — butt joint with one-sided edge flanging; *b* — with double-sided edge flanging. Two types of electron beam joints of cathode unit with EBG insulator (*c*, *d*): *c* — overlapped; *d* — with double-sided edge flanging

As a result, in the cathode unit high quality welds were produced, the fragments of which together with the general appearance of CU are presented in Figure 4.

The final and the most responsible stage of welding-in CU into a thin-walled (0.5−0.8 mm) flange of the EBG ceramic insulator is carried out in the conductor specially made in the form of seating positions of the insulator. The conductor is fixed in the rotator at an angle with a deviation from the vertical to 10°. This requirement is mandatory to provide the possibility of welding-in difficult-to-reach areas of welded CU with coaxial welds at different heights.

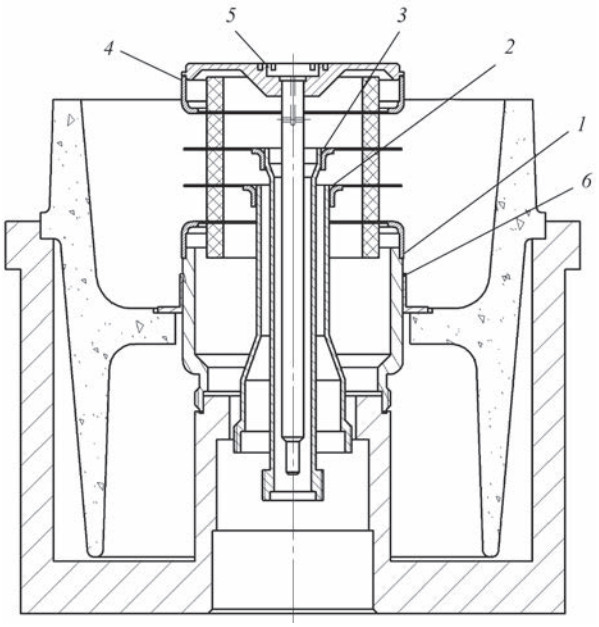

Figure 2. Sequence of assembly and welding of CU with the help of EBW: weld No.1 (Wehnelt electrode bushing with a high-voltage input); No.2 (cathode bushing with high-voltage input); No.3 (heating device bushing with high-voltage input); No.4 (lid with high-voltage input); No.5 (mounting of pin of heating device into the lid); No.6 (joining of CU with insulator)

In order to increase the manufacturability of the assembly and welding process, the design of CU was modernized. In particular, the type and shape of welded joint during welding-in CU into the insulator were changed.

Replacement of one type of welded joint – overlapped welded at a sharp angle into the end (Figure 1, *c*), i.e., a welded joint in which welded elements are arranged in parallel and partially overlap each other on a bilateral flanging (Figure 1, *d*) made it possible to

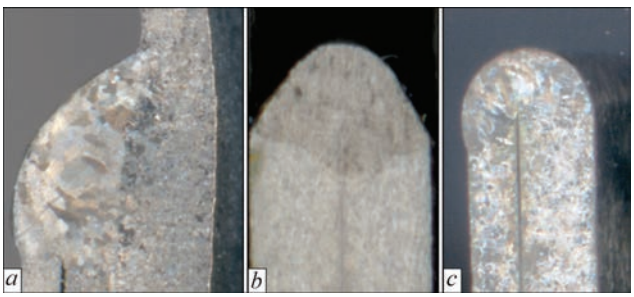

Figure 3. Macrosections of characteristic types of welded joints of cathode unit (CU): *a*−*c* — respectively welds No.1, No.5, No.6

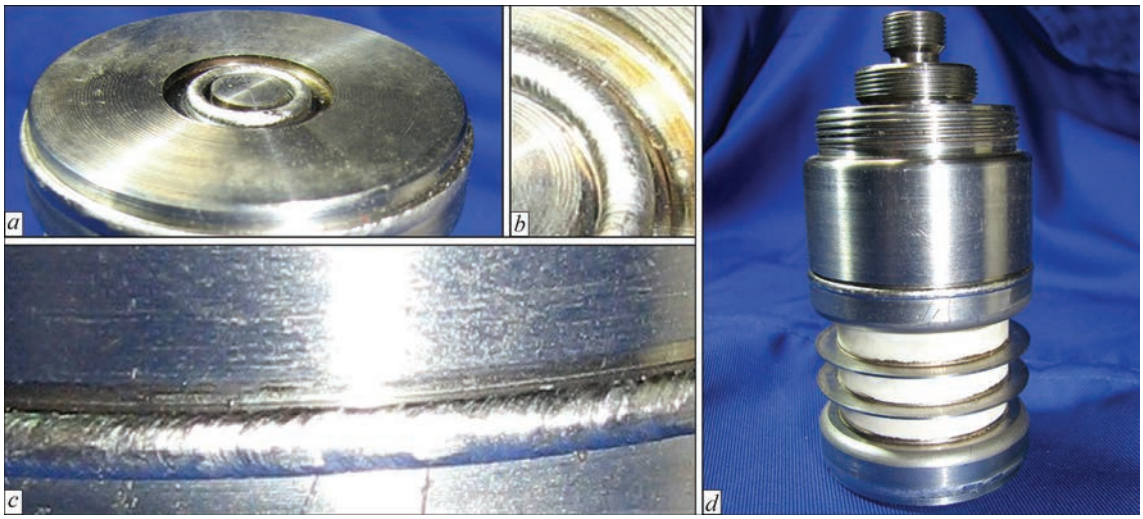

Figure 4. Fragments of welds of different parts of CU (*a*–*c*) and its general appearance as-assembled (*d*): *a* — top view on the lid of CU with welds No.4 and 5; *b* — fragment of weld No.5; *c* — fragment of weld No.1

simplify the welding scheme at the final stage. Such a scheme allowed reducing the risk of both lack of penetration as well as burn out of a thin side wall of CU. On the other hand, the probability of overheating the area near the brazed joint (flange with insulator) and, as a consequence, a violation of its vacuum density were eliminated. After completion of all welding stages, the geometric dimensions of CU were within tolerance. At the same time the time of preparatory works before welding was significantly shortened without reducing the accuracy of assembly of such products. Figure 5 shows CU as-assembled with a high-voltage insulator.

The technique of assembling thin-walled high-precision welded structures, the corresponding welding devices and the ways of their improvement are described in the literature [4, 5].

We developed a set of welding equipment for the assembly-welding of electrodes in CU and a subsequent welding into the EBG insulator.

The welding equipment represents a set of cylindrical frames, which are fixed on the rotating device, depending on the stage of welding process, (Figure 6, *a*).

Figure 5. Appearance of CU as-assembled with insulator: *1* — insulator; *2* — CU; *3* — weld

EBW of the cathode unit is a precision process and requires a minimal axial and radial beating of rotating device. With this aim, the welding equipment was manufactured in such a way that its attachment together with a welded products occurs directly on the shaft of the rotating device.

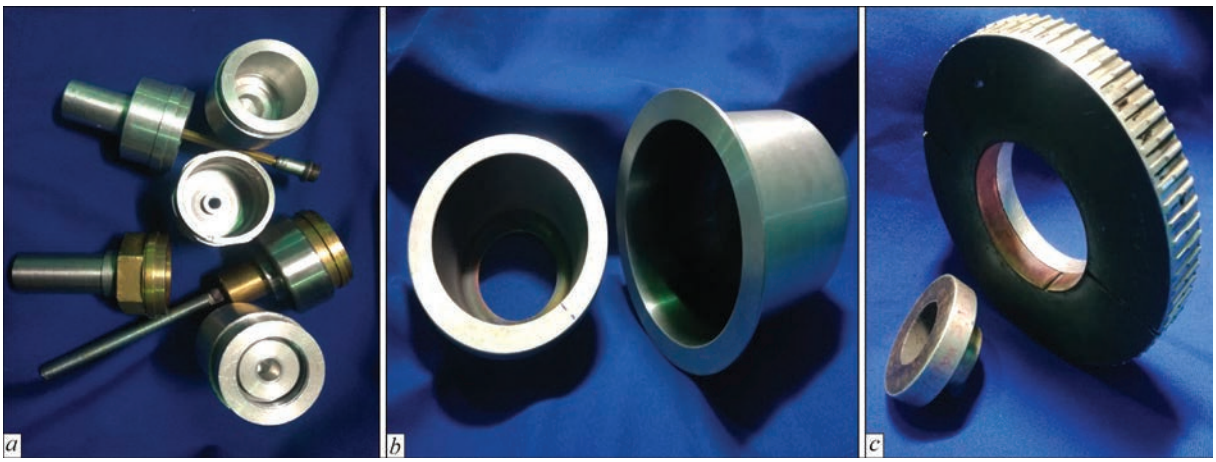

Figure 6. Welding equipment (*a*), screening device (*b*) and heat removing equipment (*c*)

Such a solution allowed minimizing the need in a software adjustment of the electron beam position relative to the butt joint during welding.

During assembly of parts for welding, the absence of a gap on the end surfaces and a guaranteed tension on the cylindrical ones were provided.

To protect the interelectrode space of CU of the electron optics from contamination with metal vapors during EBW at an operating power and avoiding short circuits of electrodes as a result of that, insulating spacers, caps and shields of nonmagnetic material were used (Figure 6, *b*, *c*). In case of welding-on bushing of the Wehnelt electrode the heat-removal equipment with a non-magnetic material of ring type with a copper insert was additionally applied (Figure 6, *c*).

Finally it can be noted that due to changes introduced to the design of CU, development of EBW technology, including on the pulsed mode, the experimental industrial batch of CU for domestic EBGs with accelerated voltage of 60 and 120 kV was manufactured.

Conclusions

1. The optimal design of the cathode unit (CU) and assembly-welding device were developed.

2. The order of assembly and welding of the cathode unit was proposed, which allowed eliminating the losses of a shape of a product, burn outs and contamination of CU electrodes with metal vapors.

3. The possibility of using EBW as a final operation during manufacture of CU was grounded providing operation reliability of the whole unit, including its connection to insulator.

1. Kostin, A.M., Labartkava, Al.V., Martynenko, V.A. (2014) Investigation of processes of interaction between titanium-containing brazing filler metal and oxide ceramics and covar. *Metallofizika i Novejshie Tekhnologii*, 36(**6**), 815–827 [in Russian].
2. Nazarenko, O.K., Lokshin, V.E., Patsiora, S.K. (1981) Reproducibility of spatial-time characteristics of welding electron beams. *Avtomatich. Svarka*, **8**, 41–43 [in Russian].
3. (1978) *Welding in machine-building*: Refer. Book. Vol. 2. Ed. by A.I. Akulov. Moscow, Mashinostroenie [in Russian].
4. Krampit, N.Yu., Krampit, A.G. (2008) *Welding accessories*. Yurga, YuTI TPU [in Russian].
5. Kurkin, S.A., Khovov, V.M., Rybachuk, A.M. (1989) *Technology, mechanization and automation of production of welding structures*: Atlas. Moscow, Mashinostroenie [in Russian].

Received 13.11.2019

https://doi.org/10.37434/tpwj2020.02.07

PROPERTIES OF JOINTS OF V1341T GRADE ALLOY UNDER THE CONDITIONS OF TIG WELDING

V.A. Koval, T.M. Labur and **T.R. Yavorska**
E.O. Paton Electric Welding Institute of the NAS of Ukraine
11 Kazymyr Malevych Str., 03150, Kyiv, Ukraine. E-mail: office@paton.kiev.ua

The paper presents the results of studying the weldability of sheet aluminium alloy of V1341T grade of Al–Mg–Si–Cu–Fe system under the conditions of manual nonconsumable electrode argon-arc welding. This alloy is characterized by high susceptibility to hot cracking in welding. The hot brittleness index is equal to A = 65.8–85.5 %. The impact of filler material chemical composition on hot cracking resistance of weld metal was studied. It is found that in welding by batch-produced wires of ZvAMg63, Zv1201, Zv1217 grades the crack resistance value is A = 30.3–53.9 %, and at application of wire of ZvAK5 grade this characteristic of welds is equal to A = 6.6–19.8 %. Manual nonconsumable electrode argon-arc welding of V1341T alloy allows producing tight sound joints of this material with strength coefficient of 0.80–0.87, which also depends on filler wire chemical composition. The average value of ultimate strength of the alloy welded joints, made using different grades of filler wire is equal to σ_t = 199.2–209.0 MPa, and the yield limit $\sigma_{0.2}$ = 136.6–147.6 MPa; relative elongation δ = 4.0–5.2 %, and bend angle α = 40–65 deg. 7 Ref., 4 Tables, 5 Figures.

Keywords: aluminium alloy, manual nonconsumable electrode argon-arc welding, filler wires, welded joints, structure, mechanical properties, hot cracks

Degree of technical excellence of flying vehicles is directly related to mastering new structural materials, which have higher technological characteristics in addition to strength. This allows manufacturing complex-shaped products. Such materials include multicomponent heat-hardenable alloy of V1341T grade (Al–Mg–Si–Cu–Fe alloying system). It also contains chromium and zirconium additives (Table 1). This alloy is designed for manufacture of typical elements of aircraft structures, namely hanging tanks, small tanks, cylinders and other products of a complex configuration, which are welded predominantly by the manual method [1].

Up to now, V1341T alloy was mainly welded by automatic methods. Investigations as to its manual welding were not performed at all, but alloy introduction into the aircraft industry for fabrication of shell-type complex-shaped structures makes urgent the investigations of its weldability under the conditions of nonconsumable electrode manual argon-arc welding.

The objective of the work was assessment of the main weldability characteristics of V1341T alloy under the conditions of nonconsumable electrode manual argon-arc welding, as well as establishing the technological possibilities of the alloy application in welded structures for aircraft construction. Selected as the weldability evaluation criteria, were the values of hot cracking resistance of weld metal and level of mechanical properties of the joints at application of fillers of different chemical composition, as well as determination of optimum conditions of sound weld formation.

Investigations were conducted on sheets 1.2 mm thick in T condition (quenching at 530 °C in water and natural ageing), which have the strength limit of 250–250.8 MPa.

The process of hot cracking in V1341T alloy under the conditions of manual nonconsumable electrode argon-arc welding was studied using «fishbone» type sample (Houldcroft samples) [2, 3]. Welding heating was performed from inverter type power source MW2000 of Fronius Company in the following modes: I_w = 54–56 A, U_a = 11.2–12.4 V. Technolog-

Table 1. Chemical composition of V1341T alloy and of the studied filler wires, wt.%

Wire grade	Mg	Mn	Cu	Si	Fe	Cr	Ti	Zr	Zn
V1341T, base metal	0.65	0.16	0.30	0.80	0.14	<0.10	0.03	<0.10	0.04
ZvAMg63	6.30	0.60	Traces	0.05	0.05	–	0.04	0.25	–
ZvAK5	–	–	0.15	5.60	0.24	–	0.12	–	–
Zv1201	0.02	0.30	6.50	0.08	0.12	–	0.12	0.15	0.04
Zv1217	–	–	10	0.02	0.04	Sc = 0.15	0.10	0.24	–

V.A. Koval — https://orcid.org/0000-0001-5154-1446, T.M. Labur — https://orcid.org/0000-0002-4064-2644,
T.R. Yavorska — https://orcid.org/0000-0003-2016-6289

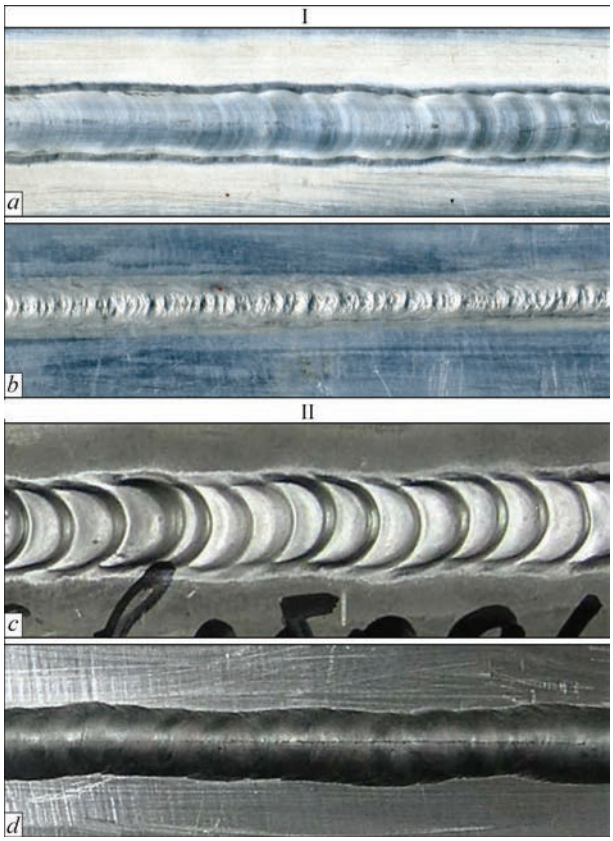

Figure 1. Appearance of face surface (*a*, *c*) and weld root (*b*, *d*) of welded joints of V1341T alloy, produced by manual arc welding without (I) and with filler wire application (II)

ical heating of V1341T alloy revealed its high sensitivity to hot cracking. The hot brittleness index in manual welding of this alloy without wire application was at a rather high level A = 65.8–85.5 %, that may be indicative of formation of an eutectic under the welding conditions and increase of the solidification range, as a result of lowering of the nonequilibrium solidus temperature [2, 3]. Results of testing 7–9 samples showed that formation of the main crack occurs in the weld center.

Table 2. Hot brittleness index (A, %) of V1341T alloy joints, produced using fillers of different composition

Wire grade	Main alloying elements, wt.%			Crack length, L_{cr}, mm	Crack resistance value $A = L_{cr}/L_{samp}$, %
	Mg	Cu	Si		
ZvAMg63	6.30	–	–	34–49	25–61.8 45.4
Zv1201	–	6.50	–	23–49	44.7–64.5 54.9
Zv1217*	–	10	–	23–42	34.4–52.6 39.6
ZvAK5	–	–	5.6	5–15	5.9–19.8 9.5

*Sc = 0.15 wt.%.

It is known [1, 3] that one of the methods to increase the hot cracking resistance of aluminium alloys in welding can be application of filler wire, which differs from the base metal by its composition. Here, its function consists in creation in the weld pool central zone of a certain metal volume in the solid-liquid state with uniform mixing of alloying components, which is a broad temperature range. This promotes healing of cracks, which form in the weld metal during its solidification [2].

Usually, there exists the possibility of application of several filler wire grades for welding each aluminium alloy. Their selection depends on the requirements to technological characteristics of the base metal and its welded joints in the product, such as: hot cracking resistance, strength, ductility and corrosion resistance. At the same time, it is practically impossible to obtain welded joints with the highest values of all the characteristics, as the maximum values of each of them are achieved at a certain combination of alloying element composition, present in the initial metal and filler wire. In this connection, in welding aluminium alloys, either general purpose wire, which provides rather high levels of the main mechanical properties of welded joints, or wire, which guarantees increase of one of these characteristics at satisfactory values of others [4]. Final selection of filler wire grades is determined by the conditions of fabrication and operation of the welded structure. Therefore, we studied the effect of chemical composition of several batch-produced 2 mm filler wires of different grades: ZvAMg63, ZvAK5, Zv1201, and Zv1217 on weldability of V1341T alloy (see Table 1).

Full penetration butt joints were produced in optimum modes, in order to evaluate the crack resistance of weld metal and conduct mechanical testing of welded joints of V1341T alloy. Technological reinforcement and weld root were removed on them with the purpose of making «fishbone» samples in keeping with the generally accepted procedure [2]. After that, repeated melting was performed along the weld by a welding arc in the mentioned modes, using filler wires of the above mentioned grades. Appearance of the produced welds after welding is shown in Figure 1. Results of crack resistance evaluation are given in Table 2, which shows the main alloying elements, promoting lowering of hot brittleness in aluminium alloys.

Analysis of the results of testing 8 to 10 samples, produced using each filler wire, showed (see Table 2) that hot crack formation also proceeds in the weld central part in the form of one main crack (Figure 2). At application of ZvAMg63, Zv1201, and Zv1217 fillers the hot cracking susceptibility remains high (A = 39.6–54.9 %). In the authors' opinion, the

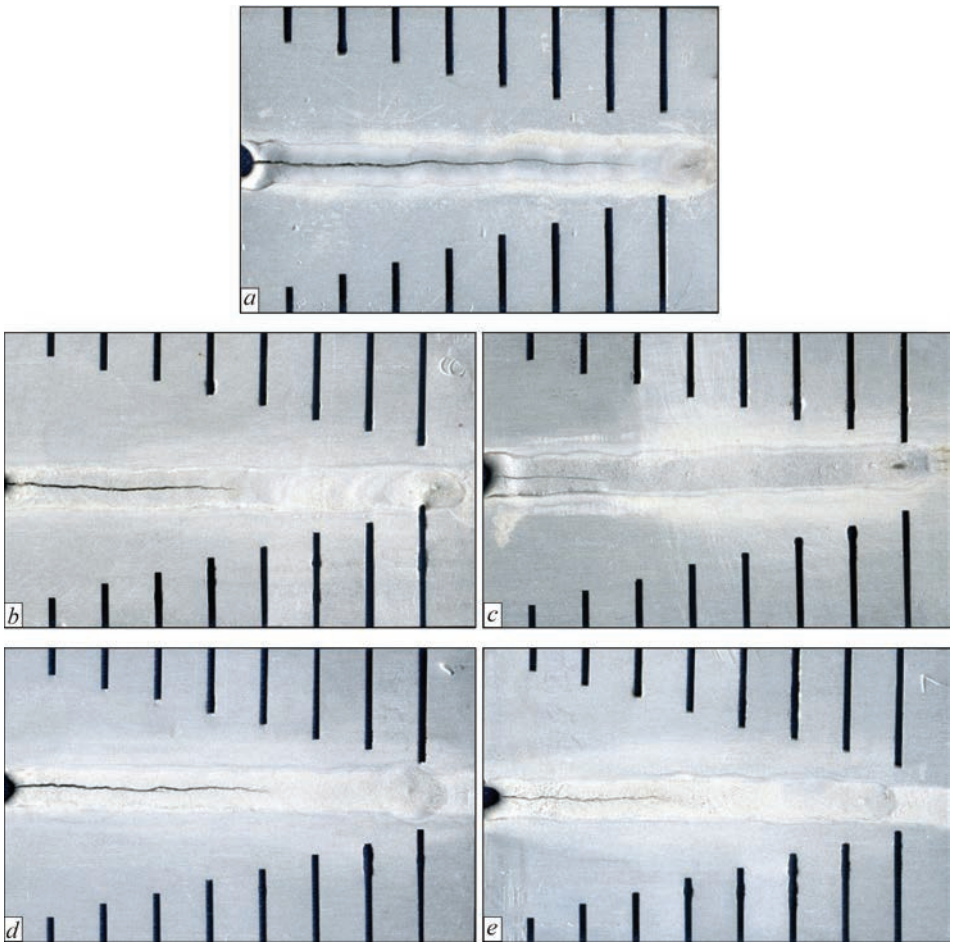

Figure 2. Hot cracking susceptibility of V1341T aluminium alloy 1.2 mm thick at manual nonconsumable electrode argon-arc welding, depending on filler wire chemical composition: *a* — without filer; *b* — ZvAMg63; *c* — ZvAK5; *d* — Zv1201; *e* — Zv1217

above-said can be associated with the presence of a significant quantity of low-melting eutectics based on Mg_2Si, which widen the temperature limits of the solid-liquid state of the metal and lead to increase of the extent of its shrinkage in the weld [5]. A positive effect was achieved at application of filler wire of ZvAK5 grade, containing up to 6 % silicon. Weld metal here has maximum values of crack resistance characteristic A = 5.9–19.8 %, compared to other wires. This occurs due to greater penetrability («healing» effect) of silicon-based eutectic [5, 6].

In order to determine the weld quality in manual nonconsumable electrode argon-arc welding, the welded joints were examined visually and using X-Ray inspection at standard sensitivity of 0.1 mm with further preparation of macrosections to study the nature of weld formation. X-Ray films were interpreted in «Densitomed» instrument, which allows determination of the metal density. Results of their analysis showed that no coarse defects classified as cracks, lacks-of-penetration, concentrated and scattered porosity of 0.5 mm and greater

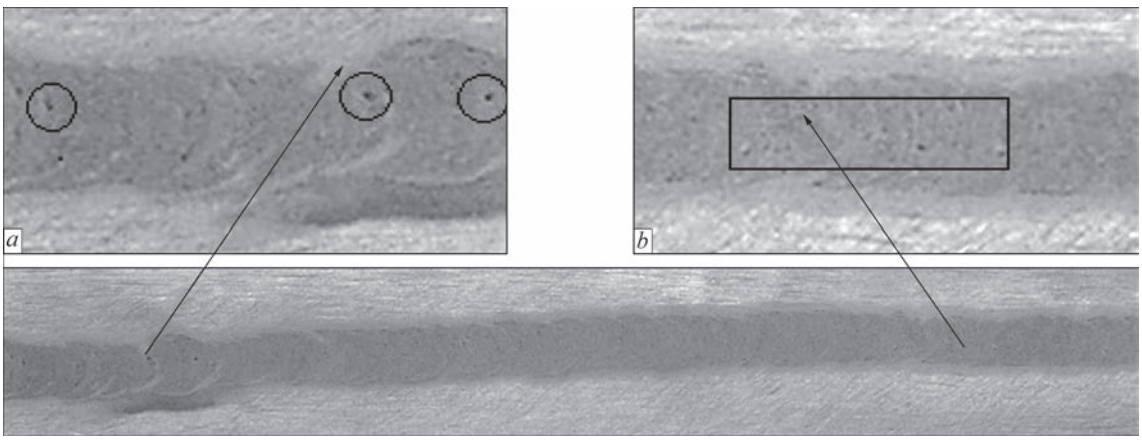

Figure 3. Surface of V1341T alloy weld after removal of technological reinforcement: *a* — isolated defects; *b* — scattered defects

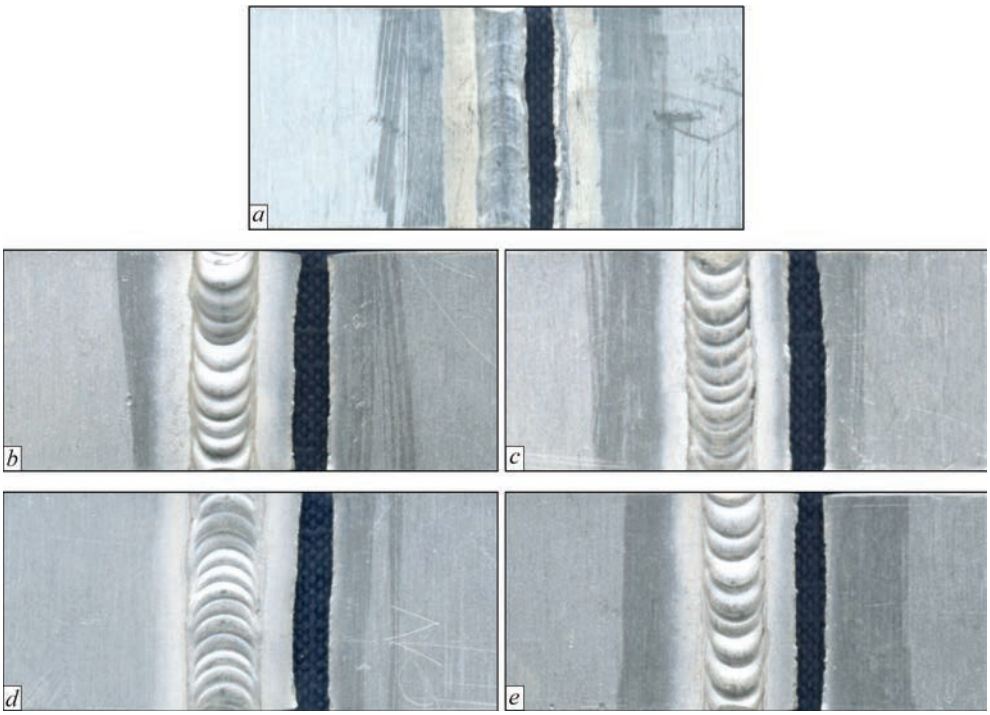

Figure 4. Fracture mode of samples of V1341T aluminium alloy 1.2 mm thick, produced by manual nonconsumable electrode welding, using different filler wire grades and without wire: *a* — without wire; *b* — ZvAMg63; *c* — ZvAK5; *d* — Zv1201; *e* — Zv1217

size are found in the joints. At visual examination of the weld surface after removal and grinding of the technological reinforcement, isolated scattered pores of up to 0.08 mm size are observed, that is 6 times lower that the admissible norms. The distance between the fine pores is equal to 11.0–15.0 mm, and the total extent is 7–8 mm on a weld section of 100 mm length (Figure 3). This is also two times smaller than the admissible values [7].

Geometrical parameters of the welds were determined by an electronic caliper APT-34460-150 with division value of 0.01 mm, and measurement accuracy of 0.03 mm. Measurement results showed (Table 3) that the optimum value of weld form factor, calculated

Table 3. Geometrical parameters and form factor of welds, produced in manual argon-arc welding of V1341T alloy (δ = 1.2 mm)

Symbols	Values of geometrical parameters of welds, mm		Weld form factor $K = \frac{B}{(b+\delta)}$	
	minimum	maximum		
Weld width *B*	3.53−4.86	4.92−5.60	2.43	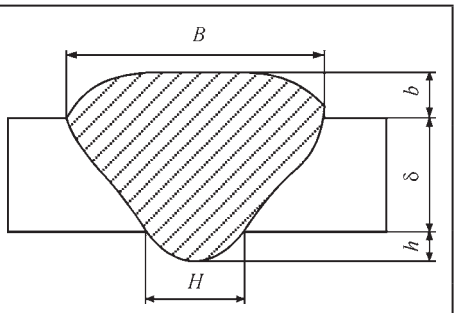
Weld root width *H*	3.15−4.15	4.2−5.1		
Technological reinforcement height *b*	0.23−0.7	0.8−1.3		
Weld root height *h*	0.17−0.68	0.85−1.15		

Table 4. Mechanical properties of welded joints of V1341T alloy 1.2 mm thick, made by manual nonconsumable electrode arc welding, using different grades of filler wires and without them

Filler wire grade	σ_t, MPa	$\sigma_{0.2}$, MPa	δ, %	α, deg	Strength coefficient
Without filler	125.3−153.3 139.0	110−144.6 130.0	0.7−1.4 0.9	30−37	0.55
ZvAMg63	196.3−207.1 199.9	141.2−144.1 142.7	3.6−5.4 4.5	55−60 58	0.8−0.82
ZvAK5	190.5−209.2 202	138.4−142.7 136.6	3.1−51.0 4.0	55−65 59	0.8−0.82
Zv1201	193.2−207.4 201.7	145.0−143.7 144.3	3.7−5.4 4.8	40−60 50	0.8−0.82
Zv1217	208.2−209.0 208.7	143.1−151.6 147.6	4.6−5.4 5.2	45−66 56	0.83−0.87

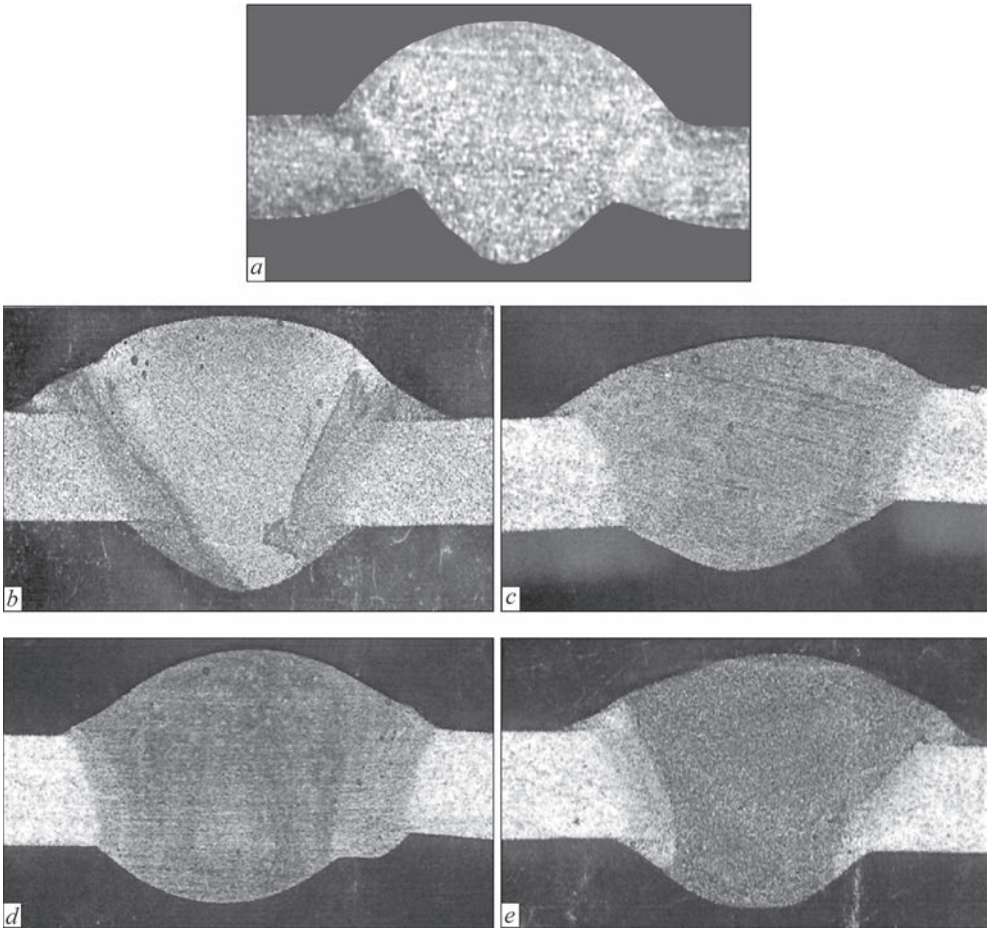

Figure 5. Microstructure of welded joints of V1341T alloy 1.2 mm thick, produced by manual nonconsumable electrode argon-arc welding without filler and using fillers of different grades: *a* — without filler; *b* — ZvAMg63; *c* — ZvAK5; *d* — Zv1201; *e* — Zv1217

by formula $K = 1(h + g)$, is 2.43 for the studied joints that corresponds to the admissible values, in keeping with normative documentation (GOST 14806−80).

Mechanical properties of welded joints of V1341T alloy were determined at testing standard samples for stretching and bending, which were cut out of butt welded joints. The samples had a technological reinforcement and weld root. Their fracture occurred along the HAZ at 3–5 mm distance from the fusion line (Figure 4). Results of mechanical testing showed that the ultimate strength and yield limit of the joints after welding are equal to σ_t = 200–208.7 MPa, $\sigma_{0.2}$ = = 136.6–147.5 MPa, irrespective of filler wire grade. The greatest values of relative elongation characteristic (δ, %) were obtained, when using filler wire of Zv1217 grade (Table 4). The strength coefficient of the weld here was equal to 0.83–0.84, compared to base metal value (σ_t = 250.8 MPa).

Ductility value α, obtained under the conditions of three-point bending of samples of a welded joint of V1341T alloy, produced with ZvAK5 and ZvAMg63 wires, is equal to 59–58 deg, respectively. In the case of application of filler wires Zv1201 and Zv1217, this welded joint characteristic is equal to 50 and 56 deg, respectively. The value of bend angle of all the welded joints decreases 4 to 6 times, compared to that of the base metal (α = 180 deg) (see Table 4).

For comparison with the mentioned joints, welds were made by manual argon-arc welding over «raised edges», i.e. without filler application (Figure 1, I). As shown by mechanical testing, such joints of V1341T alloy have low mechanical properties. The values of their ultimate strength and yield limit are smaller by 50, 30 MPa, compared to welds, produced using fillers. Values of relative elongation δ and bend angle α here decrease 4 and 2 times, respectively. The strength coefficient of the joint is equal to just 0.55 of that of the base metal (see Table 4). Deterioration of mechanical properties of welds, made without the filler, is, probably, due to the presence of stress raisers from weld root side, in the form of sharp-angled depressions in the zone of its fusion with the base metal and smaller cross-sectional area of the weld (Figure 5, *a*).

Macrostructure of welded joints of V1341T alloy was studied on transverse sections, which were cut out of the weld central part. In order to reveal their features, chemical etching was performed in a solution, which consists of three acids: 72 ml HCl + 24 ml HNO_3 + 4 ml HF. Metallographic analysis of welded joint macrostructure showed that, irrespective

of chemical composition of the used wire grades, all the welds are characterized by fine-grained uniform structure and absence of coarse defects (Figure 5, *c*–*e*). In the joint zone near the weld, areas with different degree of etching are observed, that reflects the impact of gradient conditions of the thermal cycle of welding on the morphology of structural transformations in the metal.

Conclusions

1. It is found that under the conditions of manual nonconsumable electrode argon-arc welding, aluminium alloy V1341T is characterized by a high susceptibility to hot cracking. The value of metal hot brittleness is A = 65.8–85.5 %. Application of filler wires lowers the hot cracking susceptibility of the alloy. In welding with batch-produced wires of ZvAMg63, ZV1201, Zv1217 grades, the hot brittleness value is A = 30.3–53.9 %, and when wire of ZvAK5 grade is used, this value for welds is equal to A = 6.6–19.8 %.

Application of manual nonconsumable electrode argon-arc welding of sheet aluminium alloy V1341T allows producing tight sound joints of this material with strength factor equal to 0.80–0.84 of base metal level, depending on chemical composition of filler wire grade. X-Ray inspection of the joints showed the absence of coarse defects in welds. At visual analysis of their face surface without the technological reinforcement, scattered pores of up to 0.08 mm size are observed that is 6 times lower than the admissible norms. Distance between the fine pores is 11.0–15.0 mm. Total extent of the fine pore line is equal to 7–8 mm on a 100 mm long section of the weld.

3. It is found that the average value of ultimate strength of the alloy welded joints, using different filler wire grades is σ_t = 199.9–209.0 MPa, and yield limit $\sigma_{0.2}$ = 136.6–147.6 MPa, relative elongation δ = = 4.0–5.2 %, bend angle α = 40–65 deg. Samples of the alloy welded joints fail in the base metal in the HAZ at the distance of 3–5 mm from the fusion line, irrespective of chemical composition of applied filler wires. Such a nature of fracture in this zone is due to the alloy sensitivity to technological heating, as a result of alloying component redistribution that lowers its strength.

4. Welded joints produced without filler wire application, are characterized by a lower level of mechanical properties: σ_t = 125.3–153.3 MPa, $\sigma_{0.2}$ = 110–144.6 MPa, δ = 0.7–1.4 %, α = 30–37 deg, compared to joints, produced with filler wires. Strength factor here is equal to 0.55. Proceeding from the obtained data, it should be noted that wire of ZvAK5 grade is the best one for reducing the hot cracking susceptibility of welds in manual welding of V1341T alloy, and if a complex of mechanical property values should be provided, this is Zv1217 wire. Nonconsumable electrode manual arc welding without filler is not allowed, when joining V1341T alloy.

1. Milman, Yu.V. (2008) *New high-strength aluminium alloys. Actual problems of modern materials science*. Vol. 1. Kiev, Akademperiodika, 597–612 [in Russian].
2. Ishchenko, A.Ya. (2008) Welding of aluminium alloys. *Inorganic materials science. Materials and technologies*. Vol. 2, Book 2. Kiev, Naukova Dumka, 238–253 [in Russian].
3. Yushchenko, K.A., Derlomenko, V.V. (2008) *Welding and weldability (joinability) of materials. Inorganic materials science. Materials and technologies*. Vol. 2, Book 2. Kiev, Naukova Dumka, 268–276 [in Russian].
4. Ishchenko, A.Ya., Labur, T.M. (2013) *Welding of modern structures of aluminium alloys*. Kiev, Naukova Dumka [in Russian].
5. Rabkin, D.M. (1986) *Metallurgy of fusion welding of aluminium and its alloys*. Kiev, Naukova Dumka [in Russian].
6. Lashko, N.F., Lashko-Avakyan, S.V. (1960) *Weldable light alloys*. Leningrad, Sudpromgiz [in Russian].
7. (2015) *DSTU EN ISO 10042:2015 (EN ISO 10042:2005, IDT; ISO 10042:2005, IDT)*: Welding — arc-welded joints in aluminium and its alloys. Quality levels for imperfections [in Ukrainian].

Received 11.12.2019

FEBRUARY 1, 1941 Production of Sherman tank began in the USA. Compared to riveted tank M-3, it had a larger caliber gun (75 mm), cast or welded turret. Pullman-Standard Company participated in fulfillment of the program on all-welded tank production. It developed the technology of welding the hull and turret. A conveyor line for hull assembly and welding was organized. Multilayer manual arc welding was performed in the downhand position, and after that the structure was installed into positioners. Automatic submerged-arc welding in equipment developed already in 1940, was used only for producing the heaviest part — tank wheels from low-carbon steel.

https://doi.org/10.37434/tpwj2020.02.08

ADDITIVE ELECTRON BEAM EQUIPMENT FOR LAYER-BY-LAYER MANUFACTURE OF METAL PRODUCTS FROM POWDER MATERIALS

V.A. Matviichuk and **V.M. Nesterenkov**
E.O. Paton Electric Welding Institute of the NAS of Ukraine
11 Kazymyr Malevych Str., 03150, Kyiv, Ukraine. E-mail: office@paton.kiev.ua

On the basis of small-sized equipment SV-212M for electron beam welding, a mock-up of additive technological equipment was created to reproduce the process of manufacturing parts according to set shape and properties, applying the method of layer-by-layer surfacing with the use of metal powder materials. A hardware and software platform for the control of equipment was developed, which was integrated into additive technological equipment. The platform consists of hardware controller, which was developed on the basis of the industrial controller cRIO-9039 produced by the National Instruments Company (USA) and software for 3D-printing. On the created equipment, a test specimen of the product of a set shape with the following geometric dimensions: outer diameter — 85 mm, inner diameter — 55 mm, height — 35 mm was produced. For manufacturing, the powder of VT-20 titanium of the domestic Ti-Technology Company was used. Metallographic examinations of the specimen were carried out. It was established that the surfacing structure in the body of crystallites mainly has a branchy α′-phase and a small amount of (β-phase, which is characteristic of cast titanium alloy VT-20. The grain boundaries are pure, without inclusions. Parts of the specimen are without pores, which evidences about a complete penetration of the powder layer in the process of 3D-printing. The hardness of the metal in all the areas is not significantly different and is in the range from *HV* 3960 to *HV* 4150 MPa. According to the results of investigations the conclusions were made. 10 Ref., 1 Table, 13 Figures.

K e y w o r d s : additive technologies, electron beam, surfacing, metal powder, titanium alloy, control platform, metallography, investigations

Innovative technologies of layer-by-layer manufacturing of products by the method of rapid prototyping open up new opportunities for production of parts of a set shape and structure with predicted properties.

The process of manufacturing products applying this method with the use of the electron beam is relatively new, but it has already successfully demonstrated the great prospects of its application in the industry for the production of a wide range of parts and units. It is based on the operation of layer-by-layer fusion of a metal powder in vacuum by an electron beam. This approach is distinguished by a rapid transition to the production of three-dimensional products directly from the system of automated design with the possibility of using a wide range of metals and alloys, including refractory and chemically active ones [1].

All the existing industrial specimens of similar equipment are owned by foreign companies. There is no domestic equipment of serial production [2].

From the very beginning, the technologies and equipment created by the E.O. Paton Electric Welding Institute of the NAS of Ukraine (PWI) [3] are oriented on the needs of Ukrainian enterprises. For manufacturing the user is supposed to apply necessary domestic inexpensive raw materials. Such an approach allows providing the manufacture of parts and units based on the needs of a customer and staying in close contact with him. The developed technologies will provide shortening of terms for introduction of new types of products into manufacturing, expanding their assortment and also creating principally new types of products with preliminary predicted properties, the production of which is impossible without using the methods of 3D-printing [4].

The aim of the work is the creation of the equipment for additive manufacturing of parts of a preset shape and the structure using the method of layer-by-layer electron beam surfacing of metals in vacuum with the use of powder materials.

For this purpose it is necessary:

- to develop the design documentation of the main units of additive equipment and manufacture the experimental laboratory equipment;

*Based on materials presented at 9th International Conference «Beam Technologies in Welding and Materials Processing», September 9–13, 2019, Odessa, Ukraine.

V.A. Matviichuk — https://orcid.org/0000-0002-9304-6862, V.M. Nesterenkov — http://orcid.org/0000-0002-7973-1986

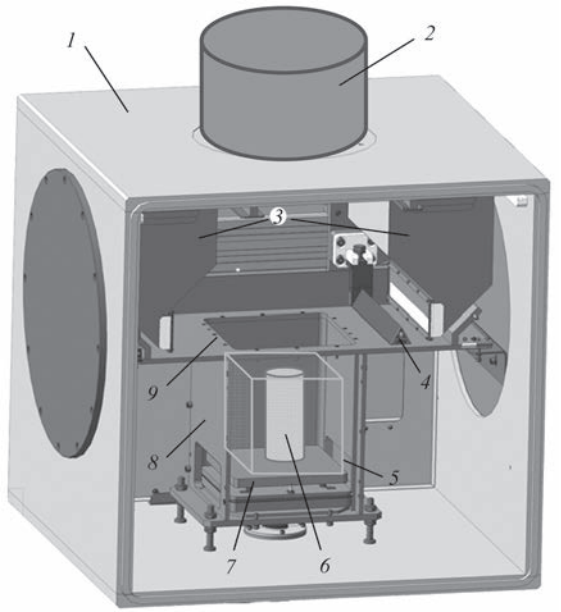

Figure 1. Scheme of equipment for additive production using metallic powder materials (see description *1*–*9* in the text)

- to develop software for investigations;
- to develop additive electron beam technologies and also investigate the properties of multilayer deposited metal;
- to create industrial model of equipment in the set with the software.

The urgent task is to develop installations based on electron beam processes using domestic powder materials, which will be certified and oriented for introduction at domestic enterprises [5].

A significant interest to the developed technologies is in the aerospace industry, power engineering, defense industry, as well as in the enterprises manufacturing products of biomedical purpose. In recent years, there has been a noticeable tendency for the introduction of additive technologies in the leading domestic companies of the aerospace industry and turbine construction: SE «Yuzhoye Design Office», JSC «Motor Sich» and SE «Zorya»–«Mashproekt» [6].

Figure 2. Equipment for electron beam 3D-printing (see description 1–4 in the text)

Equipment. To solve the specified problems, the investigations were carried out using the equipment for 3D-printing, which was created on the basis of small-sized equipment for electron beam welding of type SV-212M [7]. The equipment was used as a part of the pulsed power source of 60kV/60kW and the electron beam gun ELA-60. The equipment was developed at the PWI.

Principle of operation. The process of electron beam surfacing occurs in the vacuum chamber *1* (Figure 1). The metal powder is supplied in a bulk to the worktable *9* from the hoppers *3*. The rail *4* moves along the table *9* and on the surface of the pallet *7* it forms a layer of powder of a set thickness. In the starting position the platform stays at the top of the mine *8*. A focused electron beam formed by the electron beam gun *2* melts the powder surface along a set trajectory. Thus, according to the algorithm, the contour of the product and its layer are formed. Then, the platform *7* is lowered and the next layer of powder is deposited. The process is repeated. The product *6* is grown layer by layer. At the end of the manufacturing cycle, the workpiece should be removed from the vacuum chamber, cleaned from the nonmolten powder *5* and machined [8].

The general view of the laboratory equipment for 3D-printing is given in Figure 2.

The equipment consists of a small-sized vacuum chamber *1* with the mechanisms for moving along the vertical as well as mechanisms for supplying and distribution of the powder in the horizontal plane. The equipment includes electron beam gun *2* and high-voltage power source *4*. The electron beam gun is located on the top of the vacuum chamber. The vacuum system provides a value of vacuum of up to 10^{-4} Torr in the chamber. The elements of the equipment control system are located in cabinets *3*, where industrial computer, process controller, monitor, units for control of high-voltage source and vacuum system are located. A high-voltage source allows obtaining a regulated voltage of up to 60 kV and a beam current of electrons of up to 1000 mA [9].

The photo of the vacuum chamber is shown in Figure 3, and of the high-voltage source is in Figure 4.

Control system. Figure 5 presents a block diagram of the system of equipment control for 3D-printing.

The formation and preliminary treatment of the product model take place in a top-level computer that interacts with the MCP controller through Ethernet.

The MCP controller is created on the platform of the industrial controller cRIO-9039 with a preliminary installed peripheral modules.

To the MCP controller the following components are connected:

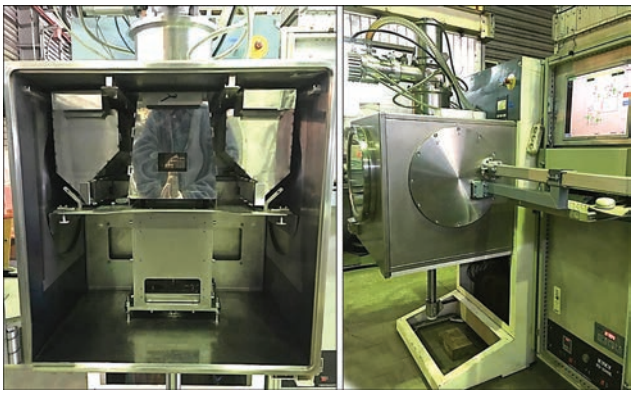

Figure 3. Vacuum chamber of additive equipment

- high-voltage source of 60 kV/60kW;
- electric drive of the movement system Siemens Sinamics S120;
- amplifiers of scanning and dynamic focusing.

MCP generates analog signals for controlling the electron beam scanning along the axis *X*/*Y*, the signals to control focusing — static and dynamic, and a signal for the electron beam current control. The scanning signals are supplied to the power amplifiers which control the current in the deflection coils of the electron beam gun (EBG). The signal of dynamic focusing I_{fd} is supplied to the power amplifier that controls the current in the coil for dynamic focusing of EBG. MCP also generates the analog signals for controlling the electron beam current I_w and the static focusing current I_f. These signals form quick-response modules of analog outputs NI-9263. The signals are supplied to the Normalizer converter, which is located in the crate of the high-voltage source. The converter converts analog signals into digital code according to the CAN bus protocol.

MCP controls the drives of the 3D printer: the drive of the mechanism for moving the platform along the vertical and the mechanism of distribution of metal powder in the horizontal plane. Through the Profibus bus the control signal from the MCP is supplied to the frequency converters Siemens Sinamics S120, which control the electric motors Siemens Simotics 1FK7 for the movement system.

The MCP interacts with the industrial computer that operates under the control of the operating system Windows 10 through the Ethernet network. Through the CAN bus the computer controls the high-voltage source of the 3D printer.

Software and hardware platform. In order to control the equipment and realization of the processes of additive manufacturing, the software and hardware platform was developed, consisting of the process controller-the hardware part and the package of application software.

The hardware part consists of:

Figure 4. High-voltage source with control cabinet

- MCP process controller.

The software consists of:

- Magics — the program for editing files of a model product;
- BuildProcessor — the program for geometric construction of a part on the platform;

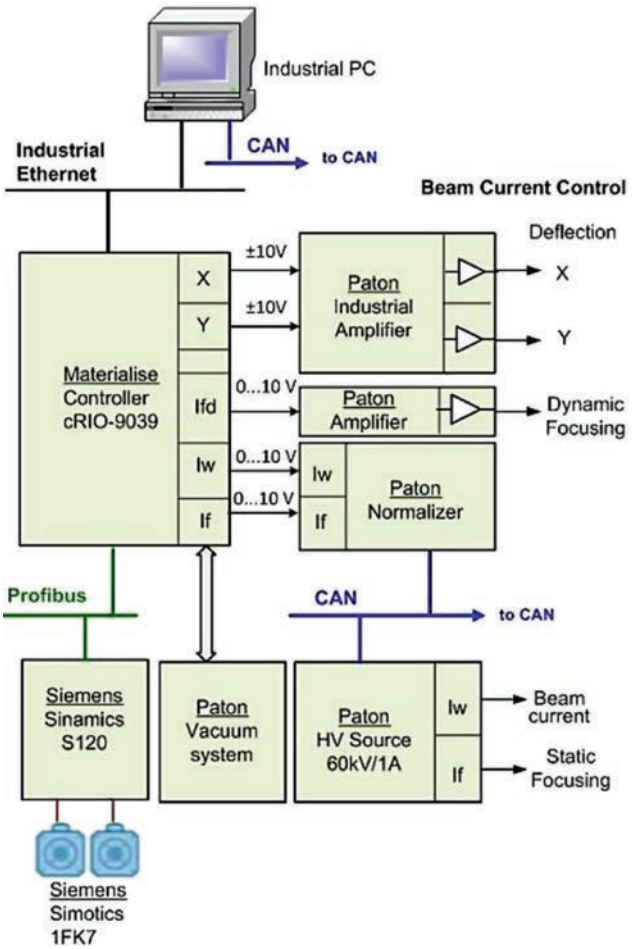

Figure 5. Block diagram of equipment control

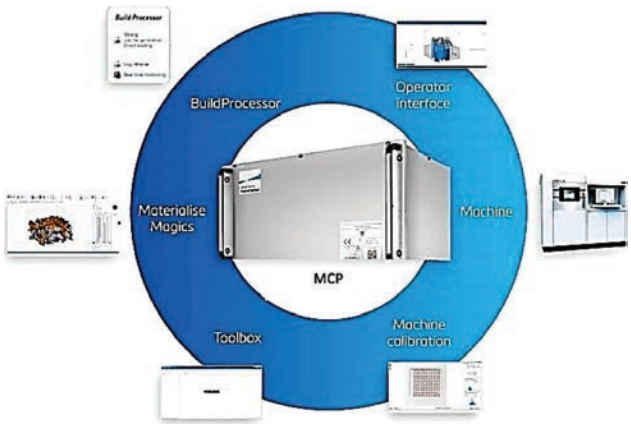

Figure 6. Structure of control platform

Figure 7. Interface of MCP controller

● Operator interface — the human-machine interface;

● Toolbox — the tool for adjustment of the process controller.

The structure of the control platform and the state of interactions between its components are presented in Figure 6.

The function of the Machine calibration is realized in the program Toolbox.

Peripheral modules of MCP controller

Type	Description
CS-PBMC	Profibus bus module
NI-9263	4-channel module of analog outputs, ±10 V
NI-9401	8-channel module of quick-response TTL outputs
NI-9425	32-channel module of discrete inputs, 24 VDC
NI-9477	32-channel module of discrete outputs
NI-9205	32-channel module of analog inputs, ±10 V

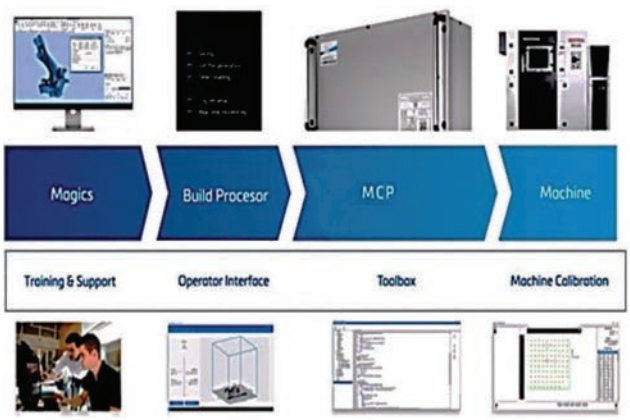

Figure 8. Interconnection between structural elements of control platform

The MCP controller is required to control the additive process equipment. The controller was developed by the experts of PWI together with the Company Materialise (Belgium) on the platform of the industrial controller cRIO-9039 produced by National Instruments (USA) (Figure 7).

The controller is equipped with peripheral modules (Table).

Software. The interconnection between the structural elements of the control platform is shown in Figure 8.

3D models of the product were created and edited using the program Magics. For this purposes any other software of the type CAD, such as NX Program of Siemens Company is also may be used.

Figure 9 provides the interface of the program Magics, where the model of a product is located — rotor blade of the gas turbine engine and technological supports are formed, which in the process of printing allow maintaining the shape of a part and reducing thermal contact with the platform.

The computer model of a product, which is prepared for printing, is further processed by the program BuildProcessor. This program allows creating assemblies of different parts on the equipment platform, de-

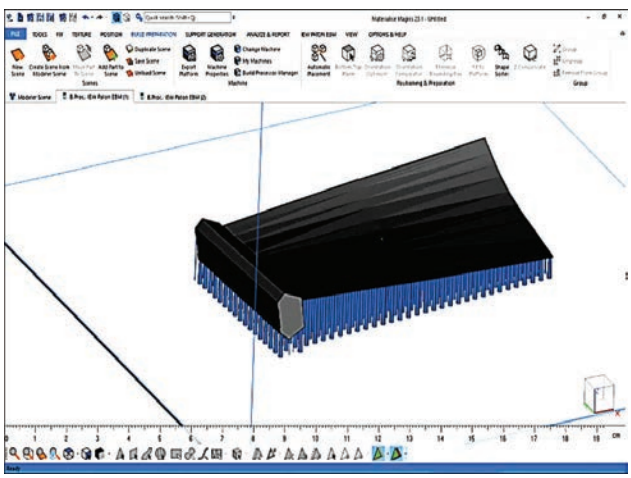

Figure 9. Interface of Magics program

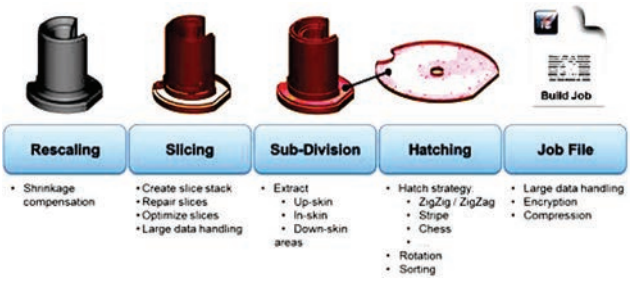

Figure 10. Functions of BuildProcessor program

composing models into layers, setting parameters and structure of forming each of the layers, determining the electron beam power, the speed of its movement and the diameter of the electron beam. The program allows choosing the material of a product and the variants of a texture to fill the layers during printing.

BuildProcessor forms an executive job-file, which is supplied to the MCP controller. Using job-file, MCP controls the process of 3D-printing.

The functions of BuildProcessor and the sequence of technological operations are presented in Figure 10.

The process of 3D-printing is controlled by the Operator interface program. In this program the technological parameters of the equipment are set and also the process of printing is monitored and displayed in real time. The program allows selecting a file of a model product, determining the time of beginning and end of the manufacturing process and its stage. The program has a three-dimensional print visualization. The appearance of the interface of the Operator interface program is shown in Figure 11.

The adjustment of the process controller and calibration of the 3D printer is performed by using the Toolbox program.

The PLC program was created to control the high-voltage source. This program allows controlling the voltage of high-voltage source, electron beam current, current and voltage of cathode bombardment, focusing current and also controlling these parameters.

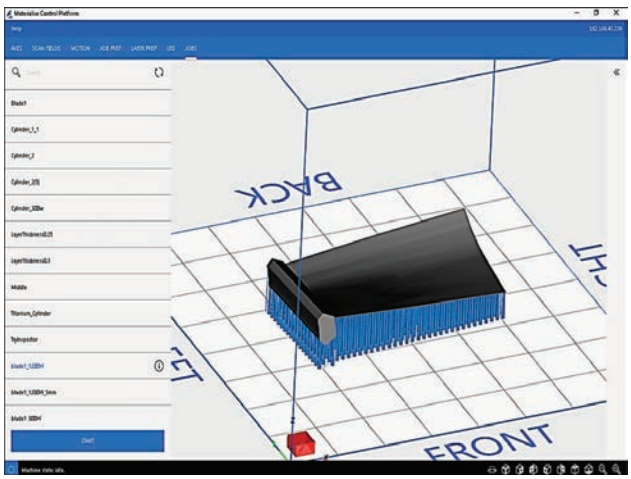

Figure 11. Operator interface program

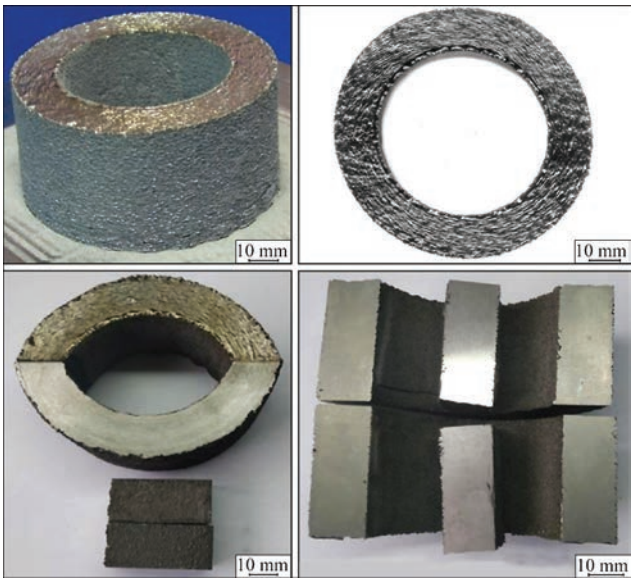

Figure 12. Specimen of product

The program has a function of monitoring and recording the current state of the high-voltage source in time.

Specimens of products. In the created equipment, an experimental product of a set shape (Figure 12) was produced with the following geometric dimensions: outer diameter — 85 mm, inner diameter — 55 mm, height — 35 mm. A photo of the printed product located on the platform in the vacuum chamber of the equipment is shown in Figure 13.

The parts were manufactured from the powder of titanium VT-20 produced by the domestic Ti Technology Company. The powder is an alloy of the Ti–Mo–Al–V–Zr system with granules of a nonspherical shape and a cast microstructure of particles. The choice of the alloy of this alloying system was predetermined by the fact that it is characterized by excellent anticorrosive, heat-resistant and mechanical properties. The alloy VT-20 is used for manufacturing parts of aircraft purpose, that are capable of operating for a long time at a temperatures of up to 500 °C [5].

The produced specimen was prepared for further metallographic examinations of the peculiarities of

Figure 13. Specimen of printed product

forming the structure of a product along and across the surfacing axis [10].

The carried out tests showed that the surfacing structure in the body of crystallites mainly has a branched α′-phase (supersaturated solid substitutional solution of alloying elements in α-titanium) and a small amount of β-phase. This is characteristic of the cast titanium alloy VT-20. The grain boundaries are clean, without inclusions.

The produced parts of the specimen are nonporous, which indicates a complete penetration of the powder layer in the process of 3D-printing.

The hardness of the metal in all the areas was not significantly different and ranged from *HV* 3960 to *HV* 4150 MPa.

Conclusions

As a result of the research and development works, the following was created:

- additive laboratory electron beam equipment;
- software and hardware platform for control of additive equipment;
- elements of additive electron beam technology of manufacturing metal parts applying layer-by-layer method with the use of powder materials;
- products of a set shape and with predicted properties which are manufactured according to the additive technology.

1. Nesterenkov, V.M., Matvejchuk, V.A., Rusynik, M.O. (2018) Manufacture of industrial products using electron beam technologies for 3D-printing. *The Paton Welding J*., 1, 24–28.
2. Matviichuk, V.A., Nesterenkov, V.M., Rusynik, M.O. (2019) Specialized technological electron beam equipment for realization of additive process of layer-by-layer manufacture of metal products using the powder materials. In: *Proc. of 9th Int. Conf. on Beam Technologies in Welding and Materials Processing - BTWMP (Odessa, 9–13 September 2019)*, 84–88.
3. Paton, B.E., Nazarenko, O.K., Nesterenkov, V.M. et al. (2004) Computer control of electron beam welding with multi-coordinate displacements of the gun and workpiece. *The Paton Welding J*., **5**, 2–5.
4. Nesterenkov, V.M., Matvejchuk, V.A., Rusynik, M.O., Ovchinnikov, A.V. (2017) Application of additive electron beam technologies for manufacture of parts of VT1-0 titanium alloy powders. *Ibid*., **3**, 2–6.
5. Nesterenkov, V.M., Matviichuk, V.A., Rusynik, M.O. et al. (2019) Microstructure of VT20 titanium alloys produced by the method of layer-by-layer electron beam fusion using domestic powder materials. *Ibid*., **9**, 2–7.
6. Zhukov, V.V., Grigorenko, G.M., Shapovalov, V.A. (2016) Additive manufacturing of metal products (Review). *Ibid*., **5–6**, 137–142.
7. Nesterenkov, V.M., Matvejchuk, V.A., Rusynik, M.O. et al. (2017) Principles of manufacture of commercial parts by method of rapid prototyping using the electron beam technologies. In: *Proc. of 9th Int. Conf. on Beam Technologies in Welding and Materials Processing — BTWMP (Odessa, 9–13 September 2019)*, 73–77.
8. Matviichuk, V.A., Nesterenkov, V.M., Rusynik, M.O. (2018) Application of additive electron-beam technologies for manufacture of metal products. *Electrotechnica & Electronica E+E*, **3–4**, 69–73.
9. Nesterenkov, V.M., Khripko, K.S., Orsa, Yu.V., Matviichuk, V.A. (2018) Electron beam technologies in aircraft construction. In: *Science of materials: Achievements and perspectives*. In: 2 Vol., Vol. 2. Kyiv, Akademperiodika [in Russian].
10. Mahale, T.R. (2009) *Electron beam melting of advanced materials and structures*: Syn. of Thesis for the Degree of Dr. of Philosophy. North Carolina State University, USA.

Received 08.01.2020

https://doi.org/10.37434/tpwj2020.02.09

INFLUENCE OF SCANDIUM ON MECHANICAL PROPERTIES OF WELDED JOINTS OF D16 ALLOY PRODUCED USING FILLER WIRES OF DIFFERENT ALLOYING SYSTEMS

A.G. Poklyatsky[1], **V.E. Fedorchuk**[1], **S.l. Motrunich**[1], **Yu.V. Falchenko**[1] and **G.P. Kisla**[2]
[1]E.O. Paton Electric Welding Institute of the NAS of Ukraine
11 Kazymyr Malevych Str., 03150, Kyiv, Ukraine. E-mail: office@paton.kiev.ua
[2]National Technical University of Ukraine «Igor Sikorsky Kyiv Polytechnic Institute»
37 Peremohy Prosp., 03056, Kyiv, Ukraine

The impact of scandium in filler wires of SvAMg6, Sv1201 and SvAK5 type, as well as arc oscillations, caused by electric current passage through the filler section, on weld structure formation was studied in nonconsumable electrode argon-arc welding of sheet aluminium alloy D16. Curves of metal hardness distribution in the welding zone are shown and strength limits of welded joints and weld metal after natural ageing of the specimens are determined. It is shown that use of scandium filler wires, similar to standard batch-produced ones, leads to formation of a fine-grained dendritic structure of weld metal. However, the subdendritic structure does not form even in welding with arc oscillations, because of a low (0.15–0.17 %) scandium content in welds. Use of scandium-containing filler wires can lower the degree of weld metal softening at lowering of the total content of the main alloying elements in them. Positive impact of scandium additives together with application of arc oscillations on the degree of softening and ultimate strength of weld metal is noticeable at application of filler wire of Al-Si alloying system. However, the maximum level of strength, both of the welded joints and the weld metal, is provided in nonconsumable electrode argon-arc welding of D16 alloy 2 mm thick using batch-produced filler wires SvAMg6 and SvAMg63. 21 Ref., 2 Tables, 3 Figures.

Keywords: D16 aluminium alloy, nonconsumable electrode argon-arc welding with arc oscillations, scandium, microstructure, hardness, ultimate strength

Aluminum alloys of different alloying systems are widely used for manufacture of space and aircraft equipment, sea and river vessels, railway and automobile transport and other structures of critical purpose [1−3]. This is largely predetermined by their high structural strength, which is provided by the optimal combination of strength characteristics, which determines the material intensity of structures and resistance to cracking, which indicates their resistance to brittle fracture and providing the reliability and life of units during their operation [4]. To produce permanent joints from the semi-finished products of these alloys in most cases, nonconsumable (tungsten) electrode argon-arc welding (NEAAW) is used, in which the weld formation occurs as a result of melting welded edges and filler wire and their subsequent crystallization [5]. At this time, the weld metal has a cast, mostly large crystalline structure with a clearly pronounced orientation of dendrites, as a result of which, its tensile strength for the most thermally hardened alloys does not exceed 50−60 % of this value for the base material [6].

Therefore, in order to increase the strength of welds, during the process of welding it is necessary to create favorable conditions for the formation of a fine-grained disoriented structure of metal in them. Among the known widely applied methods of influence on the processes of weld pool metal crystallization, the use of welding wires modified with zirconium, acting as forced crystallization centers, is of particular importance. In addition, the effectiveness of using scandium as a modifier has been long investigated, the unique influence of which is predetermined by the dimensional and structural similarity of crystalline lattices of aluminum (0.4405 nm) and $A1_3Sc$ phase (0.4407 nm), due to which the particles of the latter act as nuclei of crystallization centers in the welds [7−9]. As a result, the formation of fine-crystalline structure of welds is provided, which has a positive effect on their physical and mechanical properties [10].

A.G. Poklyatsky — https://orcid.org/0000-0002-4101-2206, V.E. Fedorchuk — https://orcid.org/0000-0002-9929-3231,
S.l. Motrunich — https://orcid.org/0000-0002-8841-8609, Yu.V. Falchenko — https://orcid.org/0000-0002-3028-2964,
G.P. Kisla — https://orcid.org/0000-0003-0791-6903

Thus, during welding of deformed thermally non-strengthened alloys of the Al–Mg alloying system due to the use of scandium alloyed wires, the dispersion hardening and structural hardening of weld metal occurs, which provides an increase in their tensile and yield strength [6, 11]. The introduction of scandium into the filler wires has a positive effect also during welding of thermally hardened aluminum alloys of the Al-Mg-Li alloying system. In addition, in order to increase the tensile strength of welds immediately after welding during heat treatment of welded joints, favorable conditions are created for their further strengthening by isolating not only strengthening particles of basic alloying elements, but also dispersed aluminum-scandium phases [6, 12, 13].

Regarding aluminum alloys doped with copper, the introduction of scandium may reveal in different way. Sometimes scandium with copper can form a chemical compound (W-phase), as a result of which its impact on refining the weld metal structure and its strengthening will be reduced [14]. In addition, an increase in the volume fraction of excess phases can lead to a decrease in the strength, ductility and fracture toughness of weld metal [15]. However, the experimental investigations carried out on alloys 1201 and 1460 indicate an increase in the tensile strength of the welds produced by NEAAW using the filler wire of type Sv1201 with 0.5 % of Sc [6]. Also a positive effect of scandium on physicomechanical characteristics of semi-finished products and welded joints of alloys of the Al–Zn–Mg–Cu alloying system is observed [6, 16].

The sharp oscillations in the melt of the welding pool caused by periodic change in the power influence of the arc as a result of pulsations of welding current or deviation from the vertical position [17, 18] can be the other effective way of changing conditions of metal crystallization during the welding process. As a result of such oscillations, periodic melting of second-order axes of the formed crystals occurs and the activity of the crystallization centers increases due to the periodic change of the metal temperature at the crystallization front. This leads to violation of crystallization continuity and formation of long oriented crystals and facilitates the formation of a fine-grained disoriented structure of the weld metal [19].

During welding thin-sheet (<3 mm) semi-finished products, when the volume of filler wire in a weld is small (<20 %), it is not possible to achieve the optimum (0.3–0.4 % [20]) concentration of scandium in the weld metal, at which the formation of subdendritic structure of weld metal is provided. Therefore, in such cases it is advisable to perform arc welding with oscillations of the weld pool melt simultaneously with the use of scandium-modified filler wires to guarantee producing a disoriented fine-grained dendritic structure over the entire volume of the weld metal [21].

The aim of the investigations is to evaluate the influence of scandium in the filler wires of the Al–Mg, Al–Cu and Al–Si alloying systems and arc oscillations caused by passing electric current through the area of filler on the formation of weld structure, softening of metal and tensile strength of welded joints and weld metal in NEAAW of thin-sheet D16 alloy.

Procedure of investigations. Automated NEAAW of butt joints of 2 mm thick sheets of aluminum D16 alloy (wt.%: 4.5 Cu; 1.7 Mg; 0.53 Mn; 0.19 Si; 0.21 Fe; 0.11 Zr; 0.06 Ti; the remnant is Al) was performed on an alternating current with a rectangular wave shape of 200 Hz with the use of the welding head ASTV-2m from the power source MW-450 (Fronius, Austria). The welding speed was 20 m/h, the value of welding current was 170 A and the feed speed of the 1.6 mm diameter filler wire was 82 m/h. During welding, the serial filler wires of three alloying systems were used: Al–Mg (SvAMg6), Al–Cu (Sv1201) and Al–Si (SvAK5), as well as the wires similar to them modified with zirconium and scandium — SvAMg63 (Al–6.2 % Mg–0.6 % Mn–0.2 % Zr), Sv1571 (Al–6.1 % Mg–0.19 % Mn–0.06 % Zr–0.015 % Ti–0.52 % Sc), Sv1201Sc (A1–6 % Cu–0.1 % Ti–0.2 % Zr–0.5 % Sc) and SvAK5Sc (A1–5 % Si–0.5 % Sc). In addition, to form a homogeneous fine-grained disoriented metal structure over the entire volume of welds the welding was performed with oscillations in the molten metal of the weld pool, caused by deviations of the arc from its vertical position due to passing of a constant («+» — to earth) current of the value of 200 A through the area of the 25 mm long filler wire directly before it gets into the welding pool [18, 21].

Before welding, chemical etching of sheets was carried out according to a generally-accepted technology and mechanical cleaning of surfaces and ends of welded edges to a depth of approximately 0.1 mm. The sheets of the alloy in the state after quenching and natural aging (tensile strength is σ_t = 445 MPa, elongation is δ = 11 %) were welded between each other along the direction of their rolling. All the investigations and tests of the specimens of welded joints were performed within 10–12 months after their welding, when their natural aging process took place.

The hardness of the metal in different zones of welded joints was measured on the facial surfaces of the specimens of the produced joints after cleaning the reinforcement and penetration of the welds flush with the base material in the Rockwell device at a load P = 600 N. The evaluation of structural features of welded joints was carried out with the use of the optical elec-

tron microscope MMT-1600V. The tensile strength of welded joints (σ_t^{wj}) was determined at a static tension of standard flat specimens with a width of a working part of 15 mm with a cleaned weld penetration in the standard servo-hydraulic complex MTS 318.25, and the tensile strength of the weld metal (σ_t^{wm}) was determined on the same specimens with the cleaned reinforcement and weld penetration.

The analysis of chemical composition of the specimens was performed in the X-ray fluorescence analyzer EXPERT3L. The chemical analysis was based on the energy-dispersive X-ray fluorescence elemental analysis according to the method of fundamental parameters with excitation of characteristic radiation of atoms of the specimen by photons of a braking spectrum of a low-power X-ray tube and recording this radiation by means of a semiconductor detector with a thermal electric cooling.

Results of investigations and their discussion. According to the results of the carried out investigations, it was established that during a conventional NEAAW of 2 mm thick D16 alloy with a serial filler wire SvAMg6, the hardness of metal in the central part of the weld is at the level of *HRB* 92.5–93.0, and in the zone of its fusion with the base material is *HRB* 97.0–97.5 (Figure 1). The use of the filler wire SvAMg63 containing zirconium as a modifier almost does not change the nature of hardness distribution of the metal in the welding zone even in NEAAW with arc oscillations caused by passing of electric current through the filler area. And, accordingly, the tensile strength of welded joints and the tensile strength of the weld metal at a static tension of the specimens produced with the filler wires SvAMg6 and SvAMg63 are approximately at the same level (Table 1). The use of the filler wire of type Sv1571, containing 0.52 % of Sc leads to a slight decrease in the hardness of the metal in the area of forming a permanent joint. Thus, in the weld produced by NEAAW with the specified wire and arc oscillations, the hardness of the metal is *HRB* 91.5–92.0 and in the fusion zone with the base material it is *HRB* 95.0–95.5. Moreover, the tensile strength of welded joints and the tensile strength of weld metal are slightly reduced to 336 and 320 MPa, respectively. The fracture of all specimens with a cleaned weld penetration produced with the investigated filler wires of the alloying system Al–Mg at a static tension occurred in the zone of fusion of the weld with the base material, and of the specimens with cleaned reinforcement and weld penetration — in the central part of the weld (Figure 2).

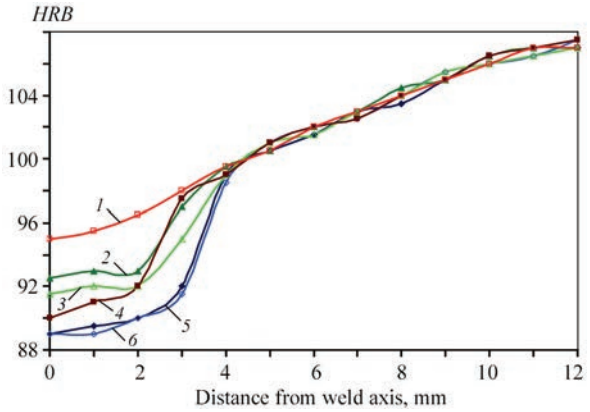

Figure 1. Distribution of hardness in butt joints of 2 mm thick D16 alloy after welding and their natural aging, produced by NEAAW using filler wires of different alloying systems and arc oscillations: *1* — SvAK5Sc with arc oscillations; *2* — SvAMg6; *3* — Sv1571 with arc oscillations; *4* — SvAK5; 5 – Sv1201; *6* — Sv1201Sc with arc oscillations

Table 1. Tensile strength of welded joints of 2 mm thick D16 alloy after their natural aging, produced by NEAAW using different filler wires

Type NEAAW	Filler wire	Tensile strength, MPa	
		$\sigma_t^{w.j}$	$\sigma_t^{w.m}$
Natural	SvAMg6	369–352 363	345–325 335
With arc oscillations	SvAMg63	364–340 359	339–321 332
	Sv1571	343–332 336	330–311 320
Natural	Sv1201	360–340 349	318–312 315
With arc oscillations	Sv1201Sc	363–341 350	319–311 315
Natural	SvAK5	347–339 342	260–255 257
With arc oscillations	SvAK5Sc	362–343 350	318–308 312

Note. In the numerator the maximum and minimum and in the denominator — the average values of the results of the test of 4–6 specimens are given.

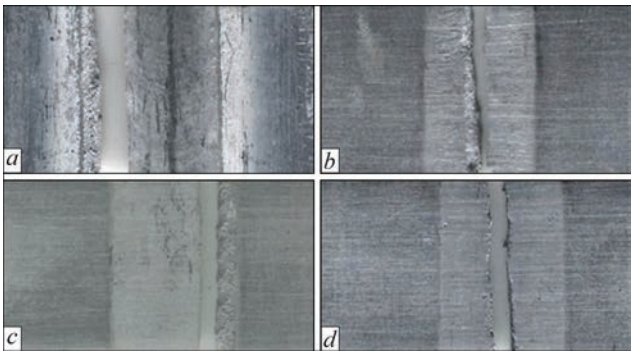

Figure 2. Appearance of working part of specimens with cleaned weld penetration (*a*) and cleaned weld reinforcement and penetration (*b*–*d*) of 2 mm thick D16 alloy after their fracture during tests produced by NEAAW using filler wires of different alloying systems: *a* — Al–Mg, Al–Cu or Al–Si; *b* — Al–Mg; *c* — Al–Cu; *c* — Al–Si

According to the results of the carried out investigations of microstructure of the specimens of the produced welded joints, it was established that, regardless of the chemical composition of filler wires and presence of scandium in them, a fine-grained dendritic structure of metal is formed in the welds (Figure 3), although dendritic parameter for weld metal can vary during welding using different filler wires. Thus, when using the wire SvAMg6 it amounts to 9.95 μm, when using the wire SvAMg63 — 10.20 μm, and the wire Sv1571 — 12.36 μm. The carried out analysis of chemical composition of the welds showed that when using the filler wire Sv1571, the content of scandium in them is at the level of 0.17 % (Table 2). Of course, such amount of scandium is not sufficient to form the primary particles of scandium aluminide in the weld metal. Therefore, the use of this filler wire even in NEAAW with arc oscillations cannot provide the necessary conditions for the formation of a subdendritic structure in the weld metal, due to which the tensile strength of the welds significantly increases. In addition, the results of the analysis of chemical composition of the welds indicate that when using these wires, the total amount of the main alloying elements in the metal of the welds, on which the tensile strength of

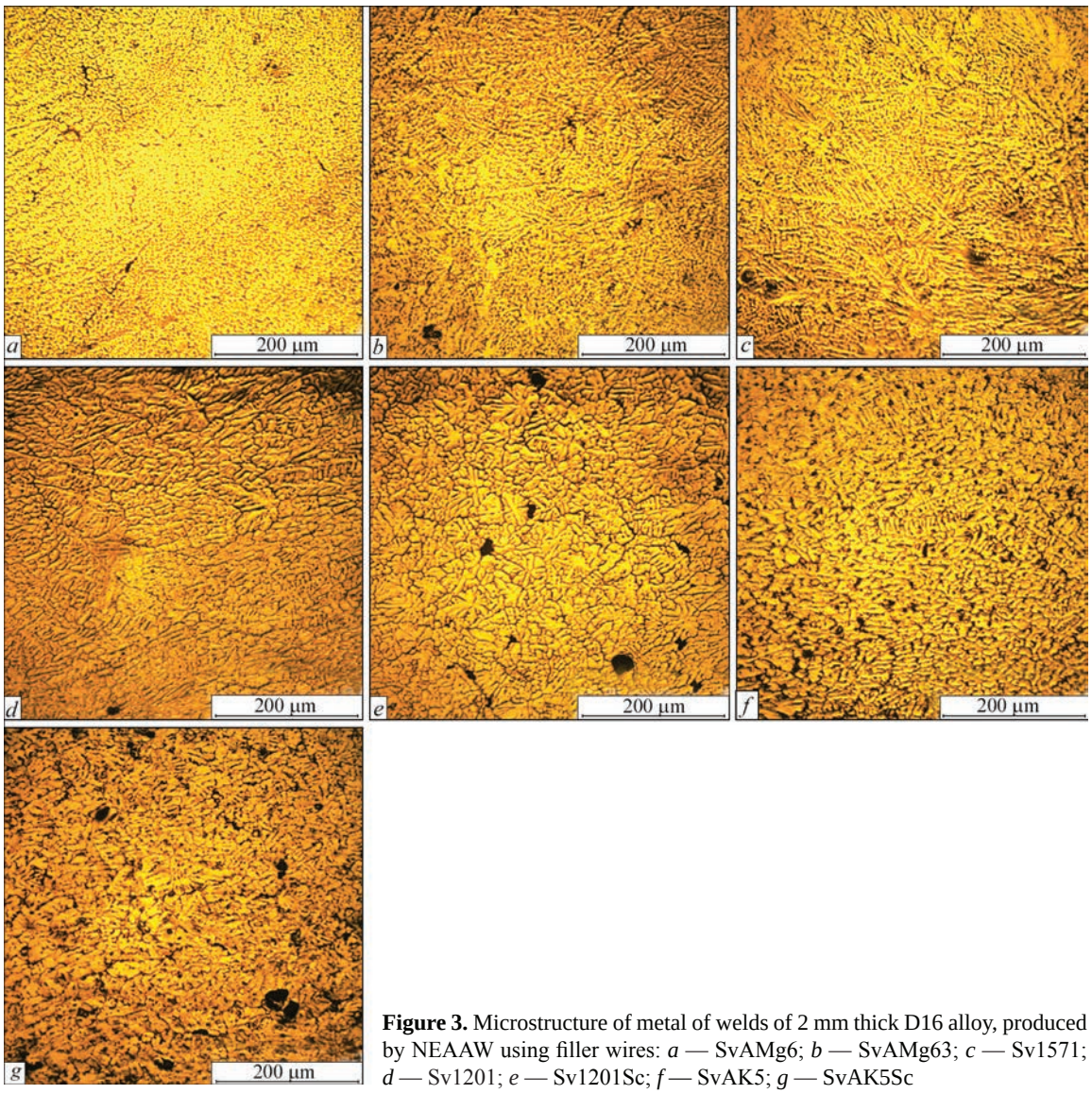

Figure 3. Microstructure of metal of welds of 2 mm thick D16 alloy, produced by NEAAW using filler wires: *a* — SvAMg6; *b* — SvAMg63; *c* — Sv1571; *d* — Sv1201; *e* — Sv1201Sc; *f* — SvAK5; *g* — SvAK5Sc

Table 2. Content of main alloying elements and modifiers in the metal of welds of 2 mm thick D16 alloy, produced by NEAAW with the use of different filler wires

Filler wire	Alloying elements, wt.%				Modifiers, wt.%	
	Mg	Cu	Si	$\Sigma_{Mg+Cu+Si}$	Zr	Sc
SvAMg6	3.22	2.79	–	6.01	–	–
SvAMg63	2.92	2.91	–	5.83	0.10	–
Sv1571	2.61	3.00	–	5.61	0.05	0.17
Sv1201	1.08	5.91	–	6.99	0.07	–
Sv1201Sc	0.86	5.70	–	6.56	0.06	0.15
SvAK5	1.02	2.63	1.99	5.64	–	–
SvAK5Sc	1.06	2.87	1.78	5.71	0.06	0.15

the latter depends, is different: for SvAMg6 it is the highest, and for Sv1571 it is the lowest.

In NEAAW of D16 alloy using the filler wires Sv1201 and Sv1201Sc by the alloying system Al–Cu, the metal hardness in the zone of forming permanent joints is at the same level — *HRB* 89.0–90.0 in the weld metal and *HRB* 91.5–92.5 in the zone of their fusion with the base material. Of course, this provides the same values of the tensile strength of welded joints (350 MPa) and the tensile strength of weld metal (315 MPa) at a static tension of the specimens produced using such filler wires. The fracture of the specimens with a cleaned weld penetration occurs along the fusion zone with the base material, and of the specimens with the cleaned reinforcement and weld penetration – along the weld metal closer to this fusion zone.

The examinations of microstructure of metal in the welds produced in NEAAW using both filler wires of the alloying system Al–Cu made it possible to establish that dendritic parameter is the same for them and amounts to 12.36 μm. But when using a scandium filler wire, the total amount of the main alloying elements in the weld metal is slightly lower than in that produced using a serial filler wire. Obviously, it is precisely due to the presence of scandium in the welds and application of arc oscillations during their welding and it is possible to provide the same values of dendritic parameter and the tensile strength of welds, as in conventional NEAAW of D16 alloy using the serial filler wire Sv1201.

The positive effect of scandium additives, together with the use of NEAAW with arc oscillations, can be observed in the use of the filler wire of the alloying system Al-Si. Thus, during a conventional NEAAW of D16 alloy using the filler wire SvAK5, the hardness of the metal in the central part of the weld is at the level of *HRB* 90.0–92.0, and in the zone of its fusion with the base material is at the level of *HRB* 97.5–98.0. The use of scandium-modified filler wire SvAK5Sc in NEAAW with arc oscillations provides an increase in the hardness of the metal in the weld to *HRB* 95.0–96.5, and in the zone of its fusion with the base material — to *HRB* 98.0–99.0. Accordingly, the tensile strength of weld metal produced using scandium filler wire is 55 MPa higher than this value for the joints produced using the serial filler wire SvAK5 and is at the level of 312 MPa. Moreover, the presence of scandium in the filler wire has a lesser effect on increasing the tensile strength of welded joints since fracture of the specimens with a cleaned weld penetration occurs in the area of fusion of the weld with the base material. And the specimens with a cleaned reinforcement and weld penetration at a static tension are fractured in the central part of the weld.

According to the result of the analysis of microstructure of the welds produced with the use of filler wires of the alloying system Al-Si, it was found that dendritic parameter for the weld metal produced using the filler wire SvAK5 was 11.66 μm and using the filler wire SvAK5Sc — 11.33 μm. In addition, the results of studying the chemical composition of the weld metal indicate a rather small increase in the total amount of the main alloying elements in them when using a scandium-containing filler wire. Therefore, the presence of scandium in the filler wire of the alloying system Al-Si together with arc oscillations during NEAAW of D16 alloy contribute to the refinement of the dendritic structure of the weld metal and increase in their tensile strength.

Conclusions

1. During nonconsumable electrode argon-arc welding of 2 mm thick aluminum D16 alloy with the investigated filler wires of the alloying systems Al–Mg, Al–Cu and Al–Si regardless of the presence of scandium in them, in the welds a fine-grained dendritic structure is formed. In addition, dendritic parameter for the weld metal can vary when using filler wires of different chemical composition.

2. The presence of scandium in the filler wire of the alloying system Al–Si together with arc oscillations during welding of this alloy by a nonconsumable electrode contribute to the refinement of dendritic structure of the weld metal and increase in their hardness and tensile strength.

3. The maximum level of strength of welded joints and weld metal is provided by nonconsumable elec-

trode argon-arc welding of 2 mm thick aluminum D16 alloy with serial filler wires SvAMg6 and SvAMg63.

4. The use of filler wires of the alloying systems Al–Mg and Al–Cu with scandium in nonconsumable electrode argon-arc welding of 2 mm thick aluminum D16 alloy with arc oscillations does not allow providing the formation of subdendritic structure of metal in welds and thus significantly increasing their strength and can only slightly reduce the degree of softening the weld metal while reducing the total amount of the main alloying elements.

1. Ishchenko, A.Ya., Labur, T.M., Bernadsky, V.N., Makovatskaya, O.K. (2006) *Aluminium and its alloys in modern welded structures*. Kiev, Ekotekhnologiya [in Russian].
2. Beletsky, V.M., Krivov, G.A. (2005) *Aluminium alloys (composition, properties, technology, application)*: Refer. Book. Ed. by I.N. Fridlyander. Kiev, KOMINTEX [in Russian].
3. Kablov, E.N. (2000) Main directions of development of materials for aerospace engineering of 21st century. *Perspektivnye Materialy*, **3**, 27–36 [in Russian].
4. Ostash, O.P. (2015) *Fracture mechanics and strength of materials*: Refer. Book. Vol. 15. Structure of materials and fatigue life of structure components. Ed. by V.V. Panasyuk, Lviv, SPOLOM [in Ukrainian].
5. Ishchenko, A.Ya., Labur, T.M. (2013) *Welding of modern structures from aluminium alloys*. Kiev, NPP NANU [in Russian].
6. Mashin, V.S., Poklyatsky, A.G., Fedorchuk, V.E. (2005) Mechanical properties of aluminium alloys in consumable and nonconsumable electrode arc welding. *The Paton Welding J.*, **9**, 39–45.
7. Davydov, V.G., Elagin, V.I., Zakharov, V.V., Rostova, T.D. (1996) On alloying of aluminium alloys with scandium and zirconium additives. *Metallovedenie i Termich. Obrab. Metallov*, **8**, 25–30 [in Russian].
8. Bondarev, B.I., Elagin, V.I. (1992) New aluminium alloys with scandium. *Tekhnologiya Lyogkikh Splavov*, **5**, 22–28 [in Russian].
9. Ishchenko, A.Ya. (2003) *Aluminium high-strength alloys for welded structures. Advanced materials and technologies*. Vol. 1, Kyiv, Akademperiodika, 50–82 [in Russian].
10. Milman, Yu.V. (2003) Effect of scandium on structure, mechanical properties and corrosion resistance of aluminium alloys. *Ibid*., 335–360 [in Russian].
11. Ryazantsev, V.I., Filatov, Yu.A. (2003) Technological aspects of arc welding of aluminium alloys with scandium. *Aviats. Promyshlennost*, **1**, 13–17 [in Russian].
12. Turkina, N.I., Semenova, B.V. (1992) Structure and properties of Al–Mg–Li system alloys with scandium. *Tekhnologiya Lyogkikh Splavov*, **1**, 57–59 [in Russian].
13. Bratukhin, A.G., Tretyak, N.G., Sklabinskaya, I.E. (1993) Structure and mechanical properties of welded joints of aluminium-lithium alloys in welding with scandium-containing test additives. *Ibid*., **12**, 11–15 [in Russian].
14. Zakharov, V.V., Rostova, T.D. (1995) Alloying with scandium of aluminium copper-containing alloys. *Metallovedenie i Termich. Obrab. Metallov*, **2**, 23–27 [in Russian].
15. Elagin, V.I., Zakharov, V.V., Rostova, T.D., Filatov, Yu.A. (1989) Some physical metallurgy principles of alloying, production technology and heat treatment of aluminium scandium-containing alloys. *Tekhnologiya Lyogkikh Splavov*, **9**, 27–34 [in Russian].
16. Fridlyander, I.N., Senatorova, O.G., Novikov, I.I. et al. (1993) Superplasticity of high-strength alloys of Al–Zn–Mg–Cu system alloyed with scandium. *Ibid*., **7–8**, 43–47 [in Russian].
17. Brodyagina, I.V. (1998) Arc welding of aluminium alloys using magnetic fields. *Svarochn. Proizvodstvo*, **9**, 48–51 [in Russian].
18. Poklyatsky, A.G., Ishchenko, A.Ya., Grinyuk, A.A. et al. (2002) Consumable-electrode argon-arc welding of aluminium alloys with arc oscillations. *The Paton Welding J*., **2**, 18–22.
19. Ishchenko, A.Ya., Poklyatsky, A.G., Lozovskaya, A.V. et al. (1990) Influence of low-frequency modulation parameters of rectangular-shaped heteropolar current on weld structure in welding of aluminium alloys. *Avtomatich. Svarka*, **9**, 23–27 [in Russian].
20. Fedorchuk, V.E., Kushnaryova, O.S., Alekseenko, T.A., Falchenko, Yu.V. (2014) Peculiarities of alloying of weld metal of high-strength aluminium alloy welded joints with scandium. *The Paton Welding J*., **5**, 28–32.
21. Poklyatsky, A.G., Motrunich, S.I. (2019) Strength of welded joints of heat-hardenable aluminium alloys in TIG and friction stir welding. *Ibid*., **2**, 13–18.

Received 23.12.2019

FEBRUARY 20, 1986 On February 20, 1986 the Soviet Union launched the scientific orbital station «Mir», replacing the orbital stations «Salyut» and became for about 15 years a single in the world manned space laboratory for long-term scientific-technical experiments and investigation of human body in space. Further on the solar-cell batteries designed at the E.O. Paton Electric Welding Institute were deployed at the station.

FEBRUARY 26, 1934 The first plant for the production of the «people's» car Volkswagen was opened. The first produced car was the famous VW Beetle. This is the most popular car in history, produced without additional consideration of the basic design. In total, 21,529,464 cars were manufactured. In its development Ferdinand Porsche (later founder of the second variant of the Tiger tank) was involved, who was keeping contact with Ford and other pioneers and actively introduced new technologies at the plant. Welding provided reliability and quick assembly of the car in the conveyor.